ISSN Print 0970 - 3268
ISSN Online 2582 - 2020

The Journal of the Indian Association of Sedimentologists

The Indian Association of Sedimentologists

Volume 40 No. 2 July - December, 2023

Photo Courtesy: G M Bhat

Eight Thousand years old remnants of Lake Deposits at Changmar Village in Shyok Valley along the right bank of Shyok River, Ladakh

**** 8 thousand years old remnants of Lake Deposits at Changmar Village in Shyok Valley along the right bank of Shyok River, Ladakh*

ISSN Print 0970 – 3268
ISSN online 2582 - 2020

The journal of the Indian Association of Sedimentologists

DOI:
https://doi.org/10.51710/jias.v40i11

Managing Editors:

The Journal of the Indian Association of Sedimentologists (IAS) is both an international open access online and print journal and is leader in its field and publishes ground-breaking research from across the spectrum of sedimentology, sedimentary geology, sedimentary geochemistry, experimental and theoretical sediment transport, mass movement fluxes, modern and ancient sedimentary environments, sequence – cyclo – chrono – and chemostratigraphy, sediment – biological interaction, palaeosols, diagenesis, stable isotope geochemistry, environmental sedimentology, neo-tectonics, geo-hazards, stratigraphy, palynology, sedimentary mineral resources and hydrocarbons, and allied branches of sedimentary - stratigraphic research. It also publishes review articles, editorials, conference reports, tributes, announcements, advertisements, etc. It is currently distributed to universities and research laboratories in India and abroad. Access is open to complete electronic journal archive. Subscribers also have the option to buy the printed journal at subsidized cost.

Indian Association of Sedimentologists

TABLE OF CONTENTS

JOURNAL INDIAN ASSOCIATION OF SEDIMENTOLOGISTS ISSN NO 2582 – 2020
Vol. 40, Issue II, 2023, pp. 3-13
DOI: https://doi.org/10.51710/jias.v40iII.304

Provenance and Diagenetic Features of Sandstones in the Surma -Tipam Transitional Sequence exposed in the Schuppen Belt, Naga Hills, NE India

Borgohain, P.* and Pandey, N.
Department of Earth Sciences, Assam University, Silchar, Silchar-788011, Assam, India
E-mail Address: pranamee14@gmail.com

ABSTRACT
The Schuppen Belt, a part of the Indo-Burma Ranges is basically comprised of molasses of Tertiary age. This tectono–stratigraphic belt is restricted by two major thrust faults, namely Disang and Naga. In the southern part of the Naga Hills a significant part is occupied by Surma–Tipam Transitional Sequences (STTS). This study deals with the petrography, provenance, and tectonic setting of the STTS sandstones. The sandstones are classified as arkose and arkosic wacke types. The major contribution of detritus has been observed from the recycled orogen, dissected arc, transitional continental and basement uplift. The geochemistry data reveals that the sandstones were derived from a collisional setting of an active continental margin. The low degree of chemical maturity indicates that the sandstones were deposited in an arid climatic condition. The diagenetic signatures observed in these sandstones such as, point, long and concavo-convex grain boundary, albitization, crushing and squashing of quartz grains, warping of mica around detrital grains, and bending of mica suggest early to a late stage deep burial diagenesis.

KEYWORDS: **Petrography, Provenance, Diagenesis, Tectonic setting, Surma-Tipam Transitional Sequences, Naga-Hills**

INTRODUCTION

Naga Hills, the northern extension of Indo – Burma Wedge occupies a significant part of the Assam-Arakan Basin. Stratigraphically it consists of Tertiary sediments, Cretaceous Ophiolites, Precambrian metasediments and limestone clasts (Table 1). The region is divided into three morphotectonic belts having NE – SW trend, from east to west namely: Schuppen Belt, Inner Fold Belt, and Ophiolite Belt (Ghose et al. 1987). The Schuppen Belt is characterized by sediments ranging from Oligocene to Recent in age (Evans, 1964). The belt consists a narrow lineament of multiple thrust slices. Besides its two bounding thrusts i.e. Naga Thrust and Disang Thrust two other prominent thrusts of the belt are Chumliyanchen and Pephima. The Inner Fold Belt, bounded by Disang Thrust and Ophiolite Belt is characterized by Disang – Barail Transitional Sequence and Disang Group. This study is focused on the Neogene Surma – Tipam Transitional Sequences (STTS) exposed in the southwestern part of the Schuppen belt in the Dimapur District. The Surma – Tipam Transitional Sequence of the study area possess a heterogeneous lithology resembling both Surma and Tipam group of rocks (Borgohain & Pandey, 2016). The argillaceous lithology of

TABLE 1:Tertiary succession of Nagaland (Modified after Mathur and Evans, 1964; DGM, 1978; Ghose et al., 2010).

Age	Group	Lithology		
		Outer and Intermediate Hills		Eastern High Hills
Recent - Pleistocene		Alluvium and high-level terraces		
	Dihing	Boulder beds		
--------Unconformity--------				
Mio-Pliocene	Dupitila	Namsang Beds		
--------Unconformity--------				
Miocene	Tipam	Girujan Clay Tipam Sandstone		
	Surma	UpperBhuban/(STTS?) LowerBhuban		
--------Unconformity--------				
Oligocene	Barail	Renji	Tikak Parbat	Jopi / Phokphur FormationTuffaceous shale, sandstone, greywacke,grit and conglomerate. Minor limestoneand carbonaceous matter
		Jenam	Baragolai	
		Laisong	Naogaon	
UpperCretaceous-Eocene	Disang	Upper		Shale/slate/phyllite with calcareous lenses in basal sections
		Lower		Metamorphosed sediments with phyllite
--------Fault/Thrust--------				

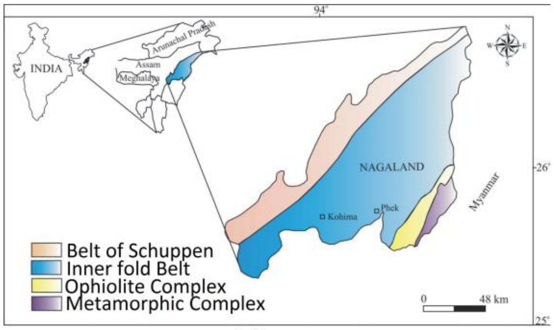

(a)

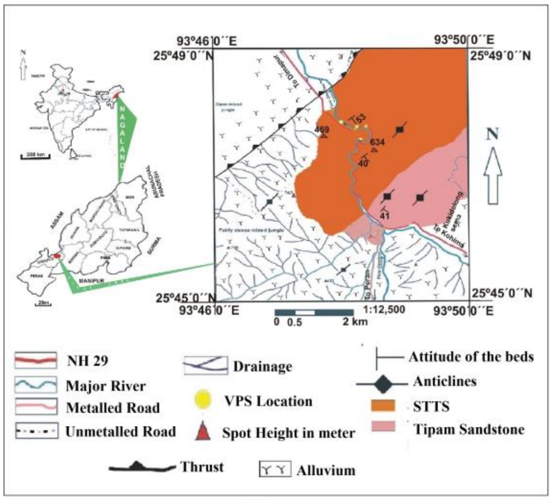

(b)

Fig (1a). Morphotectonic belts of Naga Hills after Ghose et al. (1987) **(b).** Geological map of the Study Area showing sample locations

The aim of this study is to infer the provenance, tectonic setting and diagenetic signatures of sandstones in the Surma – Tipam transitional sequences. This study investigated the maturity, provenance, transport processes and diagenetic history of sandstones. Composition of sandstones helps in deciphering the nature of petrographic province and tectonic regime that prevailed during sedimentation (Tawfik et al., 2018). It also explains the denudation history of sediments besides changes that occurred during its deposition. The present investigation is expected to help the ongoing research activities focusing on provenance studies.

STUDY AREA

The study area forms a part of the Belt of Schuppen that lies in the western margin of Nagaland (Fig 1 a). Besides well developed Surma – Tipam Transitional Sequences (Fig. 2), Tipam Sandstone Formation of the Tipam Group of Rocks and Namsang Beds of the Dupitila Group are the major lithological units observed in the study area. The Naga thrust is the major structural feature that passes through the area.

The area is bounded by the latitudes 25°45´00´´N - 25°49´00´´N and longitudes 93°46´00´´E - 93°50´00´´E of the topographic sheet no. 83G/13 of the Survey of India (Fig. 1 b). It covers almost five km distance along the NH 29 from Chumukedima town towards Kohima in Dimapur District.

sequence becomes rich in arenaceous content incorporated to the younger arenaceous Tipam Sandstone Formation. The sequence offers a local gradational passage between Surma and Tipam group of rocks instead of representing a typical Bhuban Formation in the study area.

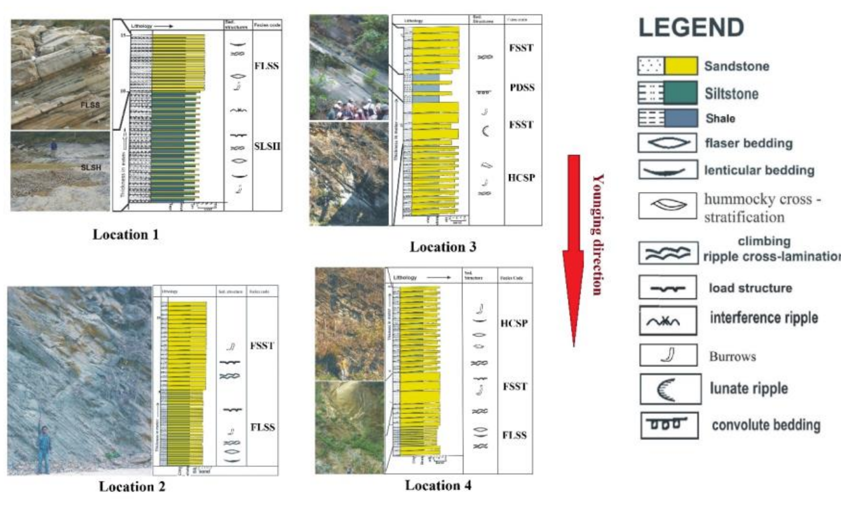

Fig 2: Vertical Profile section showing STT Ssandstones

The chemical composition of clastic sediments is a key to understand the provenance, tectonic setting, maturity, and weathering of the source region (Armstrong-Altrin et al., 2013; Basu, 2020). Numerous studies addressed the provenance of clastic sediments based on geochemistry data (Ramos-Vázquez et al., 2017; Armstrong-Altrin et al., 2021, 2022; Madhavaraju et al., 2021; Singh et al., 2023).

MATERIALS AND METHODS

Twenty-four thin sections of representative sandstone samples from the

TABLE 2**:** Modal composition of STTS sandstones; (Qmt: Monocrystalline quartz, Qpt: Polycrystalline quartz)

Sample No	Quartz	Qmt	Qpt	Feldspar	Mica	Rock fragment	Matrix	Cement
RP11	21.2	15.2	7	20.5	3	2.4	25.2	5
RP12	30	21.2	8.8	20.1	7.5	2.1	12.9	20.5
RP18	32.3	22.6	9.7	18.4	5.9	6.9	25	9.9
RP19	33.6	24.3	9.3	15	13.4	7.7	6.1	23.5
RP20	40.5	24.4	16.6	28.6	5.3	0.6	7.1	11
RP21	25	10.8	14.2	15.2	9.2	5.1	30.2	15.3
RP23	21.9	14	7.9	20.2	7.2	3.1	36.2	9.8
RP24	24.7	14.6	10.1	21	6	5.3	27.5	15.5
RP25	24.5	16.4	8.1	18.3	7.5	7	7.5	38
RP26	34	29.3	4.7	15	3	5	2	40
RP28	27.8	21	6.8	22	8.8	7.8	5.4	26.3
RP29	37.1	25.8	11.3	24.7	6.47	8.07	9.07	16.5
RP30	30.6	23.6	6.9	17.2	2.1	8.1	8.5	32.8
RP31	30.6	19	11.6	28.1	6.6	13.2	6.6	13.2
RP32	31.7	17.6	14.1	28.8	6.8	11.2	7.2	10.4
RP33	31	19.8	11.2	28.1	6.1	12.8	6.7	13.4
RP 34	33	19.5	13.5	26.1	8.3	10.6	6.1	14
RP35	34.7	18	16.7	27.3	7.2	11.7	8.3	10.8
RP36	31.9	19.7	11.3	28.5	8.2	11.4	7.9	12.1
RP37	33.6	19.4	14.2	24.3	7.9	12.1	7.7	14.4
RP38	30.7	16.2	14.5	28.2	6.7	12.8	6.8	14.8
RP42	29.9	16	13.9	18.5	2.6	7.3	9.3	30.6
RP45	29	21.2	7.8	21.1	8.5	8	11.9	21.5
RP 46	30	21.7	8.3	20.4	9.1	6.2	12.1	22.2

Neogene STTS were accomplished using Leica DM LP petrological microscope in the Department of Earth Science, Assam University, Silchar. The thin sections were prepared at the department of Geological Sciences, Gauhati University. Along with thin-section study modal analysis were also carried out. More than 400 grains were counted in each thin section following Gazzi-Dickinson method (Table 2). The data on modal composition were recalculated to 100% and the sandstones were classified by following the scheme suggested by Dott (1964) and Pettijohn et al. (1987). In this scheme quartz, feldspars and rock fragments are considered as the three poles of the triangle. The demarcation between arenite and wacke has been considered at 15% (Pettijohn et al., 1987). In addition, the QtFL (total quartz-feldspar-lithic fragments) and QmFLt (monocrystalline quartz- feldspar-lithic fragments + polycrystalline quartz) diagrams of Dickinson et al. (1983) were used to discriminate tectonic provenance of the Neogene sandstones.

To identify the heavy fractions in sandstones heavy mineral analysis was done by density separation technique suggested by Folk (1980) and Middleton (2003). Separation was done using the heavy liquid bromoform.

X-ray fluorescence (XRF) spectrometry was employed to determine the major element compositions of the sandstones. Approximately 25 gm of each powdered siliciclastic rock samples was analyzed using PANalytical AXIOS Sequential X-ray Fluorescence Spectrometer and Bruker S4 Poinner Spectrometer at Sophisticated Analytical Instrument Facility (SAIF), Gauhati University and IIT Roorkee, respectively.

RESULTS AND DISCUSSION

PETROGRAPHY

The framework grains of STTS are mainly composed of quartz, feldspars and rock fragments. Other minerals include muscovite, biotite, chlorite, glauconite and heavy minerals. The cementing materials are dominated by silica, iron - oxide and calcite (Table 2).

According to the classification scheme of Pettijohn et al. (1987), these sandstones dominantly represents arkose and arkosic wacke types (Fig. 3). Among the framework grains quartz is the most dominant variety. It includes monocrystalline undulatory non – undulatory, polycrystalline quartz grains.

Feldspars are the second most dominating framework grains of STTS sandstones. Among feldspars, plagioclase dominates over k-feldspar. K-feldspars include orthoclase, microcline and sanidine. Orthoclase dominates over the others. Feldspars grains possess sub-rounded to angular outlines. Rock fragments are composed of all three varieties, i.e. sedimentary, metamorphic and igneous. Shale, siltstone and sandstones are the common varieties of sedimentary rock fragments. While physillite and volcanic rock fragment characterize the metamorphic and igneous varieties, respectively.

(a)

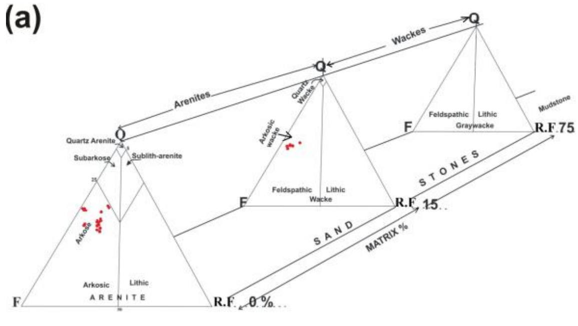

Fig 3: Classification of STTS sandstones after Pettijohn et al. (1987)

Among micas muscovite and biotite are the dominating varieties. Some flakes of chlorite, glauconite and illite are also observed in fine-grained samples. Matrix is mainly composed of sericite and chert. Different types of grain contacts such as point, long, rare concavo–convex, sutured and isolated or floating grains of STTS sandstones depicts different degrees of compaction.

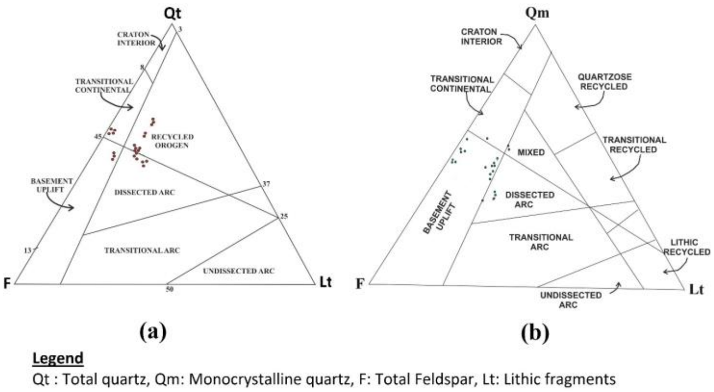

Fig 4: QtFLt and QmFLt after Dickinson and Suczek (1979) and Dickinson et al. (1983) showing the tectonic provenance of STTS sandstones.

TECTONIC PROVENANCE

Petrographic and geochemistry data have been widely used in various studies to understand the nature of the tectonic provenance of clastic sediments and rocks (Verma and Armstrong-Altrin, 2013, 2016; Verma et al., 2016; Bessa et al., 2021; Bela et al., 2023). In this study, both of the mentioned approaches have been utilized to understand the nature of the tectonic provenance of STTS sandstone. In order to interpret the tectonic setting of STTS, the triangular plots of QmFLt and QtFLt after Dickinson et al. (1983) and Dickinson and Suczek (1979) were used. On these diagrams the sandstones show a mixed contribution of dissected arc, basement uplift, transitional continental and recycle orogen, indicating an active tectonic setting in the source area (Fig 4).

HEAVY MINERALS

The nature of heavy mineral suites of STTS sandstones reflects intermingling of various provenance of the sedimentary sequence. The heavy mineral suite constitutes opaque and non – opaque varieties. Non – opaque varieties dominate over the opaque varieties. The percentage of opaque and non – opaque heavy minerals is graphically represented in Fig. 5 a. The opaque grains assumed to be iron oxide. The non–opaque transparent varieties include tourmaline, rutile, zircon, kyanite, sillimanite, sphene, dolomite, hornblende, phlogopite, clinohumite, humite, chondrodite, scapolite, staurolite, cordierite, garnet, xenotime, vesuvianite, epidote, zoisite, clinozoisite, hedenbergite, apatite and chloritoid (Fig. 6). Among the non – opaque varieties zircon, tourmaline, rutile, garnet, staurolite, chondrodite, humite and epidote dominate over the others. Most of the zircon grains possess subhedral to rounded shape. Twinned staurolite and epidote grains are not common. Among the tourmaline varieties schorlite dominates over dravite. Anatase and brookite two varieties of rutile are also observed in studied STTS sandstones. Though most of the garnets are subhedral to rounded in shape, some fine-grained euhedral grains are also observed.

MINERALOGICAL MATURITY

The mineralogical maturity of sandstone can be depicted on the basis of the presence of stable and unstable

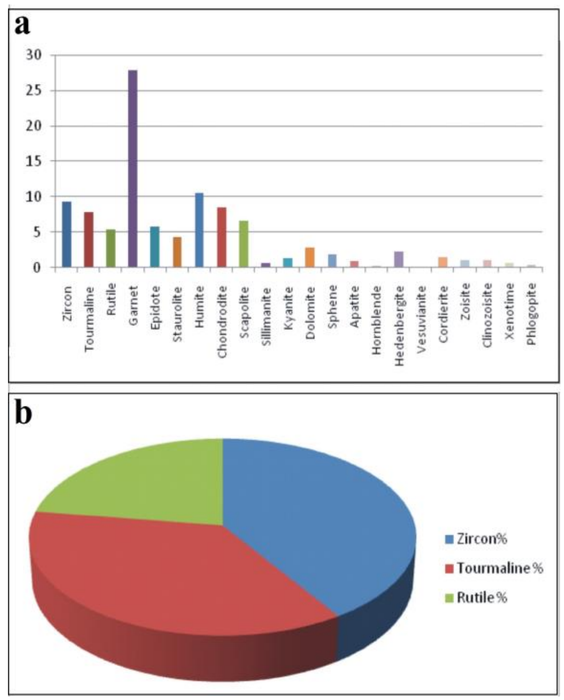

Fig 5 a: Graphical representation of heavy minerals distribution in the STTS sandstones **(b):** Graphical representation zircon tourmaline and rutile distributions in the STTS sandstones

constituents, i.e. increasing percentage of stable constituents such as quartz, chert etc. indicates higher degree mineralogical maturity and increasing percentage of unstable constituents such

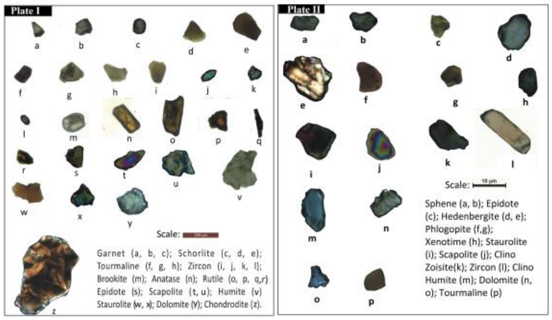

a

Fig 6: Different heavy minerals observed in STTS sandstones

s feldspars and rock fragments, suggesting lower degree of mineralogical maturity (Folk 1980). Besides these ZTR index of heavy minerals is also a good indicator of mineralogical maturity. The average ZTR index of STTS is found to be 20.9 % depicting mineralogically an immature nature. The presence of higher percentage of feldspar and rock fragments of sandstone further supports the immature to sub-mature nature of the sandstones.

TABLE 3:Major element concentrations of STTS sandstones (in wt. %)

S No	SiO_2	Al_2O_3	Fe_2O_3	MnO	MgO	CaO	Na_2O	K_2O	TiO_2	P_2O_5	Total
P4	68.61	13.7	4.91	0.04	3.240	2.15	1.71	2.94	0.60	0.14	98.04
P5	49.45	6.28	3.10	0.10	2.605	14.3	1.48	1.49	0.56	0.16	79.525
P6	38.08	6.79	5.17	0.15	2.689	20.1	1.21	2.20	0.39	0.23	77.009
P7	64.55	9.72	4.26	0.03	3.540	1.72	1.75	2.09	0.56	0.15	88.37
P8	65.16	9.99	4.61	0.04	3.849	2.01	1.74	2.10	0.58	0.16	90.239
P9	51.29	9.28	7.22	0.05	4.156	2.47	1.44	1.61	0.69	0.15	78.356
P10	64.63	10.2	4.27	0.04	1.978	0.93	1.75	2.24	0.52	0.15	86.708
P14	72.49	8.48	5.86	0.08	0.50	2.76	2.20	2.30	0.70	0.14	93.21
P15	72.40	13.01	4.45	0.07	0.60	1.84	2.17	2.13	0.45	0.16	97.28

PROVENANCE

Heavy mineral constituents can lead us to understand the nature of the tectonic provenance of sandstones. On the basis of occurrences of heavy minerals in STTS, the following four assemblages are identified along with their source rock characteristics.

(i) Humite – Clinohumite – Chondrodite – Phlogopite – Scapolite – Wollastonite – Sphene – Tourmaline (Dravite) – Vesuvianite – Epidote – Brookite – Iron oxide, which characterizes a contact dolomitic marble and scarn source rocks.

(ii) Zircon – Tourmaline (Schorlite) – Sphene – Apatite – Hornblende – Hedenbergite is an indicative of granite and granitoid sources.

(iii) Tourmaline (Schorlite) – Kyanite – Sillimanite – Staurolite – Hornblende – Hedenbergite – Rutile – Anatase – Garnet signifying a regionally metamorphosed source terrain.

(iv) Tourmaline (Scorlite and Dravite) – Garnet – Xenotime indicates pegmatitic source.

(v) Rounded reworked grains of Zircon – Tourmaline – Rutile – Dolomite etc. indicate a sedimentary source terrain.

MAJOR ELEMENT CONCENTRATIONS

A total of ten representing sandstone samples were analyzed for major element concentrations (Table 3). The SiO_2 concentration of the sandstones varies between 38 and 68 wt. %, with an average of 58 wt. %. The SiO_2/Al_2O_3 ratio of STTS sandstone is relatively high. The lower level of chemical maturity of the sediments is reflected by the binary plot of $Al_2O_3+K_2O+Na_2O$ against SiO_2 (Suttner and Dutta, 1986). The major elements can provide information about the climatic condition that prevailed during the deposition of sediments. The bivariate plot of $Al_2O_3+K_2O+Na_2O$ against SiO_2 suggest an arid climatic condition for the STTS sandstones (Fig. 7 a).

Source rock composition has a significant contribution to the chemical attributes of clastic rocks. Besides this, secondary processes like chemical weathering and diagenesis of clastic rocks like sandstone; shale etc. also have an effect on the chemical composition. It is also influenced by the nature of sedimentary processes that prevail in the depositional basin and the nature of transporting processes that occur from the source region to the depositional basin (Dickinson and Suczek, 1979). The geochemical composition of clastic rocks is a function of provenance, weathering, transportation and diagenesis (Mustafa, R. K., and Tobia, 2020). Condie et al. (1992) attempted to decipher the provenance characteristics using geochemical attributes of sandstones. The tectonic environment and type of provenance also can be interpreted from the major element geochemistry of a clastic sediments (Armstrong-Altrin 2015; Migani et al. 2015; Odoma et al. 2015; Zaid 2016, Kafy and Tobia, 2022). Accordingly, bivariate plot of Na_2O against K_2O after Crook (1974) suggests the derivation of STTS sandstones from a quartz rich

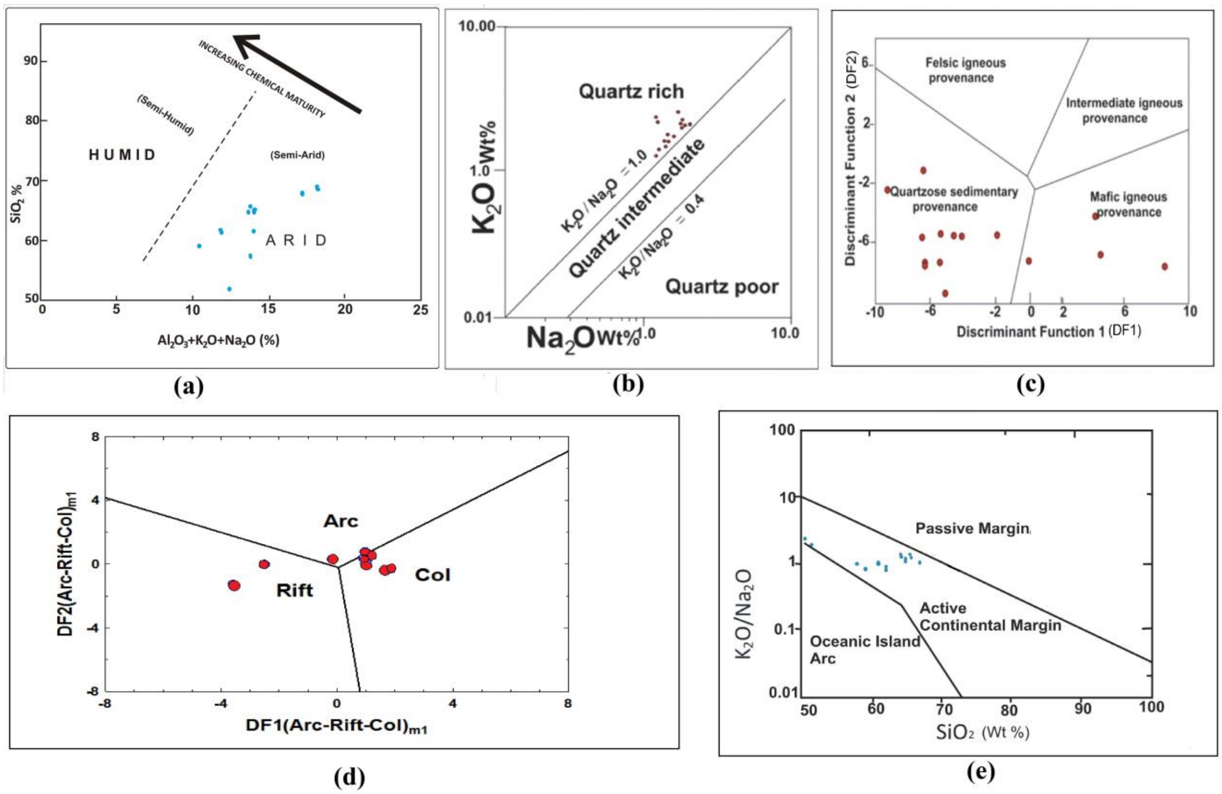

Fig 7(a): The bivariate plot of $Al_2O_3+K_2O+Na_2O$ against SiO_2 (Suttner and Dutta, 1986) suggesting an arid climatic condition forthe STTS sandstones, **(b):** Bivariate plot of Na_2O against K_2O after Crook (1974) suggests derivation of sediments from a quartz rich source, **(c):** Bivariate plot after Roser and Korsch (1988), **(d):** High-silica multidimensional diagram for the classification of tectonic settings (after Verma and Armstrong-Altrin, 2013), **(e):** Bivariate plot of K_2O/Na_2O vs. SiO_2 (Roser and Korsch, 1986) suggests an active continental margin setting for the STTS sandstones.

source (Fig. 7 b). In order to discriminate provenance, Roser and Korsch (1988) diagram has been used (Fig. 7 c). This diagram was constructed based on two discriminant functions namely DF1 and DF2, where DF1 = (-1.773^*TiO_2) + ($0.607^*Al_2O_3$) + ($0.760^*Fe_2O_3$) + (-1.500^*MgO) + (0.616^*CaO) + (0.509^*Na_2O) + (-1.224^*K_2O) + ($-$ 9.090) and DF2 = (0.445^*TiO_2) + ($0.070^*Al_2O_3$) + ($-$ $0.250^*Fe_2O_3$) + (-1.142^*MgO) + (0.438^*CaO) + (1.475^*Na_2O) + (1.426^*K_2O) + ($-$ 6.861). This diagram reveals mostly a quartzose sedimentary provenance for the studied sandstones.

The major elements geochemistry of sandstones can elucidate the tectonic setting of a sedimentary basin (Crook, 1974; Middleton, 1960). Siever (1979) and Roser and Korsch (1986) successfully related the proportion of detrital components to the bulk chemical composition of sedimentary suites that in turn reflect the tectonic setting of the basin. Bhatia (1983) developed a bivariate plot of Fe_2O_3+MgO versus K_2O/Na_2O wt. % to decipher the tectonic provenance of sandstones. Winchester and Max (1989) used the major elements as a geochemical tectonic indicator of immature sediments. However, in the present study, tectonic discrimination diagrams of Verma and Armstrong (2013) and Roser and Korsch (1986) are preferred to understand the tectonic provenance of the STTS sandstones. Since the adjusted concentrations of SiO_2 is higher than 62 wt.%, the high silica diagram of Verma and Armstrong (2013) is applied.

The multidimensional plot for high-silica $\{(SiO_2)_{adj} = > 63\% - \leq 95\%\}$ clastic sediments of Verma and Armstrong(2013) involves two discriminant functions, i.e., DF1 and DF2, where DF1(Arc–Rift–Col) m1 = (-0.263 x In$(TiO_2/SiO_2)_{adj}$)+ (0.604 x In$(Al_2O_3/SiO_2)_{adj}$) + (-1.725 x In$(Fe_2O_3{}^t/SiO_2)_{adj}$)+ (0.660 x In$(MnO/SiO_2)_{adj}$)+ (2.191 x In$(MgO/SiO_2)_{adj}$)

+(0.144 x In$(CaO/SiO_2)_{adj}$)+ (-1.304 x In$(Na_2O/SiO_2)_{adj}$) + (0.054 x In$(K_2O/SiO_2)_{adj}$)+ (-0.330 x In$(P_2O_5/SiO_2)_{adj}$) + 1.588 and DF2 $_{(Arc\text{-}Rift\text{-}Col)m1}$=(-1.196 x In$(TiO_2/SiO_2)_{adj}$)+ (1.064 x In$(Al_2O_3/SiO_2)_{adj}$) + 0.303 x In$(Fe_2O_3{}^t/SiO_2)_{adj}$)+ (0.436 x In$(MnO/SiO_2)_{adj}$)+ (0.838 x In$(MgO/SiO_2)_{adj}$) +(-0.407 x In$(CaO/SiO_2)_{adj}$)+ (1.021 x In$(Na_2O/SiO_2)_{adj}$) + (-1.706 x In$(K_2O/SiO_2)_{adj}$)+ (-0.126 x In$(P_2O_5/SiO_2)_{adj}$) – 1.068. The diagram reveals a collisional tectonic setting for the STTS sandstones (Fig. 7d). On the other hand, the K_2O/Na_2O vs. SiO_2 plot of Roser and Korsch (1986) suggested an active continental margin for the sandstones (Fig. 7 e).

DIAGENESIS

A series of diagenetic signatures involving mineralogical and textural attributes are observed in STTS sequence of the study area. These diagenetic signatures are grouped into early, intermediate and late stages (deep burial diagenesis and incipient metamorphism after Borak and Friedman, 1981). Precipitation and deposition of cement (silica, calcium carbonate and iron) is one of the processes of early diagenetic changes (Fig. 8 a). Replacement of silica cement (quartz overgrowth) by the carbonate cement was followed by iron - oxide precipitation depicting a typical order of cementation (Burley et al., 1985). The sedimentary sequences of the study area possess an eogenetic assemblage of authigenic carbonate, chlorite, glauconite, feldspar and quartz (Fig. 8 b and 8c). These authigenic growths are commonly seen on quartz and feldspars (Fig. 8 c). Sporadic occurrence of 'quartz islands' depict near complete replacement of quartz by matrix (Fig. 8 d). Presence of pseudo - matrix signifies post depositional degradation of feldspars (Fig. 8 d). On the other hand, presence of euhedral feldspars points either towards authigenic growth during deep burial phase or volcanic derivation (Fig. 8 d).

Process of albitization is a common diagenetic phenomenon observed in STTS sandstones. It occurs along the plane of weakness through hydrous reaction in which An-rich plagioclase is albitized first and followed by An-poor plagioclase (Ramseyer et al., 1992). Untwinned or slightly twinned cloudy feldspars (Fig. 8 d) in STTS sandstones bear small bleb like features that extinct differently than the grain. Such feldspar grains have been attributed to albitization process (Pittman, 1988). In addition, plagioclase grains showing discontinuous twin lamellae related to partial dissolution followed by authigenic albite infilling (Gold, 1987) resembling perthite texture. Presence of unaltered fresh plagioclase and albitized plagioclase in STTS is an indicator of albitization process. Nucleation of authigenic feldspar crystals on the surface of detrital feldspars and the recrystallization of detrital plagioclase feldspars could be the reason for albitization (Michalik, 1998). Dissolution and

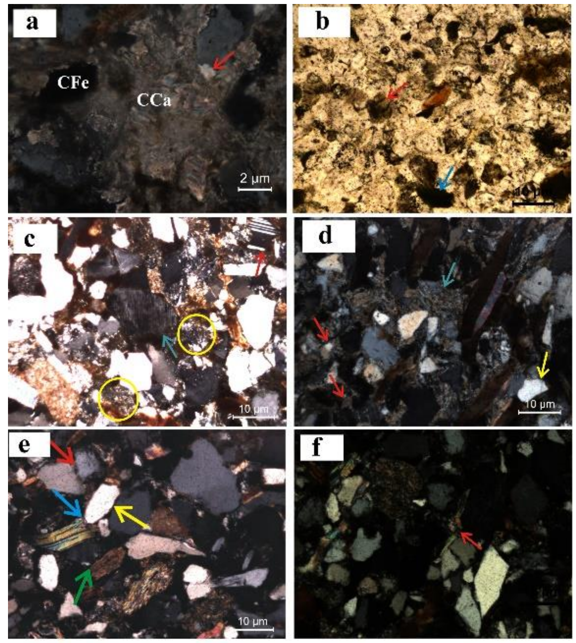

Fig 8 (a): Thin-section photograph showing typical order of cementation i.e. replacement of silica cement (red arrow) by the carbonate cement (CCa) which was followed by iron - oxide precipitation (CFe), (b): Thin-section photograph showing authigenic growth of glauconite (red arrow) and chlorite (blue arrow) as cement types, (c): Thin-section photograph showing growth of neo-quartz (yellow circle marked), authigenic growth of albite (red arrow), perthitic texture due to albitization (blue arrow), (d): Thin-section photograph showing formation of quartz by thenear complete replacement of detrital quartz by matrix (red arrow), pseudomatrix (blue arrow), fracture in quartz (yellow arrow), (e): Thin-section photograph showing different grain contacts: sutured contact (red arrow), concavo-convex contact (blue arrow), long contact (yellow arrow) and point contact (green arrow), (f): Kink bending and warping of mica around the detrital quartz grain

replacement of feldspars are the processes of formation of authigenic chlorite and glauconite which observed in some of the samples belonging to the lower part of the stratigraphic sequence. The authigenesis of chlorite could be the source of Fe cement.

Presence of calcareous cement and carbonate rock fragments in STTS sandstones indicates a depositional setting above the Carbonate Compensation Depth (CCD).

Devitrification of the volcanic glasses is considered to be one of the sources of authigenic quartz. Different phases of dissolution may have provided pore-waters with necessary components, which were essential for the authigenic growth of silica and carbonate phases (Merino, 1975 and Surdam & Boles, 1979). In the initial stage of burial, the diagenesis of detrital grains results changes in pore-water chemistry and the reaction of amorphous material and less stable detritus (Curtis, 1978).

The grain-to-grain boundaries of STTS sandstones (Fig. 8 e) show different stages of diagenesis. The concavo-convex and sutured grain-to-grain boundaries are the result of intermediate burial diagenesis. In the intermediate stage of diagenesis the grain-to-grain interlocks are formed by the dissolution of silica at the point of grain contact. Taylor (1950) suggested that the point contacts of grains are the result of two operating processes – (i) solid flow and solution and (ii) redeposition (interstitial transport of dissolved material). The compound grains are the result of increasing intensity of diagenesis that leads to the imposition of self-boundaries between two adjacent grains in close optical orientation (Dapples, 1979). The straight-line grain boundaries are the result of mobility of constituent chemical components. Under the continuous process of dip burial diagenetic evolution, the three-dimensional network of these straight-line boundaries results in the formation of the triple-junctions (Ahmad et al., 2006). Features like fracturing of detrital quartz (Fig. 8 d), crushing and squashing of detrital grains, wrappings of mica flakes around quartz grains (Fig. 8 f), pressure solutions effect and matrix are some indicator of increasing depth of burial (Burley et al., 1985). In addition, other signatures of deep burial diagenesis in the sediments of the study area include recrystallization / reconstitution of matrix and kink bending in mica (Fig. 8 f). Devitrification of volcanic glass leading to development of chert like microcrystalline aggregates, and alteration of volcanic glass into silica and clay minerals further indicate that the diagenetic processes possibly operated in a sealed environment (Pettijohn et al., 1987).

CONCLUSION

The STTS sandstones are very fine to medium- grained, sub- angular to angular, moderately to moderately well sorted. Dominating framework grains of these sandstones are quartz, feldspar, rock-fragments and micas. Different types of quartz that were found in STTS sandstones are polycrystalline undulatory, monocrystalline, recrystallized metamorphic and detrital quartz. The STTS sandstones are dominantly of arkose and arkosic wacke types.

The mineralogical composition of sandstones reveals that their source being a mixed provenance including plutonic basement, granitic intrusive, sedimentary and metasedimentary rocks. Further this inference is supported by the different provenance discriminating plots based on major elemental data.

Tectonic provenance discriminating diagrams (Qt-F-Lt and Qm-F-Lt) depict transitional continental, basement upliftment, dissected arc, and recycled orogen provenance. The tectonic discriminating plots using major elemental data reveals an active continental margin setting for the sandstones. A complex metamorphic basement and granitic intrusive sources, and an uplifted terrain like Mishimi Hills of Southern Himalaya and also Naga-Ophiolite Belt, Indo-Burma Range and prior to the Miocene sedimentary rocks of the region are considered as the most probable source rocks for STTS sandstones.

Diagenetic signatures observed in STTS belong to three different stages of diagenesis i.e. early, intermediate and late stages. Different types of grain boundaries suggest the early cementation and less compaction of the sandstone. The cementation process of the sandstone appears to be initiated by Fe cementation followed by silica cement and in some of the samples it is further followed by the calcite crystallization.

Precipitation and deposition of silica, epitaxial growth of mica around detrital quartz grains, near complete replacement of quartz by matrix and degradation of feldspars are some of the indications of early diagenetic changes of the STTS sandstone. Presence of euhedral authigenic albite represents albitization process that occurs during the burial diagenesis or intermediate stage of diagenesis. Kink bending of mica, warping of mica around quartz grains, crushing and squashing of detrital grains are indicative of deep burial diagenesis of sandstones.

ACKNOWLEDGEMENTS:

We are highly thankful to the University Grant Commission (UGC) for financial support to carry out this work. We are also thankful to the Department of USIC, Department of Geological Sciences, Gauhati University and Department of Geology, and IIT Roorkee for providing us the laboratory facility of XRF and thin section preparation. We are also thankful of Department of

Geology, Nagaland. We extend our heartfelt gratitude to the Editor of the Journal Indian Association of Sedimentologists, Dr. Amstrong-Altrin and the two reviewers of this manuscript, their suggestions and guidance improved the quality of our presentation.

DECLARATION OF CONFLICTING INTERESTS: The authors declare that they have no competing interests.

REFERENCES

Ahmad, A.H.M. and Bhat, G.M. (2006). Petrofacies Provenance and diagenesis of the dhosa sandstone member (Chari Formation) at Ler, Kachch sub – basin, Western India. Journal of Asian Earth Sciences, volume 27, pp. 857 – 872.

Armstrong-Altrin J. S. (2015). Evaluation of two multidimensional discrimination diagrams from beach and deep-sea sediments from the Gulf of Mexico and their application to Precambrian clastic sedimentary rocks; International Geological Review, volume 57, pp. 1444–1459.

Armstrong-Altrin, J.S., Nagarajan, R., Madhavaraju, J., Rosales-Hoz, L., Lee, Y.I., Balaram, V., Cruz-Martinez, A., Avila-Ramirez, G. (2013). Geochemistry of the Jurassic and upper Cretaceous shales from the Molango Region, Hidalgo, eastern Mexico: Implications for source-area weathering, provenance, and tectonic setting. Comptes Rendus Geoscience, volume 345 (4), pp. 185-202.

Armstrong-Altrin, J.S., Madhavaraju, J., Vega-Bautista, F., Ramos-Vázquez, M.A., Pérez-Alvarado, B.Y., Kasper-Zubillaga, J.J. and Ekoa Bessa, A.Z. (2021). Mineralogy and geochemistry of Tecolutla and Coatzacoalcos beach sediments, SW Gulf of Mexico. Applied Geochemistry. 134, 105103.

Armstrong-Altrin, J.S., Ramos-Vázquez, M.A., Madhavaraju, J., Marca-Castillo, M.E., Machain-Castillo, M.L., Márquez-Garcia, A.Z. (2022). Geochemistry of marine sediments adjacent to the Los Tuxtlas Volcanic Complex, Gulf of Mexico: Constraints on weathering and provenance. Applied Geochemistry, 141, no. 105321.

Basu, A. (2020). Chemical weathering, first cycle quartz sand, and its bearing on quartz arenite. Journal Indian Association of Sedimentologists, volume 37(2), pp. 3-14.

Bela, V.A., Bessa, A.Z.E., Armstrong-Altrin, J.S., Kamani, F.A., Nya, E.D.B., Ngueutchoua, G. (2023). Provenance of clastic sediments: A case study from Cameroon, Central Africa. Solid Earth Sciences 8(2), pp. 105-122.

Bhatia, M.R. (1983). Plate tectonics and geochemical composition of sandstones. Journal Geology, volume 91 (4), pp. 611–626.

Borak, B. and Friedman, G.M. (1981). Textures of sandstones and carbonate rocks in the world's deepest wells (in excess of 30,000ft. or 9.1km): Anduako Basin, Oklahoma. Journal of Sedimentary Geology, volume 29, pp. 133-151.

Borgohain, P. and Pandey, N. (2016). Lithofacies analysis of Surma-Tipam Transitional Sequences inparts of Naga Hills, Northeast India: A Case Study. Journal of Applied Geology and Geophysics, volume 5 (V), pp. 30 – 36.

Burley, S.D., Kantorowicz, J.D., Waugh, B. (1985). Clastic diagenesis. In: Brenchley, P.J. and Williams, B.P.J. (eds.). Sedimentology, Recent developments and Applied Aspects, Blackwell, Oxford, volume 18, pp. 189-226.

Condie, K.C., Boryta, M.D., Liu, J., Quian, X. (1992). The origin of khondalites: geochemical evidence from the Archean to Early Proterozoic granulite belt in the North China craton. Precambrian Research, volume 59, pp. 207–223.

Crook, K. A. W. (1974). Lithogenesis and geotectonics: The significance of compositional variation in flysch arenites (greywackes), In: R. H. Dott and R. H. Shavar (Eds.), Modern and ancient geosynclinals sedimentation, Soc. Econ. Palaeont. Min. Spl. Publ., volume 19, pp. 304 – 310.

Curtis, C.D. (1978). Possible links between sandstone diagenesis and depth-related geochemical reactions occurring in enclosing mudstones. Journal of Geological Society of London, volume 135, pp. 107–117.

Dapples, E.C. (1979). In: Larsen, G., Chinlinger, G.V. (Eds.), Diagenesis in Sandstones.Developments in Sedimentology 25A. Elsevier, The Netherlands, pp. 31–97.

Dickinson,W.R. and Suczek, C.A. (1979). Plate tectonics and sandstone compositions. American Association of Petroleum Geologists, volume 63, pp. 2164 – 2182.

Dickinson, W.R., Beard, L.S., Brakenridge, G.R., Erjave, J.L., Ferguson, R.C., Inman, K.F., Knepp., R.A., Lindberg, F.A., and Ryberg, P.P. (1983). Provenance of North American Phanerozoic sandstones in relation to tectonic setting. Geological Society American Bulletin, volume 94, pp. 222-235.

Dott, R.H. (1964). Wacke, Greywacke and Matrix—What Approach to Immature Sandstone Classification? Journal of Sedimentary Petrology, volume 34, pp. 625-632.

Ekoa Bessa, A. Z., Paul-Désiré, N., Fuh, G.C., Armstrong-Altrin, J.S., Betsi, T.B., 2021. Mineralogy and geochemistry of the Ossa lake Complex sediments, Southern Cameroon: Implications for paleoweathering and provenance. Arabian Journal of Geosciences 14, Article no. 322

Evans, P. (1964). The tectonic framework of Assam. Journal of Geological Society of India, volume 5, pp. 80 - 96.

Folk, R.L. (1980). Petrology of Sedimentary Rocks, Austin, TX, Hemphill Press, Second Edition, pp. 20 – 25.

Ghose, N.C., Agrawal, O.P. and Srivastava, S.C., 1987. Metamorphism of the ophiolite belt of Nagaland, NE India. Proceedings of National Seminar of Tertiary Orogeny, pp. 189-213

Gold, P.B. (1987). Textures and geochemistry of authigenic albite from Miocene sandstones, Lousiana Gulf Coast. Journal of Sedimentary Petrology, volume 57, pp. 353-362.

Kafy, R.H., Tobia, F.H. (2022). Geochemical signatures of provenance, chemical weathering, and tectonic setting in the Greater Zab River sediments, Iraqi Kurdistan Region. Arabian Journal of Geosciences, 15:1556**.**

Madhavaraju, J., Armstrong-Altrin, J.S., Pillai, R.B., Pi-Puig, T. (2021). Geochemistry of sands from the Huatabampo and Altata beaches. Gulf of California, Mexico. Geological Journal, 56, 2398-2417.

Merino, E. (1975). Diagenesis in Tertiary sandstones from Kettleman North Dome, California I. Diagenetic mineralogy. Journal of Sedimentary Petrology, volume 45, pp. 320 – 336.

Michalik, M. (1998). Diagenetic albite in Rotliegendes sandstones from the Intrasudetic Basin (Poland). Annales Societatis Ceologorwn Poloniae, volumen 68, pp. 85-93.

Middleton, G.V. (1960). Chemical composition of sandstones, Geological Society of America Bulletin, volume 71, pp. 1011-1026.

Middleton, G.V. (Ed), (2003). Encyclopedia of Sediments and Sedimentary rocks. Springer, pp. xxx–821.

Migani F., Borghesi F. and Dinelli E. (2015). Geochemical characterization of surface sediments from the northern Adriatic wetlands around the Po river delta, Part 1: Bulk composition and relation to local background; Journal of Geochemical Exploration, volume. 156, pp. 72–88.

Mustafa, R. K., and Tobia, F.H. (2020). Geochemical application in unraveling paleoweathering, provenance and environmental setting of the shale from Chia Gara Formation, Kurdistan Region, Iraq. Iraqi Geological Journal, volume. 53 (1A), pp. 90-116.

Odoma A. N., Obaje N. G., Omado J. I., Idakwo S. O. and Erbacher J. (2015). Mineralogical, chemical composition and distribution of rare earth elements in clay-rich sediments from southeastern Nigeria; Journal African Earth Science, volume.102, pp. 50–60.

Pettijohn, F.J., Potter, P.E. and Siever, R. (1987). Sand and Sandstone. Springer, New York, pp. 553 – 617.

Pittman, E. D. (1988). Diagenesis of Terry sandstone (Upper Cretaceous), Spindle Field, Colorado. Journal of Sedimentary Petrology, volume. 58, pp. 785–800.

Ramos-Vázquez, M., Armstrong-Altrin, J.S., Rosales-Hoz, L., Machain-Castillo, M.L., and Carranza-Edwards, A. (2017). Geochemistry of deep-sea sediments in two cores retrieved at the mouth of the Coatzacoalcos river delta, Western Gulf of Mexico, Mexico. Arabian Journal of Geosciences, volume 10 (6), pp. 148.

Ramseyer, K., Boles, J. R., and Lichtner, P. C. (1992). Mechanisms of Plagioclase Albitization: Journal of Sedimentary Petrology, volume 62, pp. 349–356.

Roser, B.P., Korsch, R.J. (1986). Determination of tectonic setting of sandstone– mudstone suites using SiO2 content and K2O/Na2O ratio. Journal Geology, volume 94, pp. 635–650.

Roser, B.P., Korsch, R.J. (1988). Provenance signatures of sandstone – mudstone suites determined using discriminant function analysis of major-element data. Chemical Geology, volume 67, pp. 119–139.

Seiver, R. (1979). Plate tectonic controls on diagenesis. Journal Geology, volume 87, pp. 127-155.

Sengupta, S.M. (1994). Introduction to sedimentology. Oxford & IBH Publishing Co., pp. 314.

Singh, Y., Haq, A.U., Pandita, S.K., Lone, B.A., Singh, A. (2023). Geoengineering properties of the Sandstones of Upper Murree Formation, Jammu and Kashmir: A case study. Journal Indian Association of Sedimentologists, 40(1), pp. 73-80.

Surdam, R.C. and Boles, J.R. (1979). Diagenesis of volcanic sandstones, In: Scholle, P.A. and Schluger, P.R. (eds.), Aspects of diagenesis: SEPM. Spec. Publ., volume 26, pp. 227-242.

Suttner, L.J., Dutta, P.K. (1986). Alluvial sandstone composition and paleoclimate, framework mineralogy. Journal of Sedimentary Petrology, volume 56, pp. 329-345.

Tawfik, H.A., Salah, M.K., Maejima, W., Armstrong-Altrin, J.S., Abdel-Hameed, A-M.T., Ghandour M.M.E. (2018). Petrography and geochemistry of the Lower Miocene Moghra sandstones, Qattara Depression, north Western Desert, Egypt. Geological Journal, volume 53, pp. 1938-1953.

Taylor, J.M. (1950). Pore-space reduction in sandstones. Bulletin of the American Association Petroleum Geologists 34, pp. 701–716.

Verma S. P. and Armstrong-Altrin J. S. (2013). New multidimensional diagrams for tectonic discrimination of siliciclastic sediments and their application to Precambrian basins. Chemical Geology, 355, pp. 117–180.

Verma, S.P., Armstrong-Altrin, J.S. (2016). Geochemical discrimination of siliciclastic sediments from active and passive margin settings. Sedimentary Geology, volume. 332, pp. 1-12.

Verma, S.P., Díaz-González, L., Armstrong-Altrin, J.S. (2016). Application of a new computer program for tectonic discrimination of Cambrian to Holocene clastic sediments. Earth Science Informatics 9, pp. 151-165.

Winchester, J. A. & Max, M. D. (1989). Tectonic setting discrimination in clastic sequences: an example from the Late Proterozoic Erris Group, NW Ireland. Precambrian Research, volume 45, pp. 19-201.

Zaid S. M. (2016). Geochemistry of shales from the Upper Miocene Samh Formation, north Marsa Alam, Red Sea, Egypt: Implications for source area weathering, provenance, and tectonic setting; Arabian Journal of Geoscience, volume 9, pp. 593.

JOURNAL INDIAN ASSOCIATION OF SEDIMENTOLOGISTS ISSN NO 2582 – 2020
Vol. 40, Issue II, 2023, pp. 14-26
DOI: https://doi.org/10.51710/jias.v40iII.309

Petrography and geochemistry of the Upper Cretaceous Gryphaea Limestones, Kallankurichi Formation, Ariyalur Group, Trichinopoly, Southern India: Implication for palaeoenvironment

M. Senthiappan[1, 2*], V. Stephen Pitchaimani[1], A.V. Udayanapillai[3], Perumal Velmayil[3], Bangarupriyanga Sundaram[3], G. Ramalingam[3], and John S. Armstrong-Altrin[4, 5]

[1] Department of Geology, V.O. Chidambaram College, Thoothukudi, Tamil Nadu, India
[2] Research Scholar, Affiliated to Manonmaniam Sundaranar University, Tirunelveli, Tamil Nadu
[3] Department of Geology & Quantum Material Research Laboratory, Department of Nano-Science & Technology, Alagappa University, Karaikudi, Tamil Nadu, India
[4] Unidad de Procesos Oceánicos y Costeros, Universidad Nacional Autónoma de México, Instituto de Ciencias del Mar y Limnología, Ciudad Universitaria, Mexico City, Mexico
[5] Department of Marine Sciences, Bharathidasan University, Tiruchirappalli, 620024, Tamil Nadu, India

ABSTRACT

Sub-surface Kallankurichi gryphaea limestone formation is observed between Archaean and Quaternary outcrops. Petrographic observation reveals that mega fossils are absent and it contains abundant skeletal fragments of pelecypods, gastropods, foraminifera, bryozoa, and symbiotic algae. X-ray diffraction (XRD) analyses reveal the mineralogical components of both carbonate and clay minerals. Carbonate minerals include calcite, siderite, witherite, malachite, smithsonite, and rhodochrosite. Clay minerals detected are kaolin, montmorillonite, and palygorskite. Major element composition represents predominance of CaO, SiO_2, Al_2O_3, and Fe_2O_3 oxides, while MgO, MnO, Na_2O, K_2O, TiO_2, and P_2O_5 oxides are depleted. Statistical analyses of correlation coefficient, principal component analysis, and cluster analysis represent the geochemical affinities and aerial distribution similarities among major elements. Palaeoclimate inferred through biotic proxies, major element geochemistry, and clay minerals represents arid and semi-arid climate.

KEYWORD: Kallankuruchi, Petrography, Major elements, XRD, Statistical analysis, Palaeoclimate,

INTRODUCTION

Marine transgressions of the Indo-Pacific Sea during the Upper Cretaceous period have occupied the continental area centered on Ariyalur town, Tamil Nadu, India. These transgressions and regressions have caused for the formation of Uttatur, Trichinopoly, Ariyalur, and Niniyur groups of various sedimentary rocks and the preservation of many marine invertebrate groups of fossils (Krishnan, 1982). Hence, this area has been reported as a Cretaceous fossil heritage site with a field museum or Cretaceous Park of Tamil Nadu (Udayanapillai et al., 2020). Numerous authors have focused their research on the Upper Cretaceous Formation of Trichinopoly in various aspects (Blanford, 1862; Krishnan, 1982; Ramasamy et al, 1991; Ayyasamy et al, 1992; Banerji, 1996; Govindan et al, 1996; Madhavaraju etal,1999, 2021; Sundaram Reddy A, N. et al,2013; Goswamy et al, 2013; Babu, 2017; Nagendra and Nallappareddy, 2017; Nagendra et al., 2011,2018; Ramkumar et al, 2018; Udayananpillai et al, 2020). Due to the widespread occurrence of Cretaceous limestone outcrops, many cement companies, like Dalmia, Chettinadu, Ramco, India cement, Gracim, Ultratech, Tancem, etc., have established their mining activities in and around the Ariyalur area.

Kallankurichi is one of the important limestone formations in the Ariyalur stage or group. It occurs as a S-type outcrop that extends from Periakuruchi village in the north and Pudupalayam village in the south. The northern band of the Kallankurichi limestone formation occurs as a surface outcrop, whereas the southern band occurs as a subsurface outcrop. A faulted structure can be observed in the 'S' type band of Kallankurichi limestone formation from the Pudupalayam mine area. There are several limestone mines in the Kallankurichi formation.

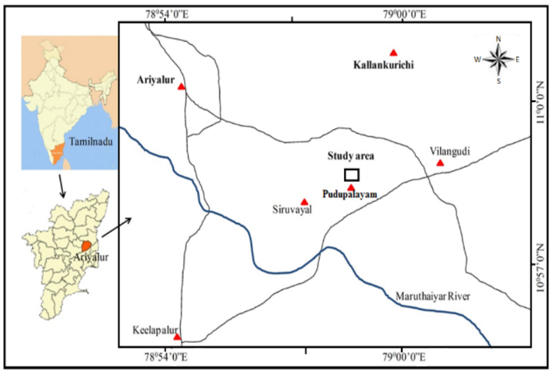

Figure 1. Location map of the study area

But still now no research has been carried out on the gryphaea limestone bed of the Pudupalayam Chettinadu mine, located in the terminal part of the Kallankurichi 'S' band limestone outcrop. In order to fulfil this gap, an attempt has been made to study the field observation, petrological observation, distribution of major elements, depositional environment and palaeoclimate

STUDY AREA

The area under investigation Pudupalayam Chettinadu limestone mine is located at 7 km from Ariyalur town, near the Ariyalur-Tiruchirappalli state highway. Proposed mine area lies at the latitude 11.10072° N and longitude 79.15059° E. The area has been well connected with Tanjore, Trichy, and Ariyalur town by state highway road networks. Physiography of the area is almost flat with an elevation range of 62 m above M.S.L. Coleroon and Maruthaiyar rivers are running from the southern side to the study area (**Fig. 1)**

GEOLOGICAL SETTING

The geological outcrop map of Ariyalur district (Nagendra et al., 2011) is shown in (**Fig. 2)**.

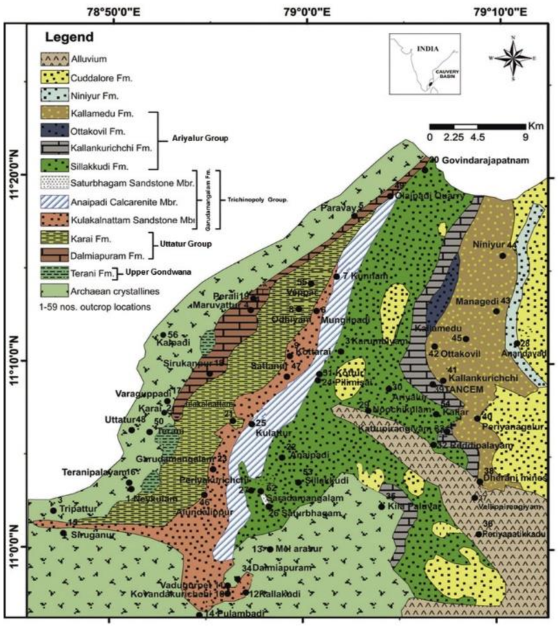

Figure 2. The Geological map of the Ariyalur district (modified after Nagendra et al., 2011).

Post-Archaean/Archaean hard basement rocks consist of granite, granitic gneiss, and charnockite. The basement rocks are unconformably overlain either by the Upper Gondwana Formation or directly rest on Upper Cretaceous group of rocks which consist of Uttatur, Trichinopoly, Ariyalur, and Niniyur stages (Krishnan, 1982). Later, over all established entire sequential stratigraphy of Upper Cretaceous rocks of Trichinopoly have been published (Sundaram et al., 2001; Nagendra et al., 2002; Udayanapillai et al., 2020) (**Table 1**). Ariyalur stage consists of several formations. The lowermost formation is Sillakudi sandstone. It is overlain by the Kallankurichi limestone formation with an unconformity and is followed by

Table 1. Litho-stratigraphy of the Ariyalur Group (Sastry et al., 1972)

Era	Stage	Formation	Lithology
Tertiary		Cuddalore	Red Sandstone
Upper Cretaceous	Niniyur	Nanniyur	Arenaceous Limestone
		Athanakuruchi	Limestone
	Ariyalur	Sendurai	Arenaceous Limestone
		Ottakovil	Arenaceous Limestone
		Kallamedu	Sandstone
		Kallankurichi	Arenaceous Limestone
			Gryphaea Limestone
			Arenaceous Limestone
			Ferruginous Gryphaea Limestone
			Conglomerate
		Sillakudi	Sandstone
	Trichinopoly	Kunnam	Shale
		Paravai	Arenaceous limestone
		Sathanur	Shale
		Kollakanattham	Clay, Arenaceous Sandstone
		Anaipadi	Red Sandstone
		Garudamangalam	Argillaceous limestone
	Uttatur	Maruvathur	Clay and shale
		Karai	Shale
		Dalmiapuram formation	Marl bedded argillaceous l.stone
			Bedded limestone
			Coralline algal limestone
		Shale	Calcareous Grey Shale
Conglomerate_unconformity			
Upper Gondwana		Therani	Variegated clay
			Purple sandstone
Conglomerate-Unconformity			
Archean		Charnockite and granitic gneiss	

Figure 3. Field photograph of Pudupalayam mine section

Kallamedu, Ottakovil, and Sendurai calcareous sandstone formations (**Table 2**). Kallankurichi limestone outcrop is bordered by the formation of the Sillakudi sandstone outcrop in the west, Kallamedu, Ottakovil and Sendurai outcrops in the eastern side, and Archaean outcrop in the south. The study area Pudupalayam Chettinadu mine is located at the southern terminal part of the ‘S’ band’ type Kallankurichi limestone outcrop.

METHODOLOGY

Intensive fieldwork was undertaken in January 2020 to investigate the nature of the Pudupalayam Chettinadu mines. Nature of the Gryphaea limestone outcrop and its other lithological associations were carefully studied with available literatures concerning the geology and geochemistry of gryphaea limestone. Gryphaea limestone is the typical characteristic bed in the Kallankurichi formation (Ramasamy et al., 2012; Nagendra et al., 2018; Ramkumar et al., 2020). Ten gryphaea limestone samples were collected at the interval of 1 foot between the occurrence of limestone profile (5-10 m) in the vertical mine profile section. Thickness of beds and intervals were measured. Then, the collected samples were properly packed and labelled with GPS co-ordination. While collecting samples, megascopic characters of limestone samples were also observed in the field. Then limestones thin sections were prepared at Suchitra polishing unit, in Chennai. In addition, limestone samples were analysed for major oxides through an XRF instrument (X-Ray Fluorescence spectroscopy) at the laboratory of the National Centre for Earth Science Studies (NCESS), Thiruvananthapuram. Three representative samples were selected for clay mineral analysis by an X-ray Diffraction (XRD) method at University Scientific Instrumentation Centre (USIC), Department of Physics, Alagappa University, Karaikudi. Photomicrographs of thin sections were taken from the laboratory at Department of Geology, University of Madras, Chennai.

FIELD OBSERVATION

Entire mine section shows Archaean, Upper Cretaceous, Sub-Recent and Recent outcrops from the bottom to the top of the mine. Lower-most Archaean granitic gneiss outcrop can be observed at the depth of 30 m in the mine area. Kallankurichi limestone of Ariyalur stage un-conformably rest on same stage Cretaceous bed of the Sillakudi sandstone formation which occurs at a depth from 11m to 26 m. A conglomerate bed of 0.5m thickness separates the Sillakudi sandstone formation and Kallankurichi limestone formation (Table2). Gryphaea limestone bed occurs between 4.5 metres and 9.5 metres depth with a thickness of 5 m. Gryphaea limestone bed is followed by marl, chert, calcrete and black soil of Quaternary age.

Gryphaea limestone collected from the Pudupalayam mine show grey, pale yellow and ferruginous colour without mega fossils. It is highly compacted and indurated. Compaction and indurations are mainly made by $CaCO_3$ mineral grains with a very few detrital grains. Entire litho-profile section of the Pudupalayam Chettinadu mine section is shown in the field photographs and table **(Fig. 3; Table 2).**

Table 2. Stratigraphy of the Ariyalur stage at Pudupalayam Chettinadu mine

Age	Stage	Formation	Lithology	Depth from Top in metres	Thickness in metres
Recent			Top soil/ Red soil/ Black soil	0 to 0.5	0.5
Holocene – Pleistocene (or) Sub - Recent			Calcrete	0.5 to 1.5	1
Upper Cretaceous	Ariyalur	Kallankurichi	Arenaceous Limestone	1.5 to 4.5	3
			Gryphaea Limestone	4.5 to 9.5	5 (study area)
			Arenaceous Limestone	9.5 to 12.5	3
			Ferruginous Gryphaea Limestone	12.5 to 22.5	10
			Conglomerate - Unconformity	22.5 to 23	0.5
		Sillakudi	Sillakudi sandstone formation	Below 23	8

PETROLOGICAL OBSERVATION

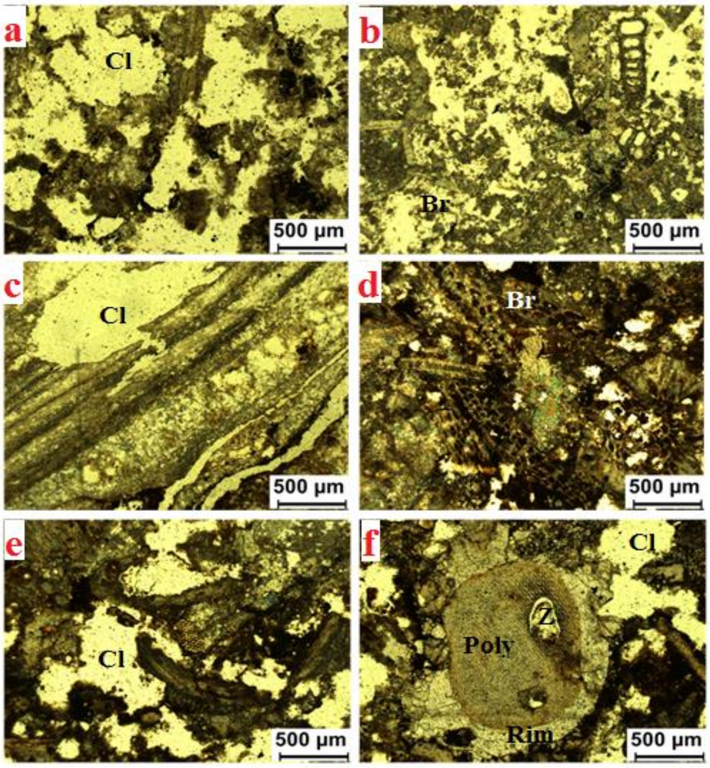

Figure 4 (a-f). Photomicrographs of gryphaea limestone of pudupalayam Chettinadu mine. a) Photomicrograph shows equal preservation of Bryozoa and more white lime mud clast in the ferruginous micritic calcite matrix. b) Photomicrograph shows preservation of uniserial chambered foraminifera Nodosaria with algal mats, gryphaea group shell fragments and also possesses more white lime mud clast preservation in the ferruginous micritic calcite matrix. c) Photomicrograph shows parallel algal mats preservation with micritic calcite and lime mud clast. d) Photomicrograph shows full of bryozoan colony within ferruginous micritic calcite matrix. e) Photomicrograph shows pelecypod shell fragments, Polyphora-Bryozoa and lime mud clast preservation in the micritic calcite matrix. f) Photomicrograph shows a large Polyphora-Bryozoa with zooecia rimmed by micritic calcite and lime mud clast in the ferruginous micritic calcite matrix.

Petrographically Maastrichtian limestones were classified as packstone/grainstone facies or as wackestone and mudstone facies (Nagendra et al., 2011). Classification of limestone has been proposed by Dunham (1962) and Folk (1968). Dunham has classified the limestone as mudstone, wackestone, and packstone, based on the fabric of the rock. Folk (1968) has classified the limestone as autochthonous and allochthonous limestones, based on grain and cement types. A revised classification was proposed by Wright (1997), based on the diagenetic pattern. Gryphaea limestone beds of Pudupalayam is a mud based biogenic limestone, as per the classification of Wright (1997). Despite large mega-fossils are being absent in the limestone, it contains numerous desmodont gryphaea group shell fragments of pelecypods, gastropods, micro-faunal distribution of foraminifera, bryozoa and algal mats. These biogenic materials are preserved in the ferruginous or calcified micritic or micro-sparitic calcite matrix. Rich iron content in the biogenic limestone indicates shallow and high energy conditions of the sea (Nagendra et al., 2011). Such similar condition may be existed in the study area. Shell fragments and algal mats have caused for the formation of ferruginous micritic calcite matrix, during diagenesis and lithification. The uniserial foraminifera Nodosaria with lime mud clast preservation was also observed in the ferruginous micritic calcite matrix. Some thin section photomicrograph shows parallel algal mats preservation with micritic calcite and lime mud clast. In general, carbonate microfacies of Pudupalayam gryphaea limestone indicates that these limestones were formed in a continental marginal platform. Such similar reports have already been reported in the other areas of the Kallankurichi formation (Nagendra et al., 2011). Photomicrographs of gryphaea limestone samples of the Pudupalayam mine are given in (**Fig. 4 a-f**).

X-RAY DIFFRACTION ANALYSIS

Numerous researchers have applied XRD technique for the identification of minerals in sediments and sedimentary rocks (Carrol 1970; Deer et al., 1979; Mitra 1989; Kile and Dennis, 2000; Jimenez-Espinosa and Jimenoz-Millan, 2003; Udayanapillai et al., 2015; Perumal and Udayanapillai, 2020; Armstrong-Altrin et al., 2021, 2022; Ramos-Vázquez et al., 2022; Udayanapillai et al., 2022). Based on high angle XRD mineral analysis (2 theta 0-80 degree), d spacing values and their relative intensities of powdered gryphaea limestone samples reveals the presence of

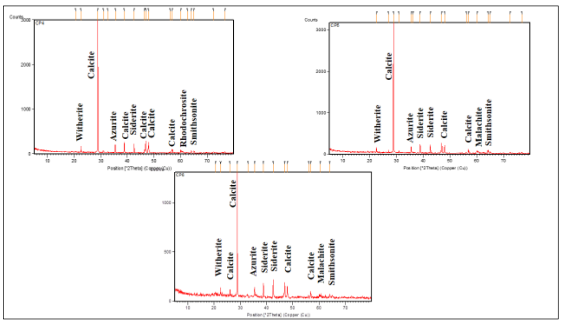

Figure 5a. XRD diffractogram pattern of the gryphaea limestone samples (all minerals) of Pudupalayam Chettinadu mine

minerals of calcite, siderite, witherite, malachite, smithsonite, azurite and rhodochrosite. Low angle XRD Clay mineralogy (2 theta 0-30 degree) analysis of powdered gryphaea limestone samples indicates the presence of clay minerals of kaolin, montmorillonite, and palygorskite. Mineralogy of gryphaea limestone with d spacing values and their intensities are given in **Figure 5 a-b** and **Table 3.**

Table 3. The clay and general mineralogy of Limestone samples of Chettinadu mine

S. no.	Minerals	D-Space values A°	Name of the mineral	Chemical Composition
1	Clay minerals	3.95	Kaolinite	$Al_4[Si_4O_{10}](OH)_3$
2		15.26	Montmorillonite	$Al_2[Si_4O_{10}](OH)_2.nH_2O$
3		3.42	Kaolinite	$Al_4[Si_4O_{10}](OH)_3$
4		4.31	Palygorskite	$Mg_3H_2Si_8O_{22}(H_2O).2H_2O$
5	Other minerals	3.09	Calcite	$CaCO_3$
6		2.53	Azurite	$Cu_3(CO_3)_2(OH)_2$
7		2.12	Siderite	$FeCO_3$
8		1.89	Calcite	$CaCO_3$
9		1.93	Calcite	$CaCO_3$
10		1.62	Calcite	$CaCO_3$
11		1.53	Rhodochrosite	$MnCO_3$
12		1.45	Smithsonite	$ZnCO_3$
13		1.43	Smithsonite	$ZnCO_3$
14		3.95	Witherite	$BaCO_3$
15		2.31	Siderite	$FeCO_3$
16		3.43	Calcite	$CaCO_3$
17		1.93	Calcite	$CaCO_3$
18		1.54	Malachite	$Cu_2CO_3(OH)_2$

GEOCHEMICAL OBSERVATION

Major element concentrations of gryphaea limestones from the Pudupalayam mine, shows a more or less similar distribution trend (**Table 4; Fig. 6**). Distribution of CaO, SiO_2, Al_2O_3, Fe_2O_3, and LOI shows higher concentration, which is above 1%, whereas other major oxides, viz. MgO,

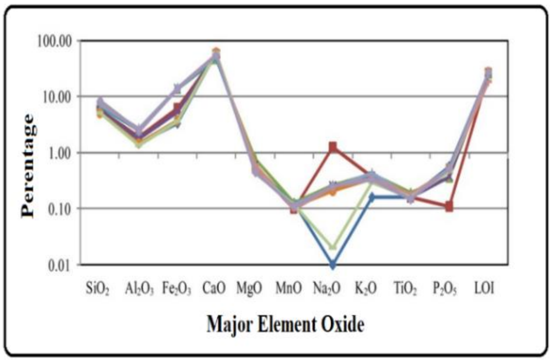

Figure 6. Comparison of Major elements distribution of Gryphaea Limestone samples of Chettinadu Pudupalayam mine

MnO, Na_2O, K_2O, TiO_2, and P_2O_5 are below 1%. Average distributions of major element concentrations of samples are taken into consideration for geochemical discussion, as they show similar distribution trend.

Average SiO_2 concentration of gryphaea limestone is 6.56, whereas the average concentration of Al_2O_3 is 2.05. Al_2O_3 concentration may generally be attributed to a good mixture of transported flux and limited SiO_2 may be due to less concentration of detrital unaltered quartz and feldspar contents (Ramasamy et al., 2007; Cox et al., 1995; Udayanapillai and Ganesamurthy, 2013; Ekoa Bessa et al., 2021a,b; Madhavaraju et al., 2021; Sopie et al., 2023). Gryphaea limestone represents less SiO_2/Al_2O_3 ratio (3.22), which indicates that the detrital concentration of quartz and feldspar is limited in the samples. Al_2O_3 is used as a proxy for clay content in limestone. K_2O/Al_2O_3 ratio of sediment can be used as an indicator of the original composition (Udayanapillai and Ganesamurthy, 2013; Anaya-Gregorio et al., 2018; Tawfik et al., 2018). K_2O/Al_2O_3 ratio of clay minerals and feldspar are different (0.00 to 0.3; 0.3 to 0.9) respectively (Cox et al., 1995;). Average K_2O/Al_2O_3 ratio in limestones is 0.16, which is close to the limit of the clay mineral range. It indicates that kaolinite,

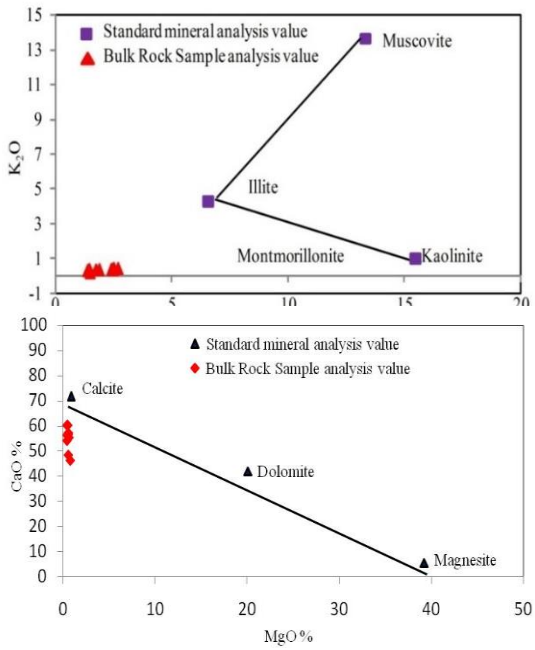

Figure 7(a). Bivariate plot K_2O vs Al_2O_3 in the gryphaea limestone samples (after Mc Queen 2006, modified with the standard analytical result of minerals analysis from Deer et al., 1978 and Udayanapillai et al., 2014), **(b).** Bivariate plot of CaO Vs MgO (after Queen, 2006, modified with the standard analytical result of minerals analysis from Deer et al., 1978 and Udayanapillai et al., 2014)

montmorillonite, and illite may be the dominant clay minerals in the limestone samples (**Fig. 7a**).

Average CaO contents shows 55.58%, whereas MgO content represents 0.54%. Lesser

Table 4: Data of major element concentrations (in wt. %) of Chettinadu Gryphaea limestones, Puthupalayam
LOI = Loss of Ignition

Major element	S-1	S-2	S-3	S-4	S-5	S-6	S-7	S-8	S-9	S-10	Average
SiO_2	5.13	5.76	8.4	5.6	6.7	5.12	7.3	8.2	5.15	8.3	6.56
Al_2O_3	1.5	1.89	2.51	1.76	2.46	1.48	2.7	2.5	1.39	2.4	2.05
Fe_2O_3	3.37	6.19	14.1	5.41	13.9	3.74	14.12	13.8	3.72	13.7	9.2
CaO	60.3	57.4	46.5	56.7	48.4	60.21	56.3	55.4	60.34	54.3	55.58
MgO	0.47	0.54	0.76	0.6	0.54	0.53	0.44	0.62	0.46	0.46	0.54
MnO	0.13	0.1	0.13	0.11	0.12	0.11	0.12	0.1	0.12	0.11	0.11
Na_2O	0.01	1.26	0.27	0.26	0.23	0.21	0.25	0.26	0.02	0.26	0.3
K_2O	0.16	0.37	0.42	0.38	0.36	0.35	0.43	0.35	0.3	0.34	0.34
TiO_2	0.16	0.16	0.2	0.16	0.17	0.16	0.17	0.18	0.16	0.15	0.16
P_2O_5	0.56	0.11	0.36	0.38	0.53	0.52	0.53	0.49	0.48	0.53	0.44
LOI	27.44	26.9	25.99	26.9	26.84	27.32	18.42	18.9	27.3	27.3	25.33

Table 5. Multiple correlation of major element concentrations

Oxides	SiO_2	Al_2O_3	Fe_2O_3	CaO	MgO	MnO	Na_2O	K_2O	TiO_2	P_2O_5	LOI
SiO_2	0.00										
Al_2O_3	0.90	0.00									
Fe_2O_3	0.93	0.98	0.00								
CaO	-0.71	-0.74	-0.78	0.00							
MgO	0.40	0.28	0.29	-0.63	0.00						
MnO	-0.04	-0.02	0.01	-0.26	0.03	0.00					
Na_2O	-0.01	0.09	-0.01	-0.04	0.13	-0.58	0.00				
K_2O	0.50	0.61	0.57	-0.52	0.41	-0.27	0.34	0.00			
TiO_2	0.55	0.53	0.53	-0.68	0.81	0.33	-0.07	0.42	0.00		
P_2O_5	0.09	0.07	0.16	0.08	-0.38	0.40	-0.89	-0.34	-0.11	0.00	
LOI	-0.50	-0.63	-0.55	0.07	-0.02	0.20	0.04	-0.39	-0.39	-0.19	0.00

concentration of MgO content indicates the absence of dolomite mineral content in the limestone samples. In general, CaO/MgO ratio in dolomite mineral 40:20 (Deer et al., 1978). Average CaO/MgO ratio in limestones of this study is 102.93. A higher value of the above ratio indicates that the samples are high-grade limestone and possess more percentage of calcite mineral than the other carbonate minerals **(Fig. 7b)**. Bulk rock containing more calcite mineral may derived from shell fragments of pelecypod, gastropod, foraminifera, bryozoa, etc. CaO shows negative correlation with SiO_2 and Al_2O_3, which indicates the effect of clastic input and detrital dilution of carbonate, during deposition (Ali and Wagreich, 2017). Fe_2O_3/Al_2O_3 ratio of limestones show a high ratio (4.16), which may be due to the preservation of sesquioxide ($Fe_2O_3Al_2O3$), clay mineral derived either from lithogenic sources or from the source of burial digenesis of Cretaceous marine invertebrate shells, due to marine transgression and regression. MnO and Na_2O in limestones are low, due to less amount of lithogenic concentration.

Titanium oxide is mainly concentrated from phyllosilicates (Ramasamy et al., 2007; Udayanapillai and Ganesamoorthy, 2013). Titanium is relatively immobile (McLennan et al., 1993; Ramasamy et al., 2007). The samples of the area show lower TiO_2 (0.16%), which indicates lesser concentration of Titanium bearing minerals in limestones. P_2O_5 content shows an average concentration of 0.44%. Low P_2O_5 may be due to the presence of a lesser amount of accessory mineral phases, such as apatite and monazite minerals (Armstrong-Altrin et al., 2018; Chougong et al., 2021).

GEO-STATISTICAL EVALUATION

Advanced statistics of Multiple correlations, Principal Component Analysis, and Cluster Analysis are carried out for the major element concentrations of the gryphaea limestone of the Pudupalayam Chettinadu mine. Geostatistical software "PAST" is used for the statistical analysis.

MULTIPLE CORRELATIONS

It is a measure of the degree of dependency between the variable with one. Many researchers have utilized this technique in various studies (Srinivasamoorthy et al., 2010; Kaliammal and Udayanapillai, 2018; Udayanapillai et al., 2022). There are very limited reports have been published on applying these techniques in shell limestones. Multiple correlations of major elements of gryphaea limestone samples of Pudupalayam mine are given in **Table 5**. Multiple diagonally symmetrical linear correlation coefficient factor numbers of eleven parameters are given in bold letters. Correlation matrix represents that CaO makes negative relations with SiO_2, Al_2O_3, Fe_2O_3, MgO, MnO, Na_2O, K_2O, and TiO_2 and positive relations with P_2O_5. Further, this relation indicates that CaO may be derived from the burial diagenetic process of Cretaceous marine invertebrates of pelecypods, gastropods, foraminifera, bryozoa, coralline algae, and brachiopod, etc. Other oxides might have been derived from continental lithogenic sources. CaO and P_2O_5 show positive correlations, which indicates both elements were derived from a similar source.

PRINCIPAL COMPONENT ANALYSIS

It is a statistical procedure in which larger data can be changed into visualized one and analysed by a set of summary indices. It finds the direction of the maximal variance of data. It examines the magnitude and direction of coefficients for the original variables. Many researchers have applied Principal Component Analysis (PCA) in various geological studies (Srivastava et al., 1998; Sridhar et al., 2014; Usman et al., 2014; Udayananpillai and Kaliammal, 2016; Kuttalingam et al., 2018; Armstrong-Altrin, 2020; Ramos Vázquez and Armstrong-Altrin, 2019, 2021; Udayanapillai et al., 2022; Botello et al., 2023). PCA is regulated by linearity, the significance of mean, covariance, and orthogonal axis fitting of data of components (Udayanapillai et al., 2022). PCA data reveal its Eigen value, Percentage of Variance, Cumulative Variance, and the selected PCA components. Eigen value 1 is considered for the selection of PCA components (**Table 6a and b)**. The canonical representation diagrams of the PCA components are given in **Figure 8**.

Four PCA components reveal 90.17% of Cumulative Variance. Each PCA component is associated with

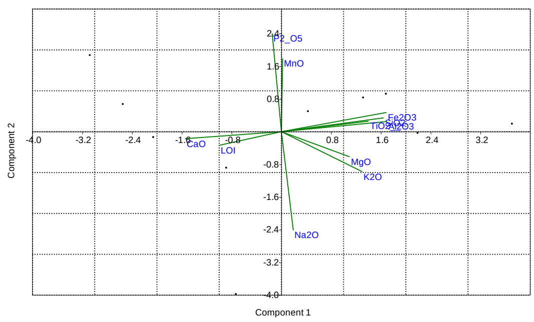

Figure 8. Canonical representation diagram of the PCA analysis.

certain major oxides and is provided as follows.

I Component - $SiO_2 + Al_2O_3 + Fe_2O_3$ + CaO + $K_2O + TiO_2$ -- 45.25% Variance

II Component - MnO+Na_2O+P_2O_5 -- 22.61% Variance

III Component – MgO +TiO_2 --15.20% Variance

IV Component – LOI -- 7.12% of Variance.

Table 6a. Principal Component Analysis of geochemical data, LOI = Loss of Ignition

PC	Eigenvalue	% variance	Cumulative variance	Components
1	4.97798	45.254	45.254	SiO_2+ Al_2O_3+ Fe_2O_3+ CaO+K_2O
2	2.48738	22.613	67.87	MnO+ Na_2O+ P_2O_5
3	1.67184	15.199	83.06	MgO+ TiO_2
4	0.783383	7.1217	90.19	LOI
5	0.46488	4.2262		
6	0.430687	3.9153		
7	0.121338	1.1031		
8	0.037837	0.34397		
9	0.024683	0.22439		

First component keeps the position of the highest amount of variation in the sample, whereas the fourth component has a lesser significance of variation. PCA component loading variations are

Table 6b. Component loading Scores
LOI = Loss of Ignition

0	Axis 1	Axis 2	Axis 3	Axis 4	Axis 5	Axis 6	Axis 7	Axis 8	Axis 9	Axis 10	Axis 11
SiO_2	0.90	0.13	-0.18	0.14	-0.18	-0.18	0.25	0.03	0.00	0.00	0.00
Al_2O_3	0.93	0.10	-0.29	0.16	0.10	-0.07	-0.05	-0.06	0.05	0.00	0.00
Fe_2O_3	0.92	0.18	-0.25	0.22	0.00	-0.06	-0.03	0.02	-0.03	0.00	0.00
CaO	-0.84	-0.07	-0.36	-0.34	0.03	-0.03	0.16	0.03	0.04	0.00	0.00
MgO	0.60	-0.24	0.64	-0.28	-0.30	-0.02	0.00	-0.06	0.07	0.00	0.00
MnO	0.01	0.69	0.55	0.10	0.45	0.00	0.09	-0.02	0.04	0.00	0.00
Na_2O	0.10	-0.93	-0.08	0.15	0.21	-0.18	-0.06	0.07	0.07	0.00	0.00
K_2O	0.71	-0.38	-0.11	-0.04	0.09	0.57	0.07	0.02	0.01	0.00	0.00
TiO_2	0.76	0.10	0.47	-0.39	0.09	-0.09	-0.04	0.11	-0.04	0.00	0.00
P_2O_5	-0.08	0.93	-0.26	0.00	-0.18	0.10	-0.10	0.08	0.08	0.00	0.00
LOI	-0.54	-0.13	0.59	0.55	-0.19	0.09	0.04	0.06	0.00	0.00	0.00

gradually reduced from the first component to the fourth component.

CLUSTER ANALYSIS

It is a statistical method that is used to group similar objects into respective categories. It can also be referred to as segmentation analysis. It confirms homogeneous and heterogeneous groups on a definite set of variables. Relative distance or proximity is taken into consideration for groups and these groups are called clusters. Cluster analysis represents a direct relationship between the variables, which function based on correlation matrices and the arithmetic average of the correlation coefficient (Davis, 1973, Harper, 1999). Numerous researchers have applied cluster analysis for various geological studies (Srivastava et al, 1998; Praus, 2007; Udayanapillai and Kaliammal, 2016; Kuttalingam et al., 2018; Udayanapillai et al., 2022).

Cluster analysis is applied here for two purposes, such as

a) To interpret the ionic similarity between major element oxide parameters in the samples.

b) Similar aerial grouping similarity concentration of cluster of the profile samples. Dendrogram of Paired group cluster method and Wards minimum variable cluster methods are used for finding out ionic similarity identification and finding out the relative distance of similarity of the profile samples (**Fig. 9 a and b)**.

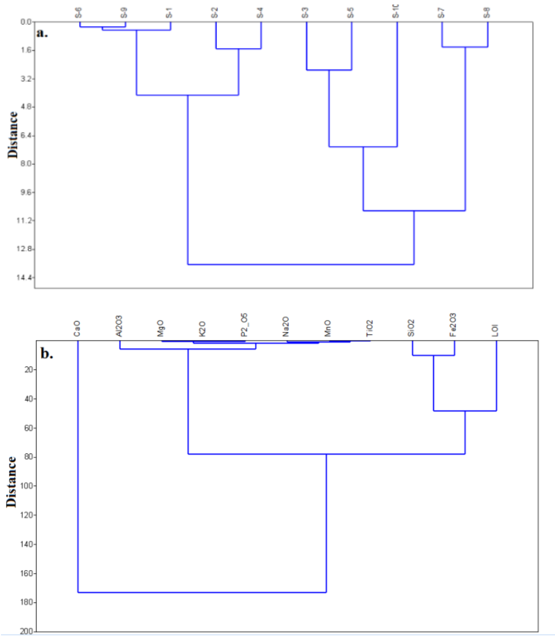

Figure 9(a). Ward method cluster analysis for aerial grouping of samples, **(b).** Paired group cluster methods of ionic similarities in the study area.

There are two paired groups of ionic clusters of major oxide are interpreted, which are as follows.

S.No	Cluster Component	Similarity of Correlation Coefficient
1	$LOI+P_2O_5-SiO_2$	50
2	$TiO_2+MnO+Na_2O+P_2O_5+K_2O+MgO+Al_2O_3$	10

The above two ionic clusters represent an average relative similarity value of 170.

There are two aerial grouping clusters by the Wards method or Euclidean method. They represent as follows:

I Cluster – S_8 - S_7 + S_{10} + S_5 - S_3 -- Relative distance --11.2

II Cluster – S_4 - S_2 + S_1 + S_9 - S_6 -- Relative distance -- 4.0

Above two aerial groups form an average relative distance of 13.6.

Thus, the relativity of major oxide parameters and the profile samples inter-relationship quality is interpreted by advanced geostatistical techniques, such as Multiple Correlations, Principal component analysis, and Cluster analysis.

PALAEOCLIMATE

Changes in climate through geological time are termed as palaeoclimate. A proxy or many numbers of proxies establish the palaeoclimate of an area. Stable isotope geochemical characters, tree rings analysis, pollen analysis, lake varves, biota or fossil evidence, ice cores, geological setting, historical documents, geochemical elements, clay minerals, etc. are some of the important proxies which represent palaeoclimate. Despite many proxies being used in the palaeoclimate studies, the palaeoclimate of the gryphaea limestone deposit of the Pudupalayam Chettinadu mine has been mainly interpreted by the proxies of biota, major element geochemistry, and clay minerals.

BIOTA PROXIES

Thin section photomicrograph reveals the presence of microfossil bryozoa, foraminifera, algal mats, pelecypod, and gastropod shell fragments. Bryozoans are chiefly identified by using skeletal characteristics, like spines, surface structure, pores, and shape and size of the colonies. Bryozoa occur both in shallow and moderately deep-water deposits (Shrock and Twenhofel, 2005). Cheilostomata, Cyclostomata, Ctenostomata Bryozoans were almost equally numerous in the late Cretaceous (David Jablonski et al., 1997; Lidgard et al., 2016). Bryozoa are dominant contributor of CaO in temperate water in marine carbonate deposits (Clark and Ligards, 2000). The presence of algal mats indicates that symbiotic algae live in shallow tropical water. Pelecypod and gastropod shell fragments along with microfossils, foraminifera and bryozoa are preserved in the shallow continental shelf marine platform of limestone deposits in the tropical climate. Since these limestone deposits are subjected to tectonic disturbances, mega fossils are damaged into small shell fragments.

GEOCHEMICAL PROXIES

Geomorphological, sedimentological, and biological factors reflect climate changes. Evaporite mineral and major element geochemistry are the two important proxies used for palaeoclimate investigation in the evaporite deposit of Tunisia and Rajasthan (Sinha et al., 2006; Smykatzkloss and Roy, 2010) and the Pandalkudi calcrete profile (Udayanapillai et al., 2021). Calcite, dolomite, halite, anhydrite, and gypsum are important evaporite minerals that represent proxies for the arid environment. Calcite and other carbonate minerals in the study area represent proxies for arid environment. Despite climate has interpreted through geomorphic landforms; mineralogical factors are mostly used as proxies to establish humid, semi-arid and arid palaeoclimatic investigations.

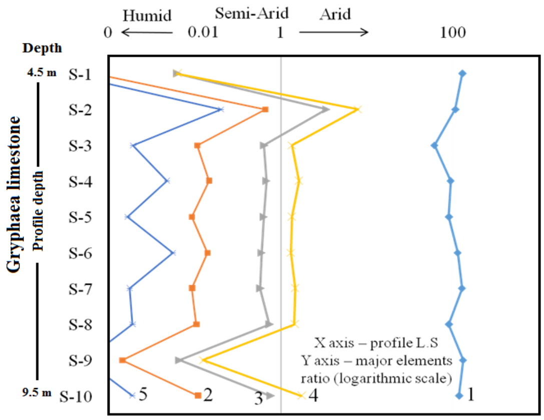

Figure 10. Ratio plot diagram of limestone samples of profile-1 (average) plotted on the climate model diagram related to depth proposed by (after Smykatz-Kloss and Roy 2010; UdayanaPillai et al., 2015). 1) CaO/MgO, 2) Na_2O/Al_2O_3, 3) Na_2O/K_2O, 4) Na_2O/TiO_2, and 5)

Highly soluble major oxides Na_2O, MgO, K_2O, and un-soluble hydrolysate TiO_2, Al_2O_3 and Fe_2O_3 are used as proxies to interpret the palaeoclimate studies of the Gryphaea limestone profile of the study area. The ratio of alkaline/hydrolysate is generally low in the humid climate and high in the arid climate (Sinha et al., 2006; Udayanapillai et al., 2021). Ratio value of Na_2O/Al_2O_3 (0.15), Na_2O/Fe_2O_3 (0.03), Na_2O/K_2O (0.88), Na_2O/TiO_2 (1.8), and CaO/MgO (102.9) of the gryphaea limestone profile samples of the study area are given in (**Table 4)** and its ratio plot for climate model diagram related to depth are given in the diagram (after Udayanapillai et al., 2015, 2021; Fig 10). The ratio value of < 0.1, 0.1 to 1, and >1 are treated as humid, semi-arid, and arid climates respectively, Geochemical ratio plots of gryphaea limestone samples collected from the study area fall on the semi-arid and arid climate prevailing during the depositional environment.

Aridity is established by Salinization. Salinization factor is established by the geochemical ratio of Na_2O/K_2O. When the above ratio is greater than 0.01, it represents a semi-arid and arid climate (Udayanapillai et al., 2015, 2021). The averageNa_2O/K_2O ratio of the limestones is 0.88. This range in the profile represents the semi-aridity or aridity of the depositional environment. Calcification character is another factor in establishing palaeoclimate. It is established by the average geochemical ratio of CaO/MgO. Average calcification ratio of the gryphaea limestone profile is 102.93. Calcification is generally high in the study area which represents an arid environment.

Na_2O/K_2O, Na_2O/Al_2O_3, and Na_2O/TiO_2 ratios are high in an arid environment and vice versa in a humid environment in limestone deposits (Sinha et al., 2006; Udayanapillai et al., 2021). Similarly, high ratio values in limestones represent an arid and semi-arid climate conditions.

CLAY MINERAL PROXIES

Limestone possesses regolith clay minerals and neo-formed clay minerals which represent climate history. Hydrolysis of weathered silicate minerals causes for the origin of clay. Meteoritic precipitation and the formation of clay minerals in the sediments help to interpret the palaeoclimate of sediments (Udayanapillai et al., 2015, 2022). Size, composition of parent material, temperature, seasonal rainfall, and time of formation of sediments are prime criteria for clay mineral composition (Udayanapillai et al., 2015, 2022). Some of the clay minerals represent the climate. Palygorskite and Sepiolite are indicating the arid climate. XRD analysis of gryphaea limestone shows the presence of clay minerals, such as kaolin, montmorillonite, and palygorskite which indicates arid and semi-arid climate conditions. Palygorskite is a neo-formed clay mineral in limestone formation that indicates an arid climate (Udayanapillai et al., 2015, 2022). Kaolin indicates a semi-arid climate (Udayanapillai et al., 2022). Gryphaea limestone of the study area represents semi-arid and arid climate conditions, during deposition.

CONCLUSION

Pudupalayam Chettinadu limestone mine is located in the southern terminal part of the Kallankurichi formation of the Upper Cretaceous Ariyalur stage, Tamil Nadu, India. Petrological observation represents that the limestone does not have mega fossils and generally a mud based biogenic limestone. However, it contains pelecypod, gastropod, shell fragments, microfossil groups of foraminifera, bryozoa, and algal mats. XRD result indicates the presence of many carbonate minerals and a few clay minerals. Geochemical results indicate elevated CaO concentration, due to the presence of more calcite minerals in the samples. Geostatistical analysis of multiple correlations, PCA, and Cluster analysis illustrates the geochemical affinities and inter-relationship between the geochemical elements. Palaeoclimate established through proxies of biota, geochemical ratio, and clay minerals indicate that the gryphaea limestone is formed under arid and semi-arid climates.

ACKNOWLEDGEMENTS

The First author expresses his sincere thanks to Shri. A.P.C.V. Chockalingam, Secretary and our Principal Dr. C. VeeraBhahu, V.O.Chidambaram College, Thoothukudi. The help was extended by Dr. P. Sivasubramanian, Professor and Head, PG and Research Department of Geology, V.O.Chidambaram College, Thoothukudi. John S. Armstrong-Altrin acknowledges the Sabbatical Research approved by PASPA, UNAM. This work is part of the PhD thesis of the first author M. Senthiappan (Reg. no: 19212232221035).

ETHICS DECLARATIONS

CONFLICT OF INTEREST

The authors declare that they have no conflict of interest.

REFERENCE

Anaya-Gregorio, A., Armstrong-Altrin, J.S., Machain-Castillo, M.L., Montiel-García, P.C., Ramos-Vázquez, M.A. (2018). Textural and geochemical characteristics of late Pleistocene to Holocene fine-grained deep-sea sediment cores (GM6 and GM7), recovered from southwestern Gulf of Mexico. Journal of Palaeogeography, 7(3), 253-271.

Armstrong-Altrin, J.S. (2020). Detrital zircon U-Pb geochronology and geochemistry of the Riachuelos and Palma Sola beach sediments, Veracruz State, Gulf of Mexico: a new insight on palaeoenvironment. Journal of Palaeogeography, 9 (4), article no. 28.

Armstrong-Altrin, J.S., Madhavaraju, J., Vega-Bautista, F., Ramos-Vázquez, M.A., Pérez-Alvarado, B.Y., Kasper-Zubillaga, J.J., EkoaBessa, A.Z. (2021b). Mineralogy and geochemistry of Tecolutla and Coatzacoalcos beach sediments, SW Gulf of Mexico. Applied Geochemistry. 134, 105103 https://doi.org/10.1016/j.apgeochem.2021.105103.

Armstrong-Altrin, J.S., Ramos-Vázquez, M.A., Madhavaraju, J., Marca-Castillo, M.E., Machain-Castillo, M.L., Márquez-Garcia, A.Z. (2022). Geochemistry of marine sediments adjacent to the Los Tuxtlas Volcanic Complex, Gulf of Mexico: Constraints on weathering and provenance. Applied Geochemistry, 141, 105321. http://doi.org/10.1016/j.apgeochem.2022.105321.

Armstrong-Altrin, J.S., Ramos-Vázquez, M.A., Zavala-León, A.C., Montiel-García, P.C. (2018). Provenance discrimination between Atasta and Alvarado beach sands, western Gulf of Mexico, Mexico: Constraints from detrital zircon chemistry and U-Pb geochronology. Geological Journal, 53(6), 2824-2848. https://doi.org/10.1002/gj.3122.

Ayyasamy, K., Radhakrishnan, K., Lingaraj, Otta (1992). Stratigraphy of the Cretaceous rock around Kilapalavur, Trichirappalli district, Tamilnadu. Palaeontological Society of India, 109-112.

Babu, K. (2017). Geochemical characteristics of sandstones from Cretaceous Garudamangalam area of Ariyalur, Tamilnadu, India: Implications of provenance and tectonic setting. Journal of Earth System Science, 126(4), 1.

Banerji, R.K., Ramasamy, S., Malini, C.S., Singh, D. (1996). Uttatur group redefined. Geological Society India, Memoirs, 213-229.

Blanford, H.F. (1862). On the Cretaceous and other rocks of South Arcot and Trichinopoly district. Memoir Geological Survey of India. 1-217.

Botello, A.V., Ponce-Vélez, G., Armstrong-Altrin, J.S., Fragoso, S.V., Velandia-Aquino, L.B. (2023). Concentration of polycyclic aromatic hydrocarbons (PAHs) in sediments from the Tampamachoco lagoon, Tuxpan River mouth, Gulf of Mexico. Arabian Journal of Geosciences, 16, 556.

Carroll, D. (1970). Clay Minerals: A guide to their X-ray diffraction. Geological Society of America Special Publication, 126:50. https://doi.org/10.1130/SPE126-p1

Chougong, D.T., Bessa, A.Z.E., Ngueutchoua G., Yongue, R.F., Ntyam, S.C., Armstrong-Altrin, J.S. (2021). Mineralogy and geochemistry of Lobé River sediments, SW Cameroon: Implications for provenance and weathering. Journal of African Earth Sciences, 183, 1-19 No. 104320. https://doi.org/10.1016/j.jafrearsci.2021.104320.

Clarke, A., Lidgard, S. (2000). Spatial patterns of diversity in the sea: bryozoan species richness in the North Atlantic. Journal of Animal Ecology, 69(5), 799-814.

Cox, R., Lowe, D.R., Cullers, R.L. 1995. The influence of sediment recycling and basement composition on evolution of mud rock chemistry in the South-western United States. Geochemical Cosmochimica Acta, 59(14), 2919-2940.

Davis, J.C. (1973). Statistics and data analysis in geology. John Wiley and Sons. New York, pp.

550. https://doi.org/10.1180/minmag.1976.040.315.20

Deer, W.A., Howie, R.A., Zussman, J. (1979). An introduction to the rock-forming minerals. The English Language book Society and Longman, p 1–528.

Dunham, R.J. (1962). Classification of carbonate rocks according to depositional textures.

Ekoa Bessa, A.Z., Paul-Désiré, N., Fuh, G.C., Armstrong-Altrin, J.S., Betsi, T.B. (2021a). Mineralogy and geochemistry of the Ossa lake Complex sediments, Southern Cameroon: Implications for paleoweathering and provenance. Arabian Journal of Geosciences, 14, Article no. 322.

Ekoa Bessa, A.Z., Armstrong-Altrin, J.S., Fuh, G.C., Betsi, T.B., Kelepile, T., Ndjigui, P-D. (2021b). Mineralogy and geochemistry of the Ngaoundaba Crater Lake sediments, northern Cameroon: implications for provenance and trace metals status. Acta Geochimica, 40, 718-738.

Folk, R.L. (1968). Bimodal super mature sandstones: product of the desert floor. Int. Geol. Congr., 23rd Sess., Proc., Sect. 8: 9--32.

Goswami, A., Prasad, G.V.R., Verma, O., Flynn, J.J., Benson, R.B.J. (2013). A trodontid dinosaur from the latest Cretaceous of India (Abstract). Nature communications Art No: 1703, Doi 10. 1038/ncomms 2716.

Govindan, A., Ravindran, C.N., Rangaraju, M.K. (1996). Cretaceous stratigraphy and planktonic foramininferal zonation of CauveriBasin,South India. Sahni, A. (eds), In: Cretaceous stratigraphy and palaeo-environments. Journal of Geological Society India, 37, 155-187.

Harper, D.A.T. (1999). Numerical Palaeobiology, John Wiley & Sons, New York.https://doi.org/10.1017/S0016756800334410

Jiménez-Espinosa, R., Jiménez-Millán, J. (2003). Calcrete development in Mediterranean colluvial carbonate systems from SE Spain. Journal of Arid Environments 53(4), 479–489.

Kaliammal, M., Udayanapillai, A.V. (2018). Aqueous geochemical modelling in the granite terrain of Pandalgudi aquifer region, Viruthunagar District, Tamilnadu, India. IJCRT, 6(2), 442-448.

Kile, D.E., Dennis, E.D. (2000). Quantitative mineralogy and particle-size distribution of Bed Sediments in the Boulder Creek Watershed. Mineralogy and Particle-size of Bed Sediments, pp. 173–184

Krishnan, M.S. (1982). Geology of India and Burma, CBS publishers and distributor (eds), 536p

Kuttalingam, U., Udayanapillai, A.V., Murugan, D., Lakshmanan, C. (2018). Advanced computational geostatistical studies of groundwater quality of Vilathikulam Region, Thoothukudi District, Tamilnadu, India. International Journal of Recent Research Aspects 20,1024-1029.

Madhavaraju, J., Ramasamy, S. (1999). Rare earth elements in limestones of Kallankurichchi Formation of Ariyalur Group, Tiruchirapalli Cretaceous, Tamil Nadu., Journal of the Geological Society of India, 54, 291-301.

Madhavaraju, J., Armstrong-Altrin, J.S., Pillai, R.B., Pi-Puig, T. (2021). Geochemistry of sands from the Huatabampo and Altata beaches. Gulf of California, Mexico. Geological Journal, 56, 2398-2417. DOI:10.1002/gj.3864.

Mitra, S. (1989). Fundamental of optical spectroscopic and X-ray. Mineralogy Wiley. http://www.worldcat.org/oclc/17300449

Nagendra, R., Kannan, B.K., Sen, G., Gilbert, H., Bakkiaraj, D., Reddy, A.N., Jaiprakash, B.C. (2018). Sequence surfaces and paleobathymetric trends in Albian to Maastrichtian sediments of Ariyalur area, Cauvery Basin, India. Marine and Petroleum Geology, 28(4), 895-905.

Nagendra, R., Nagarajan, R., Bakkiaraj, D., Armstrong-Altrin, J.S. (2011). Depositional and post-depositional setting of Maastrichtian limestone, Ariyalur Group, Cauvery Basin, South India: a geochemical appraisal. Carbonates and Evaporites, 26(2), 127-147.

Nagendra, R., Nagendran, G., Narasimha, K., Jaiprakash, B.C., Nallapa Reddy, A. (2002). Sequence stratigraphy of Dalmiapuram formation Kallakudi Quarry – II, South India, Journal of Geological Society of India, 59, 249-258.

Nagendra, R., Sathiyamoorthy, P., Pattanayak, S., Nallapa Reddy, A., Jaiprakash, B.C. (2013). Stratigraphy and paleobathymetric interpretation of the Cretaceous Karai shale formation of Uttatur Group, TamilNadu, India. Stratigraphy and Geological Correlation, 21, 675-688.

Nagendra, R., Nallapa Reddy, A. (2017). Major geologic events of the Cauvery Basin, India and their correlation with global signatures- A review. Journal of Palaeogeography, 6(1), 69-83

Nagendra, R., Nallapa Reddy, A. (2017). Major geologic events of the Cauvery Basin, India and their correlation with global signatures- A review. Journal of Palaeogeography, (1), 69-83.

Nagendra, R., Reddy, A.N., Jaiprakash, B.C., Gilbert, H., Zakharov, Y.D., Venkateshwarlu, M. (2018). Integrated Cretaceous stratigraphy of the Cauvery basin, south India. Stratigraphy, 15(4), 245-249.

Perumal, V., Udayanapillai, A.V. (2020). Calcrete profiles in Puthukulam quarry section, Sathankulam region, Southern Tamilnadu, India, implications on palaeoclimate significance. Journal of Sedimentary Environment 5:493503.

Praus, P. (2007). Urban water quality evaluation using multivariate analysis. Acta Montan. Slovaca 12(2):50–158.

Ramasamy, S., Banergi, R.K. (1991). Geology, Petrography and Stratigraphy of Pre–Ariyalur sequence in Trichirapalli district, Tamilnadu. Journal of the Geological Society of India, 577-594.

Ramasamy, S., Ramachandran, A., Velmurugan, K., David Lalhmingliana Chawngthu, B.S., Suresh Gandhi, M. (2012). Sedimentological studies of Kallamedu Formation in Ariyalur area, Tamil Nadu, India. International Journal of Geology, Earth and Environmental Sciences, 2, 218-234.

Ramasamy, S., Singh, T.S., Madhavaraju, J., Asir, G.G. (2007). Petrography and geochemistry of pre-Ariyalur sequence in Perambalur District, Tamil Nadu-Implications on depositional environment and palaeoclimate. Journal of the Geological Society of India, 69(1), 121-132.

Ramkumar, M.U. (2008). Carbonate Diagnesis in the Kallankurichchi Formation, Ariyalur Group, South India and its Implications on Petroleum Prospects. Journal of the Geological Society of India, 71(3), 407.

Ramkumar, K.B., Rajkumar, P.K., Ahmmad, S.N., Jegan, M. (2020). A review on performance of self-compacting concrete–use of mineral admixtures and steel fibres with artificial neural network application. Construction and Building Materials, 261, 120215.

Ramos-Vázquez, M.A., Armstrong-Altrin, J.S. (2019). Sediment chemistry and detrital zircon record in the Bosque and Paseo del Mar coastal areas from the southwestern Gulf of Mexico. Marine and Petroleum Geology, 110, 650-675.

Ramos-Vázquez M.A., Armstrong-Altrin J.S. (2021) Provenance of sediments from Barra del Tordo and Tesoro beaches, Tamaulipas State, north-western Gulf of Mexico. Journal of Palaeogeography, 10(1).

Ramos-Vázquez, M.A., Armstrong-Altrin, J.S., Madhavaraju, J., Gracia, A., Salas-de-León, D.A. (2022). Mineralogy and geochemistry of marine sediments in the Northeastern Gulf of Mexico. In: Armstrong-Altrin JA, Pandarinath K, Verma S. (Eds.), Geochemical Treasures and Petrogenetic Processes. P. 153-183 https://doi.org/10.1007/978-981-19-4782-7_7

Reddy, A.N., Jaiprakash, B.C., Rao, M.V., Chidambaram, L., Bhaktavatsala, K.V. (2013). Sequence stratigraphy of late Cretaceous successions in the Ramnad sub-basin, Cauvery Basin, India. In Proc. XXIII Indian Colloquium on Micropaleontology and Stratigraphy and International Symposium on Global Bioevents in Earth History. Geological Society of India Special Publications, No. 1, pp. 78-97.

Shrock, Twenhofel (2005). Principles of Invertebrate Palaeontology, Second edition, CBS, pp 1-816.

Sinha, R., Smykatz-Kloss, W., Stüben, D., Harrison, S. P., Berner, Z., Kramar, U. (2006). Late Quaternary palaeoclimatic reconstruction from the lacustrine sediments of the Sambhar playa core, Thar Desert margin, India. Palaeogeography, Palaeoclimatology, Palaeoecology, 233(3-4), 252-270.

Smykatz-Kloss, W., Roy, P.D. (2010). Evaporite mineralogy and major element geochemistry as tools for palaeoclimatic investigations in arid regions: A synthesis. Boletín de la Sociedad Geológica Mexicana, 62(3), 379-390.

Sopie, F.T., Ngueutchoua, G., Armstrong-Altrin, J.S., Njanko, T., Sonfack, A.N., Sonfack, A.N., Ngagoum, Y.S.K., Fossa, D., Tembu, L.T. (2023). Provenance, weathering, and tectonic setting of the Yoyo, Kribi, and Campo beach sediments in the southern Gulf of Guinea, SW Cameroon. Journal of Earth System Science https://doi.org/10.1007/s12040-023-02101-5

Sridhar, M., Chaturved, A., Rai, A., (2014). Locating new uranium occurrence by integrated weighted analysis in Kaladgi basin, Karnataka. Journal of the Geological Society of India, 84(5), 509–512. https://doi.org/10.1007/s12594-014-0159-2

Srinivasamoorthy, K., Vijayaraghavan, M., Vasanthavigar, V.S., Sarma, S., Chidambaram, P., Anandhan (2010). Assessment of groundwater quality with special emphasis on fluoride contamination in crystalline bed rock aquifers of Mettur region, Tamilnadu, India. Arabian Journal of Geosciences, 5, 83–94. https://doi.org/10.1007/s12517-010-0162-x

Srivastava, P., Parkash, B., Pal, D.K. (1998). Clay minerals in soils as evidence of Holocene climatic change, Central Indo-Gangetic Plains, North-Central India. Quaternary Research, 50(3), 230–239

Sundaram, R., Henderson, R.A., Ayyasami, K., Stilwell, J.D. (2001). A lithostratigraphic revision and palaeo-environmental assessment of the Cretaceous system exposed in the onshore Cauvery Basin, southern India. Cretaceous Research, 22, 743-762.

Tawfik, H.A., Salah, M.K., Maejima, W., Armstrong-Altrin, J.S., Abdel-Hameed, A-M.T., Ghandour M.M.E. (2018). Petrography and geochemistry of the Lower Miocene Moghra sandstones, Qattara Depression, north Western Desert, Egypt. Geological Journal, 53, 1938-1953.

Udayanapillai A, V., Velmayil, P., Armstrong-Altrin, J.S. (2020). Provenance, Weathering, Tectonic setting and Palaeo-oxygenation condition of the Cretaceous Calcareous Grey Shale (CGS) from the Kallakudi Dalmia Limestone Quarry No:II, Uttatur group, Trichinopoly, Tamilnadu, India. Himalayan Geology, 41(1), 11-2.

Udayanapillai, A.V., Perumal, V., Thirugnasambandam, R., Venkataraman, P., Thangavel, M. (2015). Study of micro-morphology, major element geochemistry and palaeoclimatic implications of calcrete deposits at Salukkuvarpatti Village, Near Pandalgudi, Viruthunagar District, Tamilnadu, India. Journal of Applied Geochemistry, 17(4), 421-43.

Udayanapillai, A.V., Velmayil, P., Armstrong-Altrin, J.S., Sial, A., Manavalan, S. (2022). Geochemical and stable isotope ($\delta^{13}C$ & $\delta^{18}O$) signatures of calcrete in and around Pandalgudi, Southern Tamilnadu, India and its implications on Palaeoclimate, Arabian Journal of Geosciences, 15(913), 1-19. https://doi.org/10.1007/s12517-022-10134-1.

Udayanapillai, A.V., Velmayil, P. (2021). Texture, mineralogy and geochemistry of Teri sediments from the Kuthiraimozhi deposit, Southern Tamilnadu, India: implications on provenance, weathering and palaeoclimate. Arabian Journal of Geosciences, 14(5), 1-15.

Udayanapillai A.V., Kaliammal, M. (2016). Groundwater Characterization and Quality Assessment by using GIS and Geo Statistics from Pandalgudi Region, Virudhunagar District, Tamilnadu, India. International Journal of Research in Environmental Science (IJRES)Volume 2, Issue 4, PP 1-16ISSN 2454-9444 http://dx.doi.org/10.20431/2454-9444.0204001.

Udayanapillai, A.V., Ganesamoorthy (2013). Mineralogy and Geochemistry of Red and Black sediments of Thoothukudi District, Tamilnadu, India. Journal Geological Society Sri Lanka, 15, pp. 47-56

Usman, M.O., Masago, H., Winkler, W., Strasser, M. (2014). Mid-Quaternary decoupling of sediment routing in the Nankai Forearc revealed by provenance analysis of turbiditic sands. International Journal of Earth Sciences, 103, 1141-1161.

Wright, J.L., Unwin, D.M., Lockleyl, M.G., Rainforth, E.C. (1997). Pterosaur tracks from the Purbeck limestone Formation of Dorset, England. Proceedings of the Geologists' Association, 108(1), 39-48.

JOURNAL INDIAN ASSOCIATION OF SEDIMENTOLOGISTS ISSN NO 2582 – 2020
Vol. 40, Issue II, 2023, pp. 27-39
DOI: https://doi.org/10.51710/jias.v40iII.324

Textural characteristics and distribution of ostracoda in core sediments from the Gadilam river estuary, Cuddalore, Tamil Nadu, southeast coast of India

Elumalai, K[1], Ramachandran, A[2,*], Hussain, S. M[3], and Stephen Pitchaimani, V[2]
[1]Thiru A Govindasamy Government Arts & Science College, Tindivanam, Tamilnadu, India
[2]PG & Research Department of Geology, V.O.Chidambaram College, Thoothukudi 628008, Tamilnadu, India.
[3]Department of Geology, School of Earth and Atmospheric Sciences, University of Madras, Guindy Campus, Chennai – 600025, India.
* E-mail Address: sankarramchand@gmail.com

ABSTRACT

To know the distribution of brackish water Ostracoda and to investigate the sediment characteristics, a core (105 cm) has been collected from the Gadilam river estuary and it was sub-sampled into 21 samples at 5 cm width regular interval. All the sediment samples were analyzed as per standard micropaleontological techniques in order to investigate the distribution and occurrence of ostracod fauna. A total of 27 ostracod taxa belonging to 16 genera, 12 families, 3 superfamilies and 2 sub-order of the order Podocopida, have been identified based on published articles Throughout the core (from top to bottom) the calcareous forms were noticed. The ostracod species *Kalingella mckenziei* and *Jankeijcythere mckenziei* are widely distributed in the core and they outnumbered the rest of the species. The faunal assemblages recorded are tropical, brackish to neritic (shallow marine) and benthic in nature (*Hemicytheridea paiki, Hemicytheridea bhatiai, Jankeijcythere mckenziei, Kalingella mckenziei, Neosinocythere dekrooni, Paijenborchellina* sp., *Stigmatocythere indica and Tanella gracilis)*. In the analyzed core, there is no faunal assemblage at the depth between 80-85 and 95-105 cm. The sediment characteristics such as calcium carbonate, organic matter and sand-silt-clay ratio also determined and correlated with the observed ostracod populations. Based on the detailed study, it is noticed that high calcium carbonate and low organic matter of the sediment are congenial for population abundance. From the overall distribution of Ostracoda in all the subsamples, siltysand is found to an accommodative substrate for the prosperity of Ostracoda. The statistical aspect of ostracod carapace-valve ratio has been studied to identify the rate of sedimentation which infers a faster rate of deposition of sediments in the Gadilam River estuary.

KEYWORDS: Ostracoda; Gadilam river estuary; Tamil Nadu; Environmental implications; Micropalaeontology

INTRODUCTION

Ostracoda (microscopic, aquatic Crustacea) from brackish waters provides a great potential for ecological monitoring and palaeoenvironmental analyses in different environments. This has been studied and stated in many articles during recent decades but their potential has yet to be fully developed or utilized in various studies. The analysis of ostracod species distributions, eco-phenotypic variability and stable isotopes and trace elements in ostracod shells provide valuable information about water salinity, temperature and chemistry, hydrodynamic conditions, substrate characteristics, climate, sea level variations, oxygen and nutrients availability (García-Madrigal et al., 2022). Ostracods are typically around 1 mm in size, but varying between 0.2 and 30 mm, laterally compressed and protected by a bivalve-like, chitinous or calcareous shell carapace (Barik et al., 2022). Ostracods are living in various aquatic environments, including fresh, brackish and marine waters. In the oceans, they inhabit both the sea floor and the planktonic zones. Ecologically ostracods can be part of the zooplankton, or (most commonly) they are part of the benthos, living on or inside the upper layer of the sea floor (Matzke-Karasz and Smith, 2022). Ostracods can live in an environment in with the controlling factors are temperature, bottom topography, depth, salinity, dissolved oxygen, substrate, food supply and sediment organic matter (Puri, 1966). However, the main controlling factors governing ostracod distribution in estuarine environments and continental shelf zones are salinity, water temperature and substrate (Yassini and Jones, 1995). While some ostracod species are sensitive to small changes in their environment, others are capable of withstanding a wide range of conditions, even to the extent of inhabiting heavily polluted areas. The effects of sewage pollution and oil spill on coastal ostracod fauna has been investigated by Eagar (1999, 2000) and Mostafawi (2001) from New Zealand and Pacific Atoll, Persian Gulf (Pacific atoll), respectively. These studies show that although increasing level of pollution result in reduced ostracod abundance and diversity, some species are capable of withstanding quiet high levels of contaminations. Ostracods are particularly useful for the biozonation of marine strata on local or regional scales, and they are invaluable indicators of ancient shorelines, salinities and relative sea-floor morphology. Marginal marine environments like marshy rivers, coastal lagoons, deltas, estuaries, mangrove islands, salt marshes and fluvial marine assemblages are characterized by several species, which are peculiar to these environments. Marginal – marine environmental conditions challenging physiological problems for most organisms, including ostracods, since they may have to survive in marked environmental changes over very short periods. In general, the Ostracods diversity is often low in these habitats, although abundance may be remarkably high, usually two or three species dominating. Ostracods is one of the microfaunal groups with increasing usage as biomonitors of stressed conditions in recent and Quaternary environments (Malard et al., 1996; Mosslacher, 2000; Anadon et al., 2002; Boomer and Eisenhauer, 2002). Coastal zones are very sensitive to environmental changes (Ayala-Pérez et al., 2021). Though India has a longest coastline of about 7,500 km and various marginal marine water bodies, the study on recent brackish water ostracoda and their environmental implications have received notable attention. Hence, the present study has been initiated with great concern to describe the distribution of ostracods in the Gadilam River Estuary.

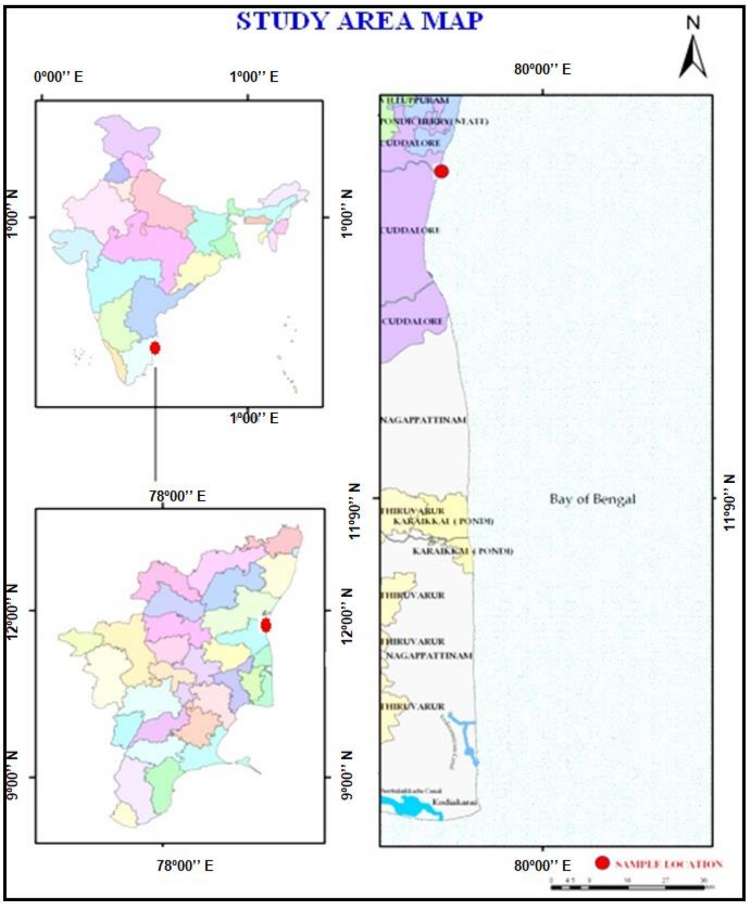

Figure 1. Location map of the study area Gadilam River Estuary

STUDY AREA

The study area is characterized by gently undulating topography with low relief sandstone and laterite hills. A mangrove forest is present near the mouth of the Gadilam river at Devanampattinam, Cuddalore. Gadilam river enters the sedimentary part of the basin from the Archaean- sedimentary contact at Thirunavallur in Ulundurpet Taluk and traverses via Thiruvamur, where Malattar confluence's the main Gadilam before confluence with Bay of Bengal. Uppanar, a backwater stream joining Gadilam, east of Devanampattinam, near Cuddalore. The southern part of the study area is drained by Manimutharu and Main Vellar river. The study area is also covered by Quaternary rocks. Central part of the study area was found to have river alluvium derived from Tertiary rocks, which comprises of lignite deposit and coastal alluvium adjacent to the coast. As it is the sedimentary basin, hydraulic boundary was extended up to the two river boundaries in the south. The study area comprises of two major hydrogeologic environments: (a) Recent alluvium and (b) sandstones in the lateritic terrain.

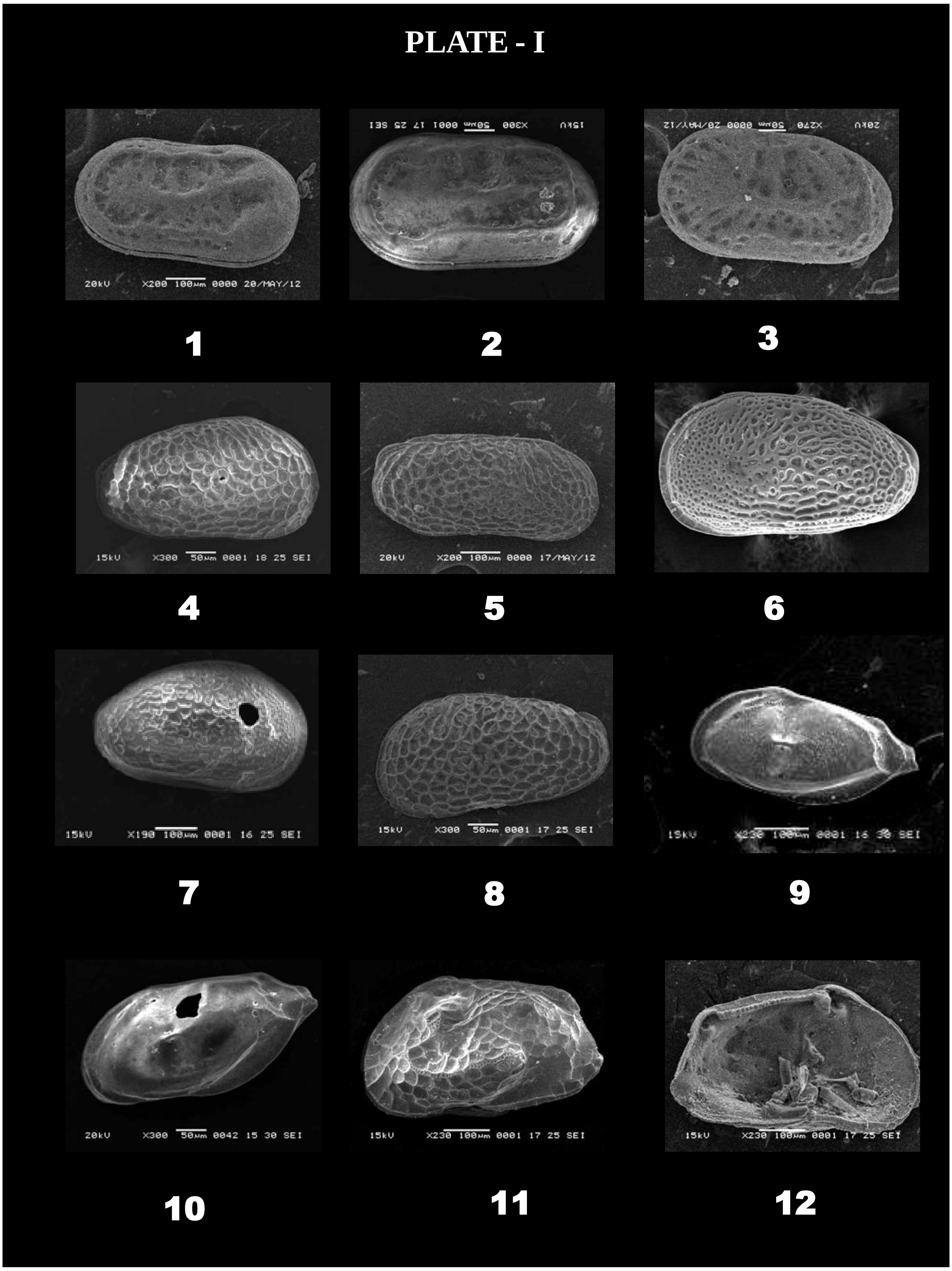

PLATE - I

(Bar scale equals 100 µm unless specified)

Fig. 1. *Cytherelloidea leroyi* Carapace, left valve external view, **Fig. 2.** *Cytherelloidea* sp1 Carapace, right valve external view, **Fig. 3**. *Cytherelloidea* sp2 Carapace, right valve external view, **Fig. 4.** *Hemicytheridea bhatiai* x 150 Carapace, right valve external view, **Fig. 5.** *Hemicytheridea khoslai* Carapace, right valve external view, Figs. 6-7 *Hemicytheridea paiki* **Fig.6**- Carapace, left valve external view, **Fig.7**- Carapace, right valve external view (single predation), **Fig. 8**. *Hemicytheridea reticulate* Carapace, left valve external view, Figs. 9-10. *Neomonoceratina jaini* **Fig. 9**- Carapace, left valve external view, **Fig.10**- Carapace, left valve external view (predated), Figs. 11-12. *Jankeijcythere mckenziei* **Fig.11** - Carapace, left valve external view, Fig.12 - Left valve internal view

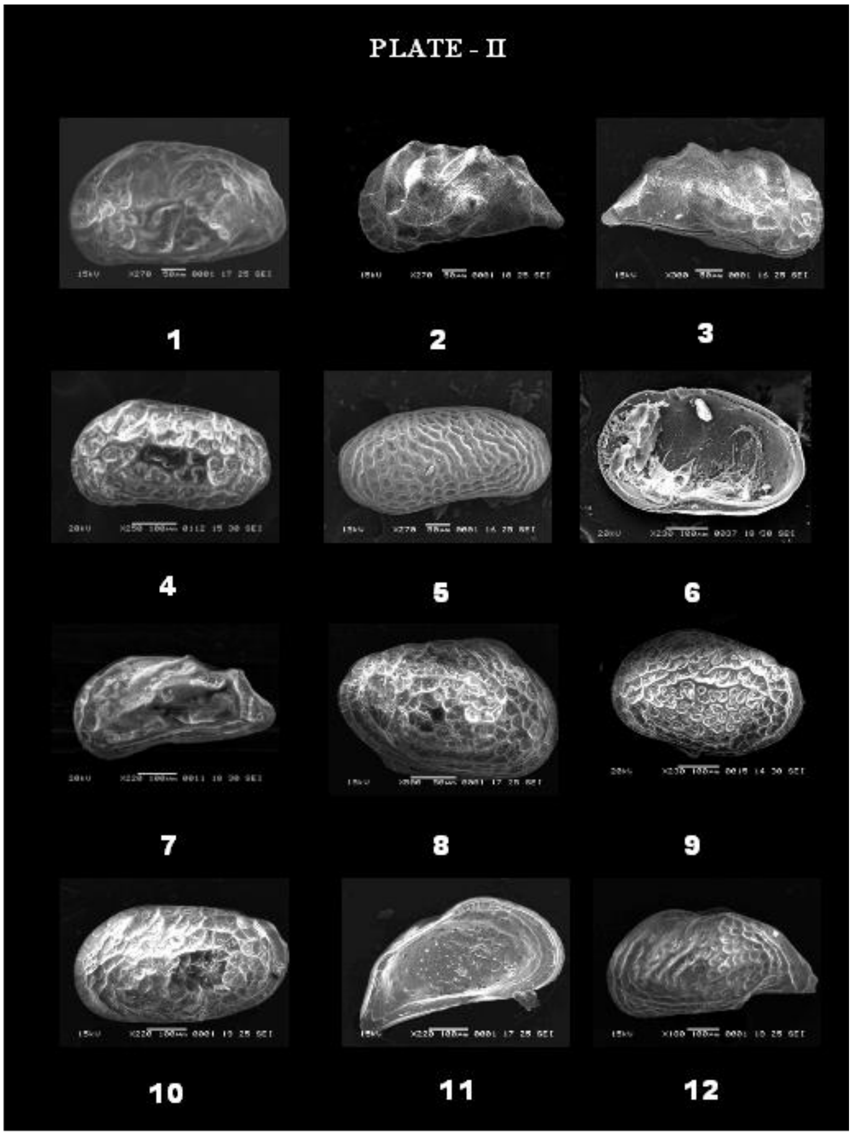

PLATE - II

(Bar scale equals 100 µm unless specified)

Fig. 1. *Jankeijcythere* sp. Carapace, left valve external view, Figs. 2-3. *Neosinocythere dekrooni* **Fig.2**- Carapace, left valve external view **Fig.3**- Carapace, right valve external view, **Fig. 4.** *Callistocythere flavidofusca intricatoides* Carapace, left valve external view, **Fig. 5**.*Tanella gracilis* Carapace, right valve external view **Fig. 6**. *Hemikrithe peterseni* Right valve internal view, **Fig. 7**.*Caudites javana* Carapace, left valve external view, **Fig. 8**. *Loxoconcha cercinata* Carapace, right valve external view, **Fig. 9**. *Loxoconcha megapora indica* Carapace, left valve external view, **Fig. 10**. *Loxoconcha tekkaliensis* Carapace, left valve external view, **Fig. 11**. *Paijenborchellina prona* Left valve internal view, **Fig. 12** *Paijenborchellina* sp. Carapace, left valve external view

MATERIALS AND METHODS

In order to fulfill the objective of this paper and to study the different microenvironmental implications of benthic brackish water ostracoda, a fieldwork was carried out and a sediment core sample was collected from the Gadilam river estuary, Cuddalore (Fig. 1). The length of the core was 105 cm. The core sample is sub-sampled at each 5 cm interval, for regular standard analysis. Thus, a total of 21 samples were obtained. The geographical co-ordinates of latitude 11° 24' 18" N and longitude 79° 46' 46" E were recorded using GPS. A mangrove species *Avicennia marina* is dominated in the estuary area. The other notable mangrove species noticed in the study area are *Acanthus ilicifolius, Egiceras corniculatum, Excoecaria agallocha* and *Rhizopora mucronata*. The sedimentological parameters such as $CaCO_3$, organic matter and sand-silt-clay ratio have been established by the standard procedures. The $CaCO_3$ content in sediments has been determined using rapid titration method (Piper, 1947). Organic matter content is determined by the procedure suggested by Gaudette et al. (1974). Fine fractions (sand, silt and clay) in the samples were analysed by the pipette method in accordance with the standard procedure adopted by Krumbein and Pettijohn (1938). The sediment type was classified by Trefethen's (1950) classification.

SYSTEMATIC PALEONTOLOGY

The classification of ostracods proposed by Hartmann and Puri (1974) has been followed in the present study. In total, 27 ostracod taxa belonging to 16 genera, 12 families, 3 superfamilies and 2 suborders of the order Podocopida have been identified from the Gadilam river estuary sediments, Tamil Nadu, southeast coast of India. A checklist of the ostracod fauna identified in the Gadilam river

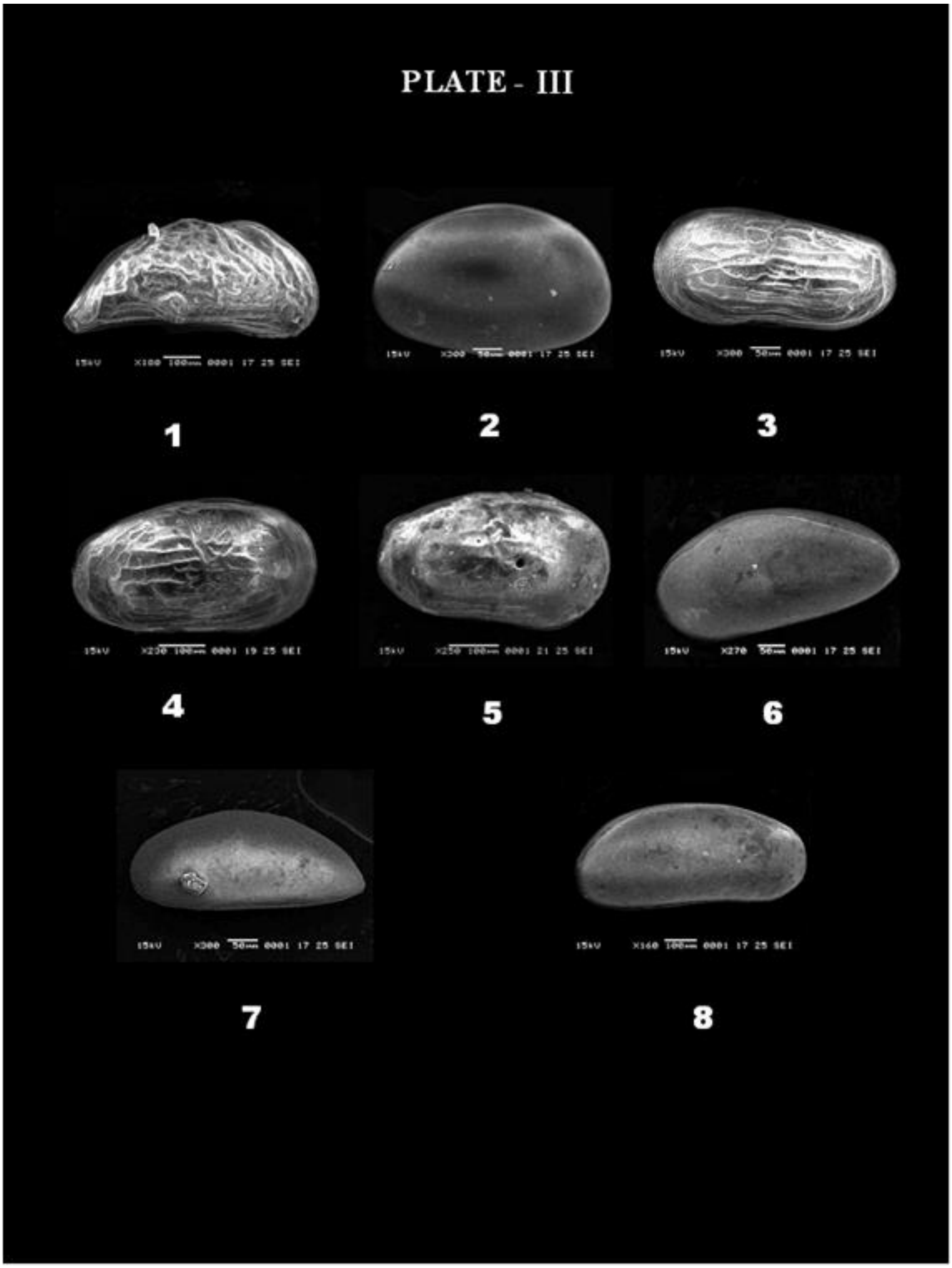

PLATE - III

(Bar scale equals 100 µm unless specified)

Fig. 1. *Paijenborchellina* sp. cf. *P. indoarabica* Carapace, right valve external view, **Fig. 2**. *Xestoleberis variegate* Carapace, left valve external viewFig. 3-4. *Kalingella mckenziei*, **Fig. 3**- Carapace, male left valve external view, **Fig. 4**- Carapace, female right valve external view, **Fig. 5.** *Kalingella* sp. Carapace, right valve external view (Predated), **Fig. 6.** *Propontocypris* (*Schedopontocypris*) *bengalensis* Carapace, left valve external view, **Fig. 7**. *Paracypris* sp. Carapace, left valve external view, **Fig. 8**. *Phlyctenophora orientalis* Carapace, Right valve external view

Table 1. Distribution of $CaCO_3$ OM, sand, silt, and clay with type of sediments and ostracod populations in Gadilam River Estuary, Cuddalore, Tamil Nadu

Samp. No	Depth in cm	$CaCO_3$ %	OM %	Sand %	Silt %	Clay %	Sediment type	Ostracod Population
1	0-5	5.0	2.30	56.04	29.46	14.50	Siltysand	80
2	5-10	5.5	1.32	62.03	25.47	12.50	Siltysand	77
3	10-15	4.5	2.09	61.59	23.91	14.50	Siltysand	66
4	15-20	5.5	1.73	52.19	45.31	2.50	Siltysand	72
5	20 -25	4.5	1.40	57.43	34.57	8.00	Siltysand	66
6	25-30	1.0	1.03	72.72	21.78	5.50	Siltysand	49
7	30-35	1.0	1.80	61.19	37.81	1.00	Siltysand	39
8	35-40	2.0	1.41	56.12	43.38	0.50	Siltysand	36
9	40-45	0.5	1.31	67.79	26.71	5.50	Siltysand	15
10	45-50	1.5	1.65	68.69	30.31	1.00	Siltysand	66
11	50-55	1.0	1.76	59.25	39.75	1.00	Siltysand	45
12	55-60	2.0	1.17	61.88	28.12	10.00	Siltysand	47
13	60-65	1.0	2.10	55.91	32.59	11.50	Siltysand	41
14	65-70	2.0	2.28	72.10	15.90	12.00	Siltysand	25
15	70-75	3.0	1.43	56.33	33.17	10.50	Siltysand	40
16	75-80	2.5	1.80	69.85	19.65	10.50	Siltysand	22
17	80-85	3.5	1.01	65.40	21.60	13.00	Siltysand	73
18	85-90	1.5	1.22	63.15	26.85	10.00	Siltysand	0
19	90-95	3.0	2.10	68.77	19.73	11.50	Siltysand	38
20	95-100	1.5	1.50	63.15	35.35	1.50	Siltysand	0
21	100-105	2.0	1.98	76.02	22.98	1.00	Siltysand	0
Average		2.6	1.64	63.22	29.26	7.52		897
Maximum		5.5	2.30	76.02	45.31	14.50		
Minimum		0.5	1.01	52.19	15.90	0.50		

estuary is given below and the SEM microphotographs depicting different views are presented in Plates I – III. Among these, 3 species belong to the suborder Platycopa and the remaining to suborder Podocopa. The following species, namely *Basslerites liebaui*, *Jankeijcythere mckenziei, Kalingella mckenziei*, *Neomonoceratina jaini* and *Propontocypris (Schedopontocypris) bengalensis* are endemic to Indian waters only.

Checklist of the ostracod fauna encountered in the Gadilam river estuary.

1. *Cytherelloidea leroyi*
2. *Cytherelloidea sp.1*
3. *Cytherelloidea sp.2*
4. *Hemicytheridea bhatiai*
5. *H. paiki*
6. *Hemicytheridea khoslai*
7. *H. reticulata*
8. *Neomonoceratina jaini*
9. *Jankeijcythere mckenziei*
10. *Jankeijcythere sp.*
11. *Neosinocythere dekrooni*
12. *Callistocythere flavidofusca intricatoides*
13. *Tanella gracilis*
14. *Hemikrithe peterseni*
15. *Caudites javana*
16. *Loxoconcha cercinata*
17. *L. megapora indica*
18. *L. tekkaliensis*
19. *Paijanborchellina prona*
20. *P. indoarabica*
21. *Paijanborchellina sp.*
22. *Xestoleberis variegata*
23. *Kalingella mckenziei*
24. *Kalingella sp.*
25. *Paracypris sp.*
26. *P.Schedopontocypris) bengalensis*
27. *Phyctenophora orientalis*

OSTRACOD DISTRIBUTION AND POPULATION

In the Gadilam river estuary sediment core, 27 taxa have been recognized from 897 specimens of ostracods, picked from 21 subsamples and are studied in detail. Among them, species belongs to Cytheracea are represented by 95% of the population. The minimum ostracods population size is 15 nos. in the interval of 40-45 cm and maximum population size of 80 specimens are noted at the surface, 0-5 cm interval. In the sediment core, ostracod population is abundant in the middle and top portions, while it is less abundant in the bottom section. No ostracod species are recorded between 85 - 90 cm and 95 - 105 cm intervals.

SEDIMENT CHARACTERISTICS

CALCIUM CARBONATE ($CaCO_3$)

The source of carbonate content in sediments is due to the abundance broken shell fragments of molluscs and also due to the dilution of biogenic calcite (Ramos-Vázquez and Armstrong-Altrin, 2021). Similar observation was documented by Sebastian et al. (1990) in the Mahe estuary sediments, West Coast of India. The association of $CaCO_3$ with sand fractions is indicating its association with sand fraction. Similarly, Hussain et al. (1997) also observed a relationship between $CaCO_3$ and sand fractions in the Gulf of Mannar sediments, off Tuticorin.

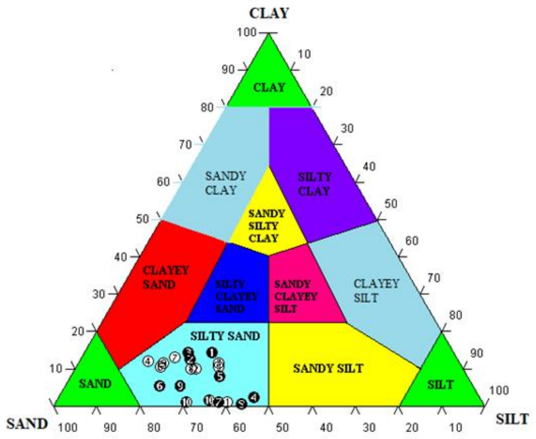

Figure 2. Sand, silt and clay ratio plot for the Gadilam River estuary sediments (after Trefethen, 1950)

The calcium carbonate percentage in the sediment cores ranges from 0.5 to 5.5 % (Table 1), which is higher particularly in the top portion of the core between 0 and 25 cm. The $CaCO_3$ content in the remaining subsamples is showing less percentage compared to top portion of the core. Hence, it is inferred that the calcium carbonate content of the sediment is one of the important parameters, which governs the population of Ostracoda, especially its vertical distribution. Similarly, the calcium carbonate content is directly proportional to the population size of the Ostracoda.

ORGANIC MATTER

Subba Rao (1960) observed that the silty clay materials of the Pennar, Krishna and Godavari rivers, are poor in organic matter. In the Suddagedda river estuary, sandy sediments have been found to be poor in organic matter content, while fine-grained materials are rich in organic matter (Venkata Rao and Subba Rao, 1974; Armstrong-Altrin et al., 2015). These authors further documented that the sandy types are poor in organic matter, while materials containing higher amount of clay are rich in organic matter. According to Joy and Clark (1977), organic carbon being directly related to food supply, is one of the major environmental parameters, which influence the distribution of benthic ostracods. Whatley and Quanhong (1987, 1988) considered the nature of substrate to be the main controlling factor for the abundance of ostracod; highest values occur in association with medium to coarse-grained sand rich in organic debris, and lower values with gravels and sands poor in carbonate. From off Tuticorin, Gulf of Mannar, Hussain et al. (1997) observed that a relative decrease in the organic matter content of the sediments favours a maximum population of Ostracoda.

In the present study, organic matter content was determined for all the 21 sub-samples of core sediments. The analytical concentration of organic matter varies from 1.01 to 2.30 %, in which the lower value is noticed at 80-85 cm interval and moderately high value (2.30 %) is noticed from 0 to 5 cm interval (Table 1). The concentration of organic matter is relatively high in the bottom and top portions of the core. Overall, the organic matter content in all the subsamples exhibits lower values. The impact of this parameter on the distribution of ostracod fauna in all the intervals appears insignificant level.

SUBSTRATE AND OSTRACODES

Annapurna and Rama Sarma (1982) documented that ostracods prefer areas high in sand and clay rather than areas rich in silt, in the Bimili back waters and the Balacheruvu tidal stream. Such a relationship has also been observed in the marine marginal water bodies of many other localities (Alvarez Zarikian et al., 2022).

The substrate sediment texture has a control on the ostracod fauna that can colonize a particular sediment type (Brasier, 1980). The texture stability of the sediment composing the substrate exerts a strong influence on marine ostracods, just as it does on brackish water and fresh water forms. Smooth shelled forms are predominant in fine-grained muds whereas, more ornamented forms are being found in coarse-grained, or in more calcareous sediments (Brasier, 1980).

In the Bimili backwaters and Balacheruvu tidal stream, Annapurna and Rama Sarma (1982) have noted that the genus *Phlyctenophora* occurs in forms such as *Tanella, Loxoconcha*, *Pajenborchellina* and *Kalingella* occur in considerable numbers in the sandy areas. Al-Abdul Razzaq *et al.* (1983) stated that ostracoda occur more in fine-grained sediments due to the greater quantities of organic material in those fractions which provide nutritive material. Hussain (1992), noticed in the Gulf of Mannar, off Tuticorin, that silty sand has been found to be the favourable substrate for the ostracod population abundance.

All the subsamples collected in the study area were analyzed for sand, silt and clay ratio. The sand content in the core sample varies from 52.19 to 76.02 % with an average of 63.22 %; silt percentage is recorded in ranging from 15.90 to 45.31 % at an average of 29.26 %. Clay content has an average of 7.52 % and ranges from 0.50 to 14.50 % (Table 1). The relative abundance of sand-silt-clay ratio of core sample were plotted on a trilinear diagram (Trefethen, 1950) and its sediment type in the core is composed by only silty sand (Fig. 2).

SURFACE ORNAMENTATION AND SEDIMENT TEXTURE

The carapace of few ostracods has smooth surface, and devoid of any sculpture. However, in many species, the carapaces are with simple to complex surface ornamentation. Hence, surface ornamentation serves as direct evidence for ecological interpretations.

Although there are research papers on taxonomy, systematic studies on internal character such as the normal pore system, muscle scar pattern and ocular sinuses of these micro crustaceans, papers pertaining to surface ornamentation of Ostracoda are relatively rare (Jones, 1956; Benson, 1961; Hulings and Puri, 1964; Puri, 1966; Krutak, 1972; Brasier, 1980; Annapurna and Rama Sarma, 1982; Vaidya et al., 1995; Sridhar et al., 1998 and Hussain et al., 2002). Hence, an attempt has been made to study briefly on the relationship between the sculpture in Ostracoda and grain size of the substrate based on direct observations by a Scanning Electron Microscope (SEM).

The substrate sediment texture has a control on the kind of ostracod fauna that can colonise a particular sediment type (Brasier, 1980). The texture stability of sediment comprising the substrate exerts a strong influence on marine ostracods. Smooth forms are predominant in fine-grained muds, whereas more ornamented forms are being found in coarser or in more calcareous sediment (Brasier, 1980).

In the present study, 4 types of ornate forms of Ostracoda (including smooth ones) have been noticed (Plates I – III). They are categorized as follows: **Smooth and fragile forms:** *Paracypris* sp., *Phlyctenophora orientalis*, *P*. (*Schedopontocypris*) *bengalensis* and *Xestoleberis variegata;* **Moderately calcified and pitted forms:** *Hemicytheridea bhatiai*, *H. khoslai*, *H. paiki*, *Neomonoceratina jaini*, *Neosinicythere dekrooni*, *Kalingella mckenziei*, *Kalingella* sp., *Paijenborchellina indoarabica*, and *Paijenborchellina* sp., **Fine to moderately reticulate and ridged forms:** *Cytherelloidea leroyi*, *Cytherelloidea* sp1., *Cytherelloidea* sp2., *Caudites javana*, *Hemicytheridea reticulata*, *Hemikrithe peterseni*, *Jankeijcythere mckenziei*, *Jankeijcythere* sp., *Loxoconcha cercinata*, *L. megapora indica*, *L. tekkaliensis* and *Tanella gracilis* and **Conspicuously ornate forms (typical box type, spinose and nodose etc.):** *Callistocythere flavidofusca intricatoides* and *Paijenborchellina prona*.

The surface sculptures of ostracod carapaces have direct relationship with the substrate type. Puri (1966) and Malz and Lord (1976) are of the opinion that more ornate and rather heavily calcified forms are present commonly in shallow water high-energy environments and inhabit sandy substrates in modern seas. In the Bimili backwaters and Balacheruvu tidal stream, Annapurna and Rama Sarma (1982) noticed that the genus *Phlyctenophora* occurs in sand dominated areas and not in muddy areas. They further noticed that the moderately ornamented forms like *Tanella*, *Loxoconcha*, *Paijenborchellina* and *Kalingella* occur in considerable numbers in sandy areas. Vaidya et al. (1995) observed good faunal content in the substrates consisting of medium to fine-grained sand, whereas poor occurrence was noticed in the clean, coarse-grained sand. Sridhar et al. (1998) found a greater number of species in siltysand and sandy substrates and less in fine-grained materials.

OSTRACOD CARAPACE –VALVE RATIO

The application of statistical data on Ostracoda, such as juveniles and adults, closed and isolated valves, males and females, right and left valves, and smooth and ornamented forms, etc. Besides colour variation, pyritization and predation to interpret the environment of deposition, rate of deposition and to assess the potentiality of sediments as source rocks for hydrocarbons has attained importance, during the last five decades.

Honnappa and Venkatachalapathy (1978) studied the carapace-valve ratio to interpret the rate of deposition of sediments in the Mangalore Harbour area, southwest coast of India. They found that the occurrence of open valves is much more in number than the closed one (ratio being 24:1). According to them, this is an indicative of a slow rate of sedimentation in more agitating waters. While comparing Eocene/Oligocene ostracods from southeastern Australia and India for petroleum potential indicators, McKenzie and Guha (1987) inferred a rapid rate of sedimentation through the presence of high percentage of carapaces. Sreenivas et al. (1991) found rapid rate of sedimentation in

Table 2. Distribution of Ostracod Carapaces and open valves in core sediments recovered from the Gadilam river estuary

S.No	Species Name	Carapace	Valve	Total
1	*Cytherlloidea leroyi*	8	1	9
2	*Cytherlloidea sp.1*	3	0	3
3	*Cytherlloidea sp.2*	1	0	1
4	*Hemicytheridea bhatiai*	98	2	100
5	*Hemicytheridea paiki*	35	3	38
6	*Hemicytheridea khoslai*	15	0	15
7	*Hemicytheridea reticulata*	106	4	110
8	*Neomonoceratina jaini*	3	0	3
9	*Jankeijcythere mckenziei*	144	5	149
10	*Jankeijcythere sp.*	9	1	10
11	*Neosinocythere dekrooni*	45	4	49
12	*Callistocythere flavidofusca intricatoides*	3	0	3
13	*Tanella gracilis*	85	7	92
14	*Hemikrithe peterseni*	6	1	7
15	*Caudites javana*	3	0	3
16	*Loxoconcha cercinata*	4	0	4
17	*L.megapora indica*	41	4	45
18	*L.tekkaliensis*	7	0	7
19	*Paijanborchellina prona*	10	1	11
20	*P.indoarabica*	4	0	4
21	*Paijanborchellina sp.*	2	0	2
22	*Xestoleberis variegata*	2	0	2
23	*Kalingella mckenziei*	190	8	198
24	*Kalingella sp.*	8	0	8
25	*Macrocyprina decora*	7	0	7
26	*Propontocypris (Schedopontocypris) bengalensis*	6	0	6
27	*Phyctenophora orientalis*	10	1	11
Total		**855**	**42**	**897**

Pulicat lake estuary on the basis of occurrence of a greater number of closed carapaces. Sridhar (1996) from the Palk Bay, off Rameswaram identified the carapace to valve ratio to 5:1 indicative of the fairly faster rate of sedimentation.

Hussain and Rajehswara Rao (1996) observed a greater number of carapaces than open valves along inner shelf sediments, the east coast of India. While the number is much less from the sediments from off the west coast of India. From this observation, they inferred that the rate of sedimentation is rapid on the east coast, whereas it is slow on the west coast of India, which is attributed to a greater number of streams/rivers flowing and debouching the sediments into the Bay of Bengal. Hussain et al. (2002) studied carapace and valve ratio and observed faster rate of sedimentation in the inner shelf of Gulf of Mannar, off Tuticorin, southeast coast of India. They counted four – fold occurrence of carapaces to open valves, which was attributed to the inflow of sediments through Tamirabarani River. Faster rate of deposition of the sediments favours conversion of organic matter into hydrocarbons, in reduced aquatic conditions, under optimum temperature and pressure. Ganesan and Hussain (2010) observed a faster rate of sedimentation in Tamiraparni Estuary, Punnaikayal, near Tuticorin, Tamil Nadu. Scott (2009) has inferred comparatively a faster rate of deposition of sediments in the Ennore creek, near Chennai. Kalaiyarasi (2010) has also noticed a very high rate of sedimentation in the Mullipallam creek, near Muthupet through the carapace and valve ratio of Ostracoda.

In the present work, the ratio between the carapaces and open valves has been taken into consideration for the determination of the rate of sedimentation in the study areas. The distribution of the carapaces and open valves found down core in the study area is given in Table 2. From a total of 21 sub-samples of this core, as many as 897 ostracod shells were recovered including 855 specimens are carapaces and remaining 42 specimens are open valves.

DISCUSSIONS

Of the 27 species encountered in the study area, only 4 are smooth forms while the remaining are either moderately calcified, moderately reticulate and ridged, pitted or highly ornate forms. The Gadilam river estuary is considered to be shallow and the substrate is mainly silty-sand in nature. Certain forms are slightly calcified, whereas most of the other forms are ornamented with strong reticulations, sinuosity and tubercles. These forms are *Callistocythere flavidofusca intricatoides*, *Paijenborchellina prona*, *Cytherelloidea leroyi*, *Cytherelloidea* sp1., *Cytherelloidea* sp2., *Caudites javana*, *Hemicytheridea reticulata*, *Hemikrithe peterseni*, *Jankeijcythere mckenziei*, *Jankeijcythere sp.*, *Loxoconcha cercinata*, *L. megapora indica*, *L. tekkaliensis* and *Tanella gracilis*. The silty-sand substrate carrying some organic debris yielded a good number of Ostracoda. These sediments also contain numerous other micro-organisms such as foraminifera and micro gastropods. The present material incorporates numerous carapaces and few open valves, but there are fewer dimorphic forms and juveniles. The number of carapaces, valves and sex ratio reflect ambient energy conditions.

Most of these species are indicative of typical marginal marine brackish water taxa. They frequently occur in the mangrove habitats. Their distributions in the core samples deduce a medium to low energy environmental conditions of deposition of sediments. It also reflects in the type of sediments deposited. The occurrence of taxa such as *Cytherelloidea leroyi*, *Paijenborchellina prona*, *Phlyctenophora orientalis*, *P. (Schedopontocypris) bengalensis* and *Xestoleberis variegata* represents shallow marine to neritic habitat forms (Zhao and Whatley, 1988; 1989a). Their distribution in the core may be attributed to the tidal fluctuations and deposition of the sediments due to the shallow water currents. However, the persistent occurrence of *T. gracilis* in the core indicates that this species is considered as cosmopolitan in nature (White, 1993; Ganesan and Hussain, 2010). The spatial distribution of ostracods is largely in influenced by the nature of substrate besides other environmental factors. Hence it is inferred from the microfaunal assessment of the shelf region off Chennai–Cuddalore that this area experiences well-oxygenated, alkaline, high-moderate energy conditions within a tropical environmental setting (Tabita Symphonia and Senthil Nathan, 2021). The statistical analysis is the easiest method available to understand the ostracod species diversity in an area (Hammer et al., 2001; Rajkumar et al., 2020).

CONCLUSIONS

Among 27 ostracod species identified in mangrove areas of Gadilam river estuary, the sediment ecological discussion for the following nine species namely, *H. paiki, H. reticulata, Jankeijcythere mckenziei, Kalingella mckenziei, Loxoconcha megapora indica, L. tekkaliensis, Neosinocythere dekrooni* and *Tanella gracilis* is found that they are typical brackish water ostracod fauna occur in fine to medium-grained sediments (silty-sand substrate) and they are considered as a widespread and abundant persistent taxa in the mangrove environments. The interpretation on ornamentation of ostracod carapace reflects that the forms, which are smooth and finely pitted, prefer finer substrate, while the highly calcified and ornamented forms prefer coarse-grained sediments.

In the Gadilam river estuary, it is observed that the calcium carbonate content of the sediment is one of the important parameters, which governs the population of Ostracoda, especially its vertical distribution. The calcium carbonate content is generally found to be directly proportional to the population size. The organic matter content shows lower values in the entire core collected in the Gadilam river estuary. The impact of this parameter on the distribution of ostracod fauna down the core is insignificant level.

The high numbers of ostracod diversity values are noticed in middle portion of the core samples, it is also inferred that silty-sand is the favorable substrate for the thriving and abundance of the fauna. The relatively higher diversity index encountered in the samples is attributed to the nature of substrate, silty-sand. The domination of siltysand sediments in the entire core without any textural variations may be due to the presence of uniformly more or less medium energy environmental conditions of deposition of sediments in the mangrove area of core collection.

The distribution of carapaces and open valves, in Gadilam River estuary core sediments (considering all adults and juveniles together), reveals that the carapaces outnumbered open valves, which may be concluded that relatively a very faster rate of sedimentation prevails in the core sample as the carapace to valve ratio is 20:1. In the core sediments, almost all the carapaces are light yellow and white in colour, supporting the fact that the sediments were deposited under normal oxygenated environment.

ACKNOWLEDGEMENTS

Authors are thankful to Professor and Head, Department of Geology, University of Madras for the encouragement and for providing SEM facility through the UGC-COSIST Programme.

REFERENCES

Al. Abdul Razzaq, S., Shublaq, W., AI. Sheikh, Z. and Kittaneh, W. (1983). Ecology and distribution of ostracods in Kuwait Bay. Micropaleontology, v. 2, pp.39 - 45.

Alvarez Zarikian, C.A., Nadiri, C., Alonso-García, M., Rodrigues, T., Huang, H-H, M., Lindhorst, S., Kunkelova, T., Kroon, D., Betzler, C. and Yasuhara, M. (2022). Ostracod response to monsoon and OMZ variability over the past 1.2 Myr. Marine Micropaleontology, v. 174, pp. 102105.

Anadon P., Ghetti, P., and Gliozzi, E. (2002). Sr/Ca, Mg/Ca ratios and Sr and stable isotopes of biogenic carbonates from the Late Miocene Velona Basin Central Apennines, Italy) provide evidence of unusual nan-marine Messinian conditions. Chemical Geology, v. 187, pp. 213-230.

Annapurna, C. and Rama Sarma, D. V. (1982). Sediment-ostracod relationship in the Bimili backwaters and Balacheruvu tidal stream. Proceedings. Indian Academy of Science. (Anim. Sci.), v. 91(3), pp. 297-303.

Armstrong-Altrin, J.S., Machain-Castillo, M.L., Rosales-Hoz, L., Carranza-Edwards, A., Sanchez-Cabeza, J.A., Ruíz-Fernández, A.C. (2015). Provenance and depositional history of continental slope sediments in the Southwestern Gulf of Mexico unraveled by geochemical analysis. Continental Shelf Research, v. 95, pp.15-26.

Ayala-Pérez, M.P., Armstrong-Altrin, J.S. and Machain-Castillo, M.L. (2021). Heavy metal contamination and provenance of sediments recovered at the Grijalva River delta, southern Gulf of Mexico. Journal of Earth System Science, v. 130, article no. 88.

Barik, S.S., Singh, R.K., Hussain, S.M., Tripathy, S. and Alvarez Zarikian, C.A. (2022). Spatial and seasonal distribution of Ostracoda in a lagoonal environment along the northeastern coast of India: Implications to assess coastal ecology and paleoenvironment. Marine Micropaleontology, v. 174, no. 102082.

Benson, R.H. (1961) Ecology of ostracod assemblages, In: Treatise on Invertebrate Paleontology, Part Q, Arthropoda 3, Ostracoda, Moore, R.C. (Ed.), Geological Society of America, pp. Q_{56}-Q_{63}.

Boomer, I. and Eisenhauer G., (2002). Ostracod faunas as palaeoenvironmental indicators in marginal marine environments. In: J. Holmes and A. Chivas (Eds.) The Ostracoda: Applications in Quaternary Research, D.C. v. 131, pp. 135–149, American Geophysical Union, Washington

.Brasier, M. D. (1980). Microfossils, George Allen and Unwin Ltd., London, pp. 193.

Eagar S.H., (1999). Intraspecific variation in the shell ornamentation of benthic Ostracoda (Crustacea) from Kiribati, Pacific Ocean. Ocenologica Acta, v. 22, pp. 603-608.

Eagar, S. (2000). Ostracoda in detection of sewage discharge on a Pacific Atoll. In R. Martin (ed.), Environmental Micropalaeontology, Kluwer, New York. Pp. 151-165.

Ganesan, P. and Hussain, S.M. (2010). Distribution of Recent benthic Ostracoda in Tamiraparni Estuary, Punnaikayal, near Tuticorin, Southeast Coast of India – Implications on microenvironment. Gondwana Geological Magazine (ISSN 0970-261 X), Special Issue on Applied Micropaleontology. (Eds. Kundal and Humane), v. 25, pp. 103-114.

Ganesan.P (2006). Systematics, Distribution and Ecology of Recent Ostracoda in Tamiraparani Estuary and Adjoining Shelf Area Off Punnaikayal, Tuticorin, Tamil Nadu, Southeast Coast of India Ph.D Thesis, University of Madras, Chennai, India.

García-Madrigal, A., Ruiz-Angulo, A. and Mischke, S. (2022). Intertidal Ostracoda from Fossvogur and Kópavogur bays (SW Iceland): Diversity and distribution. Journal of Sea Research, v. 190, article no. 102303.

Gaudette, H. E., Flight, W. R., Toner, L. and Folger, D. W. (1974). An inexpensive titration method for the determination of organic carbon in recent sediments, Journal of Sedimentary Petrology, v. 44, pp. 249-253.

Hartmann, G. and Puri, H.S. (1974). Summary of Neontological and Palaeontological classification of Ostracoda. Mitt. Hamburg. Zool. Mus. Institute, v. 70, pp. 7-73.

Hammer, Ø., Harper, D.A., and Ryan, P.D. (2001). PAST: Paleontological statistics software package for education and data analysis. Palaeontologia electronica, v. 4(1), no. 9.

Honnappa and Venkatachalapathy, V. (1978). Paleoecological and ecological interpretations of sediments of Mangalore Harbour area, west coast of India, on the basis of colour variation of ostracod shells, Current Science, v. 47(20), pp. 772-773.

Hulings, N. C. and Puri, H. S., (1964). The ecology of shallow water ostracods of the west coast of Florida, Stazione Zoology, Napoli Publication, supp., v. 33, pp. 308-343.

Hussain, S. M. (1992). Systematics, ecology and distribution of Recent Ostracoda from the Gulf of Mannar, off Tuticorin, Tamil Nadu, Ph.D. thesis, 218p, submitted to the University of Madras.

Hussain, S.M. and Rajeshwara Rao, N. (1996). Faunal affinity, zoogeographic distribution and review on Recent Ostracoda from the east and west coasts of India. Bulletin Pure Applied Science, v. 15 (1), pp. 37-50.

Hussain, S.M., Manivannan, V. and Ragothaman, V. (1997). Sediment-Ostracoda relationship in the Gulf of Mannar, off Tuticorin, east coast of India. Jour. Nepal Geological Society, v. 15, pp. 33-37.

Hussain, S.M., Mohan, S.P and Jonathan, M.P (2010). Ostracoda as an aid in identifying 2004 tsunami sediments: An example from SE coast of India. Natural Hazards, v. 55, pp. 513-522.

Hussain, S.M., Mohan, S.P. and Manivannan, V. (2002). Microenvironmental inferences of Recent Benthic Ostracoda, from Gulf of Mannar, off Tuticorin, east coast of India; In: Proceedings. National Seminar Mazaine. Natural Resources, Sankara Pitchaiah, P.(ed)., 23-43, Nagarjuna University.

Jones, D. (1956). Introduction to Microfossils. Harper and Brothers, Publishers, 406p, New York. Journal of Palaeontological Society of India, v. 20, pp. 366-381.

Joy, J.A and Clark, D.L. (1977). The distribution, ecology and systematics of the benthic ostracods of central Arctic Ocean. Micropaleontology, v. 23 (2), pp. 129-154.

Kalaiyarasi. (2010). A study on the distribution of recent ostracoda and sediment geochemistry of Mullipallam creek (Muthupet area), Nagapattinam and Thiruvarur district, Tamil Nadu, southeast coast of India, Ph.D Thesis, University of of Madras, Chennai, India.

Krumbein, W. C. and Pettijohn, F. J. (1938). Manual of Sedimentary Petrography,166-168, D. Appleton Century Co. Inc, 549p, New York.

Krutak, P.R (1972). Some relationship between grain size of substrate and carapace size in modern brackish water Ostracoda. Micropaleontology, v. 18 (2), pp. 153-159.

Malard F, Mathieu J, Reygrobellet J-L, Lafont M, (1996). Biomonitoring groundwater contamination. Application to a karst area in Southern France. Aquatic Science, 58, 2, pp. 159–187.

Malz, H. and Lord, A. (1976). Gammacythere n. g. (Ostracoda) and its occurrence in Lower Jurassic of NW Europe. Lethaia, v. 57 (416), pp. 249-263.

Matzke-Karasz, R., Smith, R.J. (2022). A review of exceptional preservation in fossil ostracods (Ostracoda, Crustacea). Marine Micropaleontology, v. 174, no. 101940.

McKenzie, K.G. and Guha, D.K. (1987). A comparative analysis of Eocene/Oligocene boundary Ostracoda from south-eastern Australia and India with respect to their usefulness as indicators of petroleum potential. Trans. Royal Society S. Australia; III, pt.l, 15-23.

Mosslacher, F. (2000). Sensitivity of groundwater and surface water crustaceans to chemical pollutants and hypoxia: implications for pollution management. Archiv fur Hydrobiologie, v. 149(1), pp. 51–66.

Mostafawi, N. (2001). How severely was the Persian Gulf affected by oil spills following the 1991 Gulf war? Environmental Geology, v. 40, pp. 1185-1191.

Piper, F.B. (1947). Soil and plant analysis. University of Adelaide Press, 368p, Aldelaide.

Puri, H.S. (1966). Ecologic and distribution of Recent Ostracoda, Proc. Symp. Crustacea, Pt.I, Marine Biology Association. India, pp. 457-495, Mandapam.

Ramos-Vázquez, M.A., Armstrong-Altrin, J.S. (2021a). Provenance of sediments from Barra del Tordo and Tesoro beaches, Tamaulipas State, northwestern Gulf of Mexico. Journal of Palaeogeography, v. 10(20), pp. 1-17.

Rajkumar, A., Hussain, S. M., Nishath, N.M., Dewi, K., Sivapriya, V. and Radhakrishnan, K. (2020). Recent ostracod biodiversity from shelf to slope sediments of Gulf of Mannar, India: Ecologic and Bathymetric implications. Journal of the Palaeontological Society of India, v. 65(1), pp. 73-80.

Ravi, G. (1999). Taxonomy, Distribution and ecology of recent ostracoda from the Bay of Bengal, Off Karikkattukuppam, south of Chennai, Tamil Nadu, India. Unpublished Ph.D. thesis, University of Madras, Chennai.

Scott, A. (1905). Report on the Ostracoda collected by Professor Herdman at Ceylon in 1902, In: Report to the Government of Ceylon on the Pearl Oyster Fisheries of the Gulf of Mannar, Pt.3, 22, pp. 365-384.

Scott Immanuel Dhas, C. (2009). Sediment geochemistry, distribution and ecology of recent ostracoda from the Ennore Creek, Chennai, Tamil Nadu, Southeast coast of India, Ph.D Thesis, University of Madras, Chennai, India.

Sebastian, S., George, R. and Damodaran, K.T. (1990). Studies on the distribution of sediments of Jaigad, Amdwah and varvada bays, Maharashtra. Journal of Geological Society, India, 49, 567.

Sreenivas, K., Raju, B.N. Honappa and Reddi, K.R. (1991). Ostracoda in the estuarine sediments, Pulicat Lake estuary, east coast of India. Journal of Geological Society. India, v. 37(5), pp. 492-499.

Sridhar, S. G. D. (1996). Ecology, distribution and systematics of Recent Ostracoda from the Palk Bay, off Rameswaram, Tamil Nadu, Published Ph.D. thesis, University of Madras, Chennai.

Sridhar, S.G.D., Hussain, S.M., Kumar, V. and Periakali, P. (1998). Benthic ostracod responses to sediments in the Palk Bay, off Rameswaram, south-east coast of India. Journal of Indian Association Sedimentology, 17 (2), pp. 187-195.

Subba Rao, M. (1960). Organic matter in marine sediments off east coast of India. Bulletin. American Association of Petroleum, v. 44 (10), pp. 1705-1713.

Subba Rao, M. and Mahadevan, C. (1957). Distribution of calcium carbonate in the marine sediments off Visakhapatnam. Geology Department, Andhra University, Waltair, pp.149-152.

Tabita Symphonia, K and Senthil Nathan D. (2021). Recent marine Ostracoda from East Indian shelf-slope sediments and their response to marine hydrodynamics. Journal of Earth System Science, v. 130, no. 195 //doi.org/10.1007/s12040-021-01685-0.

Trefethen, J. M. (1950). Classification of sediments. American Journal of Science, v. 248, pp. 55-62.

Vaidya, A.S. and Mannikeri, M.S. (1994). Faunal affinity and zoogeography of Recent marine Ostracoda from Karwar, west coast of India. Current Science, v. 67 (9 & 10, 10 & 25), pp. 735-738.

Vaidya, A.S., Mannikeri, M.S. and Chavadi, V.C. (1995). Some relationship between the bottom sediments and Recent Ostracoda: A case study. Journal Indian Association of Sedimentology, v. 14, pp. 83-88.

Venkata Rao, T. and Subba Rao, M. (1974). Recent foraminifera of Suddagedda Estuary, east coast of India. Micropaleontology, 20 (4), pp. 398-4l9.

Venkata Rao, T. and Subba Rao, M. (1976). Recent foraminifera of Chipurupalle Stream, east coast of India. Marine Science, v. 4, pp. 29l-307.

Whatley, R.C. and Quanhong, Z. (1987). Recent Ostracoda of the Malacca Straits. Pt.1, Revista Espanola de Micropaleontologia; XIX (3), pp. 327-366.

Whatley, R.C. and Quanhong, Z. (1988). Recent Ostracoda of the Malacca Straits. Pt.II, Revista Espanola de Micropaleotologia; XX (1), pp. 5-37.

Witte, L. (1993). Taxonomy and biogeography of West African beach ostracods, proceeding, Koninkl. Nederl. Akad. 39, 13-105, Wetensch.

Yassini, I. and Jones, B. G. (1995). Recent Foraminifera and Ostracoda from Estuarine and Shelf Environments on the Southeastern Coast of Australia, University of Wollongong Press, 484 p, Wollongong.

Zhao Q and Whatley, R. (1988). The genus Neomonoceratina (Crustacea: Ostracoda) from the Cainozoic of the West Pacific Margins. Acta Oceanologica Sinica, v. 7 (4), pp. 562-577.

Zhao Q and Whatley, R. (1989a). Recent Podocopid Ostracoda of the Sedili River and Jason Bay, south-eastern Malay Peninsula. Micropaleontology, v. 35 (2), pp. 168-187.

JOURNAL INDIAN ASSOCIATION OF SEDIMENTOLOGISTS ISSN NO 2582 – 2020
Vol. 40, Issue II, 2023, pp. 40-48
DOI: https://doi.org/10.51710/jias.v40iII.326

Landslide susceptibility assessment along the National Highway-244 from Batote to Doda, J & K, India: A study based on the Frequency Ratio Method

Yudhbir Singh[1], **Muzamil Liaqat**[2], **Shifali Chib**[1*], **Bashir Ahmad Lone**[1], **Sumit Johar**[1], **and Arvind Bhutiyal**[1]
[1]Department of Geology, University of Jammu
[2]Department of Geography, Jamia Millia Islamia
E-mail Address: shifali.chib@jammuuniversity.ac.in

ABSTRACT

The National Highway-244 is highly susceptible to landslide occurrences, frequently resulting in road blockades and causing significant hardships for the local population. These landslides pose a threat to human lives, property and the environment, leading to substantial losses. In this study, an attempt has been made to carry out landslide susceptibility assessment through frequency ratio method along the National Highway-244 utilizing GIS and statistical computations. It considers eight parameters, which include topographical (slope, slope aspect, slope curvature, hill shade, and relief), anthropogenic (distance to road and distance to river) and geological parameters that mostly influence the occurrence of landslides in the area under investigation. The present study focuses only along National Highway-244 and data has been gathered from field visits and secondary sources. The results of the study inferred that the area under investigation falls into different susceptibility zones, namely very high, high, moderate, low, and very low, covering approximately 15%, 31%, 27%, 19%, and 8%, respectively of the total area. This study reveals that a considerable proportion, around 73%, of the study area falls within very high to moderate susceptibility zones. The conclusions drawn from this study hold significant implications for stakeholders and also provide valuable insights for future planning and infrastructure development, enabling them to make informed decisions. By considering the susceptibility zones identified in this study, stakeholders can implement appropriate measures to mitigate the impact of landslides, ensuring the safety and stability of the region.

Keywords: Landslide susceptibility, National Highway-244, Frequency ratio, GIS.

INTRODUCTION

The term landslide in our national language has been referred as “Bhuskhalan” where the word ‘Bhu’ stands for “earth” and the word “skhalan” stands for “movement” which undoubtedly articulates that it is the movement of earth under the influence of gravity. Landslide phenomenon is one of the most widely spread natural hazard in India particularly in hilly regions and along road networks. Every year, India experiences a considerable number of landslides events, particularly during rainy seasons or incessant rainfall, inflicts huge losses in terms of life and property (Singh and Bhat, 2010, 2011). The problem of landslides is of grave concern, especially during monsoon season as it seriously affects the livelihood of people by disrupting various networks, which are very critical for sustaining daily life. Landslide events are primarily triggered by heavy precipitation, earthquakes and anthropogenic activities (Bhat et al., 2002; Sangra et al., 2017; Hussain et al., 2018; Singh et al., 2018). The thorough understanding about the frequency, character, pattern and size of slope plays a decisive role in the effective management of landslide hazard. Landslide is one of the most frequent natural disasters which resulted in vast amounts of destructions (infrastructure, property, and lives) around the world. According to Gyawali et al., (2021) the highest number of fatalities due to landslides in recent years has been reported from China (695) followed by Indonesia (465), India (352), Nepal (168), Bangladesh (150) and Vietnam (130). An estimated 89.6% of all fatalities across the world were brought on by landslides triggered by heavy rain (Petley, 2008). With regard to understanding, evaluating and investigating landslide hazards, this concept emphasizes the necessity of anticipating both location-based spatial probability and time/frequency-based temporal probability (Tien et al., 2012; Hussain et al., 2019).

Landslide susceptibility (LS) assessment provides a relative estimation of the spatial occurrences of landslides in a mapping unit, which aids in quantifying the volume or area and the spatial likelihood of a landslide event depending on the geology of the area. It involves the integration of various geospatial data and factors that contribute to landslide occurrences. It aims to identify areas with a higher potential for landslides, allowing for better understanding and management of landslide hazards. In landslides susceptibility mapping (LSM), frequency ratio method is one of the most widely used technique among bivariate statistical procedures (Chimidi et al., 2017; Hamza and Raghuvanshi, 2017; Girma et al., 2015; Lee and Min,

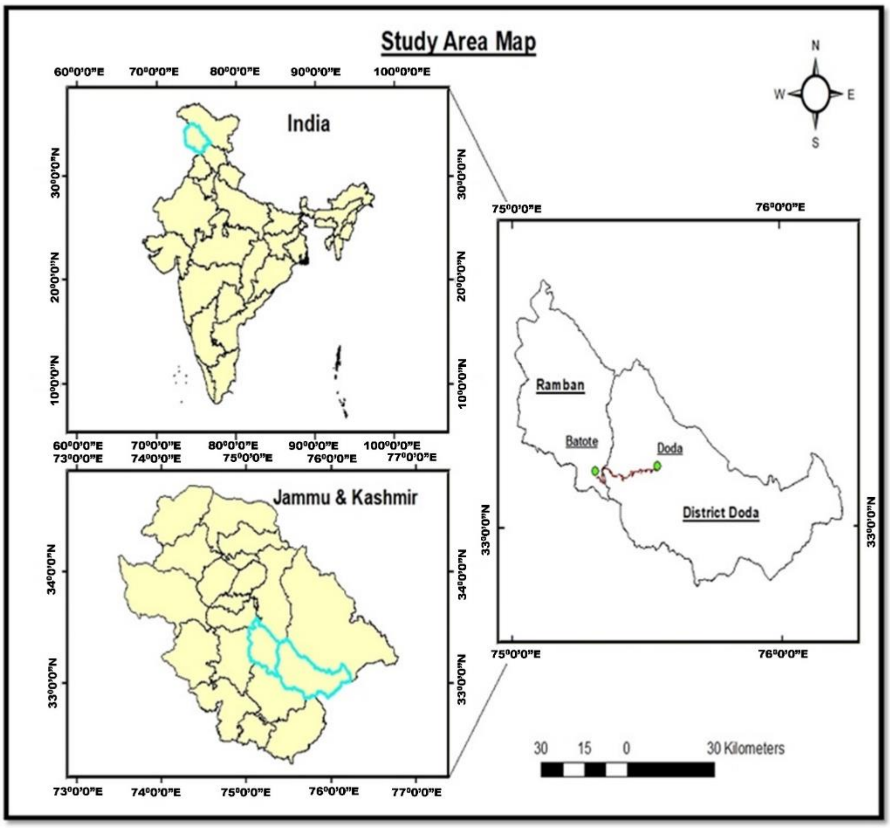

Figure 1. Location map of the study area (divaGIS).

2001). This approach makes use of the relationships between the spatial distribution of previous landslides in the area and that of relevant contributory factors (Lee, 2005; Pradhan and Lee, 2009; Akgun et al., 2012; Girma et al., 2015; Moung-Jin et al., 2014; Chimidi et al., 2017). Landslide susceptibility mapping, a significant approach (Chen et al., 2018) involves the result of combining all factor maps based on their weight for classifying the landslide susceptibility index into several susceptibility categories. The frequency ratio technique for landslide susceptibility mapping has been employed by various authors (Yilmaz, 2009; Fayez et al., 2018; Khan et al., 2019; El Abidine and Abdelmansour, 2019) in their studies to analyze vulnerability and to assess the association of different factors and landslide occurrences. Several studies (Gabet et al., 2004; Kanungo et al., 2006; Guzzetti et al., 2007; Alvioli et al., 2014) have focused on creating landslide susceptibility maps in mountainous regions, including the Himalayas to understand the causes of landslides. The frequency ratio value greater than one indicates a significant correlation of the factor class with landslide occurrences, while as the ratio less than one suggests a reduced correlation (Lee and Min, 2001; Girma et al., 2015; Chimidi et al., 2017). Shahabi et al., (2012) also conducted a landslide susceptibility study in Iran using variables such as slope, slope aspect, distance to road, distance to drainage network, distance to fault, land use, precipitation, elevation and geological factor. Overall, landslide susceptibility assessment has witnessed significant advancements, with various models and techniques being employed worldwide to understand and predict landslide occurrences based on causal factors and their associations. The present study attempted to classify the study area into different susceptibility categories using frequency ratio model.

STUDY AREA

The present study is confined between Batote and Doda sector of the National Highway-244 (NH-244) which falls in the Outer and Lesser

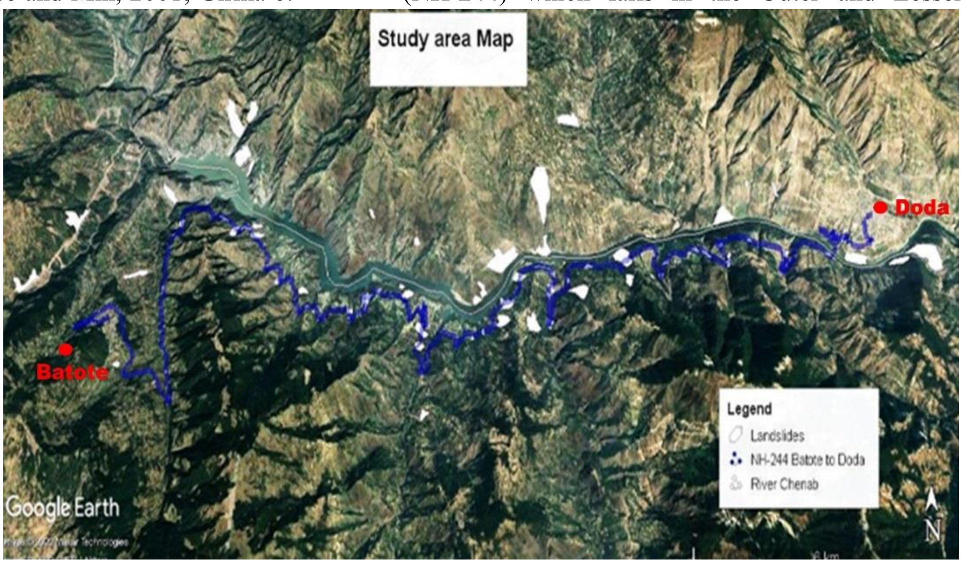

Figure 2. Google Earth image showing landslide locations of the study area (Google earth Pro).

Himalaya tectonic zones of the northwestern Himalaya. The proposed study area covers parts of Batote (latitudes 33°07'18.46"N and longitudes-75°19'17.66"E) and Doda (latitudes 33°08'45.53"N and longitudes 75°32'52.81"E) within Ramban and Doda districts of Jammu and Kashmir (Figs. 1 and 2). In this belt, about 90% of the region is made up of structural hills, which are mostly inhabited by Salkhalas, Jutogh group (Rocks of Panjal Thrust zone in J&K which includes Bhimdasa Formation, Sincha Formation etc.) and granites. The area is characterized by prominent structural units i.e., Murree thrust and Panjal thrust.

MATERIALS AND METHODS

In this study, three sets of key parameters (topographical, anthropogenic and geological) that influence the origin of landslides were considered for analysis. The topographical parameters include slope, slope aspect, slope curvature, hill shade, and relief. On the other hand, the anthropogenic factors considered are the distance to road and the distance to river and the third parameter is geology of the study area. These parameters were analyzed to determine their respective influences on the origin of landslides. The methodology employed for landslide susceptibility mapping includes GIS and statistical calculations involves several key steps. Initially, a landslide inventory is prepared by creating polygons to represent the precise locations of landslides. These layers were transformed into a raster format for each factor considered for investigation and layers are resampled into uniform pixel size. To facilitate analysis, the raster layers are categorized based on specific themes and reclassified accordingly. To analyze the relationship between landslides and the factors, the tabulated area tool in the Arc-GIS toolbox has used to obtain a table for each factor after reclassification. Then overlay and clip operations are employed to calculate pixel statistics of landslides within each class of a particular factor. The weight of each factor is determined based on the landslide inventory. These weights are then used to combine all thematic layers, resulting in the creation of the Landslide Susceptibility Index (LSI) map. Finally, the study region is divided into five relative landslide susceptibility zones: Very low, low, moderate, high, and very high.

LANDSLIDE SUSCEPTIBILITY ASSESSMENT USING FREQUENCY RATIO METHOD

The important aspect of landslide susceptibility involves the combination of several causative factors based on their weight, which are determined by various statistical approaches. In present study, the frequency ratio (FR) approach has been chosen as the primary analysis method for conducting a preliminary probabilistic assessment. This approach is favored due to its mathematical simplicity and relatively quick evaluation time. The quantitative relationship between landslide occurrences and other causal factors can be described as a frequency ratio (Pradhan et al., 2012). The frequency ratio value greater than 1 indicates a good correlation, while values lower than 1 indicates a low correlation (Lee and Min, 2001; Girma et al., 2015; Chimidi et al., 2017). The formula used for calculating the Frequency Ratio is as follows:

$$FR = \frac{Nlp / N}{Nlpi / N_l}$$

Where, Nlp = the number of pixels in each landslide conditioning factor class;
N = the total number of pixels in the research region;
Nl = total number of landslide pixels in the study region and
Nlpi= number of landslide pixels in each landslide conditioning factor class.

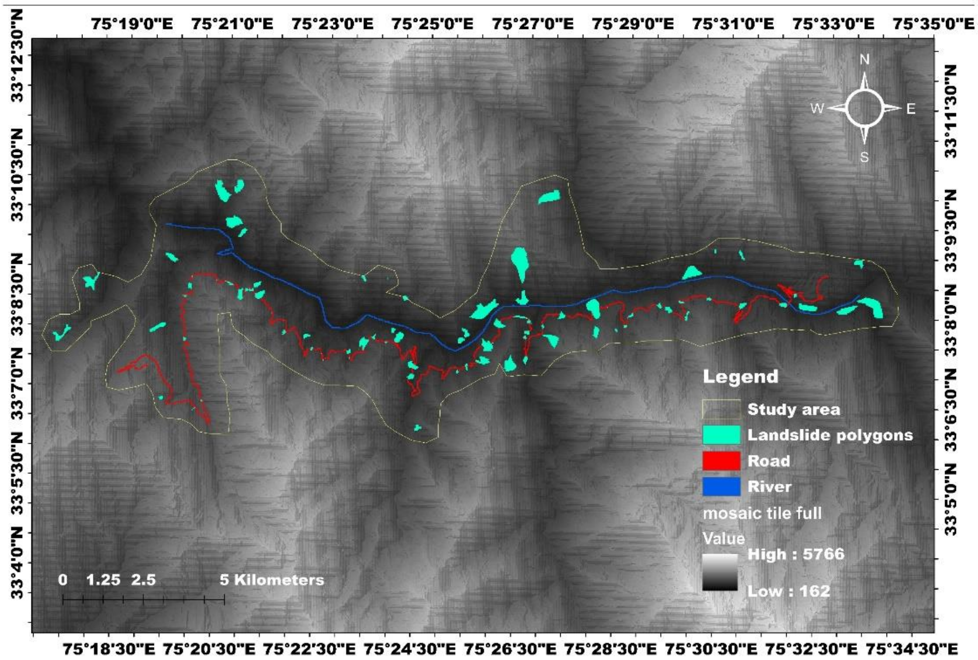

Figure 3. Landslide inventory of the study area.

LANDSLIDE INVENTORY

The landslide inventory generally refers to a comprehensive record of land sliding events within a specific area. It includes the locations, characteristics, and attributes of individual landslides, providing valuable information for landslide susceptibility and hazard assessment studies. This is considered as a base for determining a site's susceptibility to landslides. For the purpose of forecasting future landslides, the data's accuracy greatly depends on past and present landslides (Reichenbach et al., 2018). The landslide inventory (Fig. 3) offers insights into the many types of landslides, their failure mechanisms, their locations, their triggers, as well as their frequency of occurrence, density and damage (Van Westen et al., 2008). In this study, a comprehensive landslide inventory map was developed by identifying and mapping a total of 150 landsliding events. Field visits were conducted to verify the accuracy and validity of certain locations within the inventory.

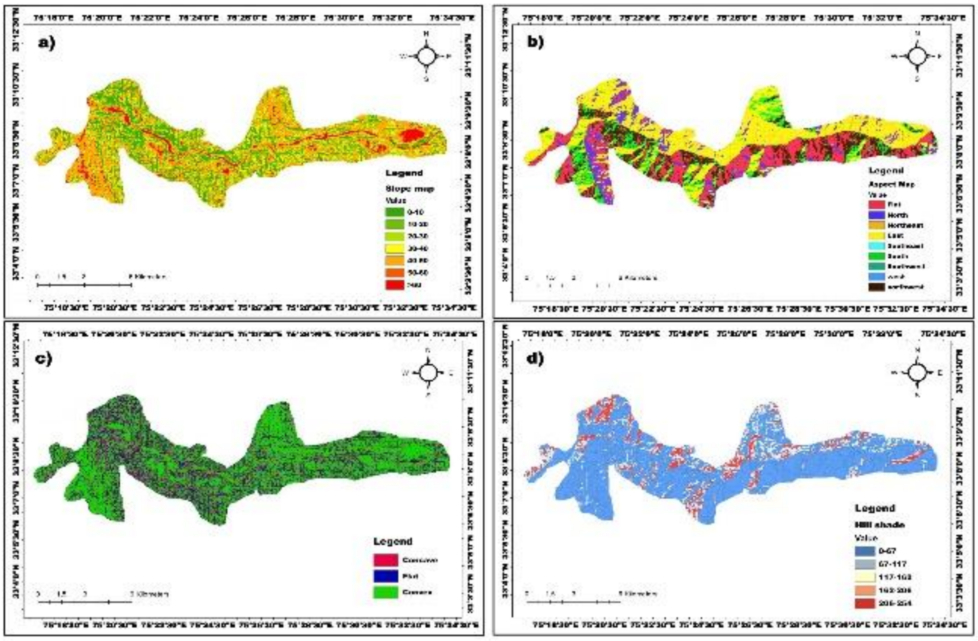

Figure 4 (a-d). Showing conditioning factors of the study area: a) Slope map, b) Aspect map, c) Curvature map, and d) Hill shade map.

RESULTS AND DISCUSSION

The frequency ratio (FR) is a statistical method used to assess the relationship between landslide occurrences and other causative factors. It involves calculating the ratio of the frequency of landslides within specific categories of a particular factor to the frequency of landslides within the entire study area. The frequency ratio approach is being utilized in this study in order to quantify the association between landslides and various causal factors (Fig. 4), aiding in the assessment of landslide susceptibility. The frequency ratio values obtained for the various conditioning factors are given in Tables 1 and 2. The stronger link between the parameters and the likelihood of a landslide is represented by a higher value of FR (>1).

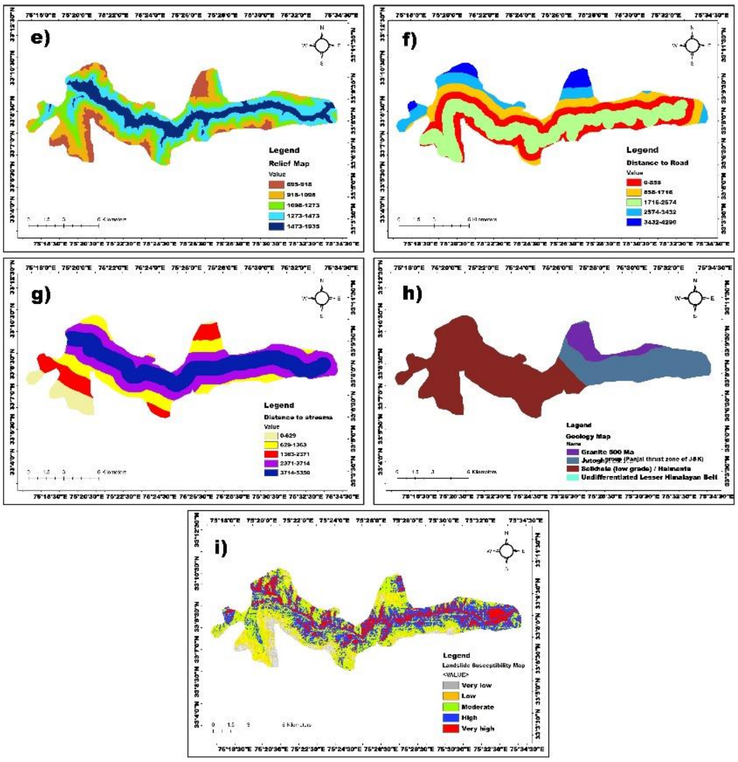

Figure 4 (e-i). Showing conditioning factors of the study area: e) Relief map, f) Distance to road map, g) Distance to river map, h) Geology map, and i) Landslide susceptibility zonation map.

The results reveal important insights into the susceptibility of landslides based on various factors. In slope sub-categories, the highest frequency ratio value (3.305) is observed in the range of 0-10^0, indicating the highest possibility of landslides (Fig. 4a). The high probability of landslides within 0-10^0 slope range can be attributed to poor geological conditions, increased anthropogenic activities which effect natural drainage system of the area and result soil erosion, particularly during incessant rainfall. These factors jointly emphasize the highest probability of landslides occurrences within 0-10^0 of slopes in the area. On the other hand, the slope sub-categories 50^0-60^0 and >60^0 exhibit the lowest frequency ratios (0.476 and 0.145) respectively indicating low possibilities of landslides. Additionally, slope sub-categories 10^0-20^0, 20^0-30^0, 30^0-40^0, and 40^0-50^0 also have frequency ratios greater than 1 (2.109, 2.108, 1.554, and 1.028), suggesting a significant risk of landslide occurrences in those areas as well. The slope map of the study area inferred that flat regions (2.10) have greatest impact on landslide occurrence (Fig. 4b). This suggests that areas with flat slopes are more susceptible to landslides compared to other slope aspects. The north aspect (1.55) suggests that it has a notable influence on landslide occurrence within the study area. North-facing slopes receive less direct sunlight, leading to reduced evaporation and potentially increased moisture retention. This increased moisture content can contribute to soil saturation and reduced stability, making north-facing slopes more susceptible to landslides. Similarly, the northeast and southeast aspect indicating moderate to low impact on landslide occurrence. The slope curvature map indicates highest frequency ratio value for flat curvature (1.11), which suggest that it has the greatest impact on landslides (Fig. 4c). The absence of slope in flat areas can contribute to the accumulation of water and instability of the soil, increasing the likelihood of landslides. The convex curvature (0.96) on the other hand has a lower frequency ratio compared to flat curvature but still shows a significant impact on landslides whereas, convex terrain features are characterized by slopes that curve outward or away from the observer. These areas may experience landslides due to the concentration of water and increased erosion along the convex slopes, leading to instability. The concave curvature has the lowest frequency ratio (0.756) among the three curvatures mentioned. However, it still demonstrates a moderate impact on landslides. The hill shade results inferred that the smaller hill shade range has a more pronounced influence on landslide occurrence compared to the greater hill shade range (Fig. 4d). The relief map of study area suggests that areas with low relief have greater influence on landslide occurrence due to water accumulation, reduced soil stability, and increased pore pressure. In contrast, areas with high relief have lower landslide susceptibility due to enhanced drainage, reducing the chances of landslides (Fig. 4e). The distance to road map of the study suggests that farthest distance from road (3432-4290 m) with a frequency ratio value (1.821) has highest impact on landslide occurrence (Fig. 4f). This may be attributed to factors such as limited accessibility for maintenance and monitoring, potentially leading to increased instability. The areas in closer proximity to the road indicate the lowest impact on landslide occurrence. This may be due to better accessibility, maintenance, and monitoring, leading to reduced landslide susceptibility compared to areas farther from the road. Similarly, the distance to river map of the study area suggests that areas in close proximity to the river within 0-629 m range are highly susceptible to

Table 1. The Frequency Ratio (FR) values obtained for slope, Aspect and Curvature parameters

S. No.	Parameters	Classes	Class Pixels	Class Pixels %	Landslide Pixels	Landslide Pixels %	FR
1.	Slope	0-10^0	8526	8.220	105	2.487	3.305
		10^0-20^0	16479	15.887	318	7.532	2.109
		20^0-30^0	21187	20.426	409	9.687	2.108
		30^0-40^0	22828	20.008	598	14.164	1.554
		40^0-50^0	19072	18.387	755	17.883	1.028
		50^0-60^0	11288	10.882	965	22.856	0.476
		>60^0	4348	4.192	1072	25.391	0.165
Total			103728		4222	100	10.745
2.	Aspect	Flat	15843	15.274	307	7.271	2.100
		North	13062	12.593	342	8.100	1.555
		Northeast	11516	11.102	385	9.119	1.217
		East	9535	9.192	396	9.379	0.980
		Southeast	11565	11.149	441	10.445	1.067
		South	10440	10.065	447	10.587	0.951
		Southwest	9314	8.979	481	11.393	0.788
		West	9309	8.974	645	15.277	0.587
		Northwest	13144	12.672	778	18.427	0.688
Total			103728		4222	100	9.933
3.	Curvature	Concave	17450	16.424	917	21.720	0.756
		Flat	65018	61.196	2325	55.069	1.111
		Convex	23777	22.379	980	23.212	0.964
Total			106245		4222	100	2.831

landslides (Fig. 4g). This may be due to river erosion, water saturation and high pore pressure which decreases slope stability and increased landslide risk in these areas. In contrast, the areas farther away from the river are less prone to landslides. These areas may experience less direct influence from river-related processes, such as erosion or fluctuating water levels, resulting in reduced landslide susceptibility. The geological set-up of the area also plays a significant role in landslides. The Jutogh group (has a higher FR value of 0.0565, followed by the Salkhalas with a FR value of 0.0338, and the granites with a FR value of 0.0269 (Fig. 4h). Because just a small portion of the research region is located in the undifferentiated lesser Himalayan belt, so it does not have a significant impact. These observations indicate a clear relationship between various parameters and landslide vulnerability. However, it is essential to consider these observations within the context of the specific study area and the limitations of the frequency ratio method, as landslide susceptibility is influenced by various factors beyond these parameters such as geology, rainfall, anthropogenic activities and land cover to gain a comprehensive understanding of landslide susceptibility.

Table 2. The Frequency Ratio (FR) values obtained for Hill shade, Relief, Distance to road, Distance to river.

S. No.	Parameters	Classes	Class Pixels	Class Pixels %	Landslide Pixels	Landslide Pixels %	FR
4.	Hill shade	0-67	8962	8.708	928	22.006	2.527
		67-117	17625	17.125	889	21.081	1.231
		117-162	22010	21.386	764	18.117	0.847
		162-206	26689	25.932	736	17.453	0.673
Total			102919		4217	100	6.073
5.	Relief	695-918	20894	19.666	1112	26.313	1.338
		918-1098	29509	27.774	1423	33.673	1.212
		1098-1273	25133	23.656	1081	25.580	1.081
		1273-1473	19844	18.678	528	12.494	0.669
		1473-1935	10865	10.226	82	1.940	0.190
Total			106245		4226	100	4.490
6.	Distance to road	0-858	41127	38.691	1713	40.554	1.048
		858-1716	29740	27.978	923	21.851	0.781
		1716-2574	17347	16.320	614	14.536	0.891
		2574-3432	12291	11.563	555	13.139	1.136
		3432-4290	5791	5.448	419	9.920	1.821
Total			106296		4224	100	5.677
7.	Distance to river	0-629	36202	34.058	1871	44.295	1.301
		629-1363	33181	31.216	1461	34.588	1.108
		1363-2371	17895	16.835	383	9.067	0.539
		2371-3714	11181	10.519	401	9.493	0.903
		3714-5350	7837	7.373	108	2.557	0.347
Total			106296		4224	100	4.197
8.	Geology	Undifferentiated Lesser Himalayan belt	23	0	0	0.000	0
		Granite	9143	0.086	246	0.058	0.0269
		Salkhala	63266	0.624	2239	0.530	0.0338
		Jutogh group	30804	0.290	1739	0.412	0.0565
Total			106296		4224	100	0.1171

Landslide Susceptibility Index (LSI) is a quantitative parameter used in landslide susceptibility analysis. It is a numerical value assigned to different locations within a study area to represent their relative susceptibility to landslides. The LSI is typically derived through a combination of various factors and variables that contribute to landslide occurrence, such as topography, geology, slope, land cover, rainfall, and historical landslide data. Landslide susceptibility mapping based on the LSI allows for the identification and delineation of areas with different levels of landslide hazard. The creation of a landslide susceptibility map of the study area involves dividing the Landslide Susceptibility Index (LSI) into distinct classes that define different levels of susceptibility. This is achieved by applying the following equation to assign each LSI value to a specific class representing its susceptibility level.

LSM_{Fr} = Total sum of (weight* factor map)

The landslide susceptibility index values obtained help in the categorization of the area under investigation into five zones: very low, low, moderate, high, and very high (Fig. 4i). The area covered by each class of landslide susceptible map using the FR approach is presented in Table 3. The results of the study inferred that study area falls into five susceptibility zones, namely very high, high, moderate, low, and very low. The distribution of these classes in terms of the area's percentages has been illustrated through a pie chart (Fig. 5a). It revealed that the very high and high landslide susceptibility zones account for 15% and 31% of the total area, respectively. The high-susceptibility zone dominates with the highest percentage (31%). Significantly, the study reveals that a considerable proportion, around 73%, of the study area falls within susceptibility zones ranging from very high to moderate. The overview of the distribution of landslide susceptibility classes and the general relationship between landslide likelihood and each susceptibility class, emphasizing the significant presence of the high-susceptibility zone within the study area (Fig. 5b) is also established. The landslide susceptibility results of the study area have been quantified and categorized into different zones, indicating varying levels of risk.

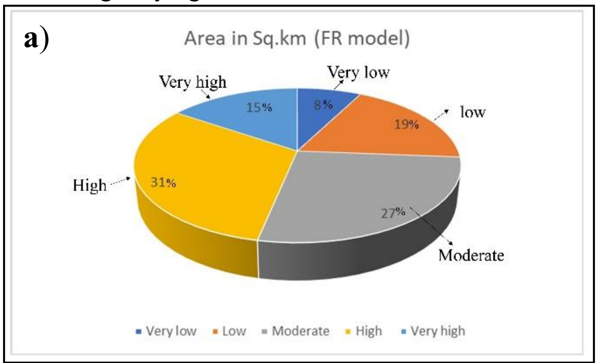

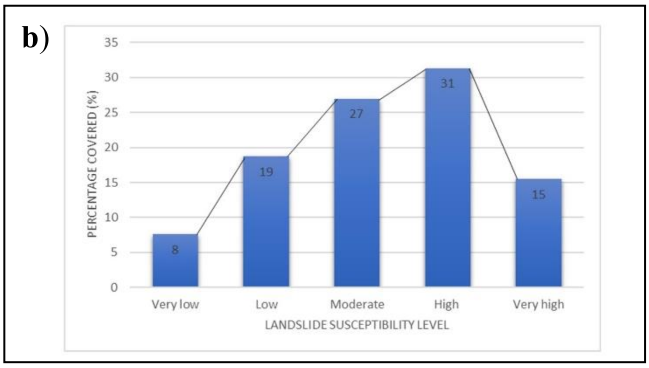

Figure 5 (a-b). a) Showing % age distribution of landslide susceptibility zonation using FR and b) Relationship between % age of areas of landslide and susceptibility level

Table 3. Landslide susceptibility zonation of the study area using frequency ratio approach.

S. No.	Category	Area in sq. km	Percentage (%)
1	Very Low	7.005	8
2	Low	17.313	19
3	Moderate	24.975	27
4	High	28.980	31
5	Very High	14.315	15
Total		92.587	100

CONCLUSIONS

The study utilized eight conditioning factors, including slope, slope aspect, slope curvature, hill shade, relief, distance from road, distance to river, and geology along with landslide inventory, to determine the Landslide Susceptibility Index (LSI) within a GIS environment. The model used in this study predicts the landslide susceptibility along the national highway-244 (NH-244) from Batote to Doda Road stretch with a reasonable level of accuracy. The findings of the present study suggest that anthropogenic activities in conjunction with factors like slope morphometry, geology, and rainfall play a key role influencing landslide occurrences. The growing population has led people to unplanned activities on slopes which increases the vulnerability to landslides. The susceptibility maps derived from this study can serve as essential tools for future construction projects, aiding in the planning and management of the area to mitigate the risk to life and property. High and very high susceptibility zones require additional attention regarding engineering, geological and geotechnical considerations, while low susceptibility zones generally present a safer environment for construction activities. It is crucial to urgently address the risk of landslides particularly in high and very high susceptibility locations, to prevent disruptions along Batote to Doda highway-244, which can result in significant inconvenience, financial losses, and human casualties.

ACKNOWLEDGEMENTS

We are grateful to the Department of Geology University of Jammu for providing the infrastructure for this research work. We also thank the two anonymous reviewers for their insightful comments and constructive suggestions, which significantly aided in the improvement of this paper.

CONFLICT OF INTEREST

The authors declare no conflict of interest.

REFERENCES

Alvioli, M., Guzzetti, F., and Rossi, M. (2014). Scaling properties of rainfall induced landslides predicted by a physically based model. Geomorphology, v. 213, pp. 38-47.

Akgun, A., Kıncal, C. and Pradhan, B. (2012). Application of remote sensing data and GIS for landslide risk assessment as an environmental threat to Izmir city (west Turkey). Environmental monitoring and assessment, v. 184, pp. 5453-5470.

Bhat, G.M., Pandita, S.K., Dhar, B.L., Sahni, A.K. and Haq, I.U. (2002). Preliminary geotechnical investigation of slope failures along Jammu-Srinagar national highway between Batote and Banihal. Reprinted from Aspects of Geology Environment of the Himalaya, v. 2, pp. 275-288.

Chen, W., Pourghasemi, H.R. and Naghibi, S.A. (2018). A comparative study of landslide susceptibility maps produced using support vector machine with different kernel functions and entropy data mining models in China. Bulletin of Engineering Geology and the Environment, v. 77, pp. 647-664.

Chimidi, G., Raghuvanshi, T.K. and Suryabhagavan, K.V. (2017). Landslide hazard evaluation and zonation in and around Gimbi town, western Ethiopia—a GIS-based statistical approach. Applied Geomatics, v. 9, pp. 219-236.

El Abidine, R. Z. and Abdelmansour, N. (2019). Landslide susceptibility mapping using information value and frequency ratio for the Arzew sector (North-Western of Algeria). Bulletin of the Mineral

Research and Exploration, v. 160(160), pp. 197-211.

Fayez, L., Pazhman, D., Pham, B.T., Dholakia, M.B., Solanki, H A., Khalid, M. and Prakash, I. (2018). Application of frequency ratio model for the development of landslide susceptibility mapping at part of Uttarakhand State, India. International Journal of Applied Engineering Research, v. 13(9), pp. 6846-6854.

Gabet, E.J., Burbank, D.W., Putkonen, J.K., Pratt-Sitaula, B.A. and Ojha, T. (2004). Rainfall thresholds for landsliding in the Himalayas of Nepal. Geomorphology, v. 63(3-4), pp. 131-143.

Girma, F., Raghuvanshi, T.K., Ayenew, T. and Hailemariam, T. (2015). Landslide hazard zonation in Ada Berga District, Central Ethiopia–a GIS based statistical approach. Journal of Geomorphology, v. 9(i), pp. 25-38.

Guzzetti, F., Peruccacci, S., Rossi, M. and Stark, C.P. (2007). Rainfall thresholds for the initiation of landslides in central and southern Europe. Meteorology and Atmospheric Physics, v. 98, pp. 239-267.

Gyawali, P., Aryal, Y.M., Tiwari, A., Prajwol, K.C. and Ansari, K. (2021). Landslide Susceptibility Assessment Using Bivariate Statistical Methods: A Case Study of Gulmi District, western Nepal. VW Engineering International, v. 3, pp. 29-40.

Hamza, T. and Raghuvanshi, T.K. (2017). GIS based landslide hazard evaluation and zonation–A case from Jeldu District, Central Ethiopia. Journal of King Saud University-Science, 29(2), 151-165.

Hussain, G., Singh, Y. and Bhat, G.M. (2018). Landslide susceptibility mapping along the national highway-1D, between Kargil and Lamayuru, Ladakh Region, Jammu and Kashmir. Journal of the Geological Society of India, v. 91, pp. 457-466.

Hussain, G., Singh, Y., Bhat, G.M., Sharma, S., Sangra, R. and Singh, A. (2019). Geotechnical characterisation and finite element analysis of two landslides along the national highway 1-A (Ladakh Region, Jammu and Kashmir). Journal of the Geological Society of India, v. 94, pp. 93-99.

Kanungo, D. P., Arora, M. K., Sarkar, S. and Gupta, R. P. (2006). A comparative study of conventional, ANN black box, fuzzy and combined neural and fuzzy weighting procedures for landslide susceptibility zonation in Darjeeling Himalayas. Engineering Geology, v. 85(3-4), pp. 347-366.

Khan, H., Shafique, M., Khan, M.A., Bacha, M.A., Shah, S.U., and Calligaris, C. (2019). Landslide susceptibility assessment using Frequency Ratio, a case study of northern Pakistan. The Egyptian Journal of Remote Sensing and Space Science, v. 22(1), pp. 11-24.

Lee, S. and Min, K. (2001). Statistical analysis of landslide susceptibility at Yongin, Korea. Environmental Geology, v. 40(9), pp. 12-18.

Lee, S.A.R.O. (2005). Application of logistic regression model and its validation for landslide susceptibility mapping using GIS and remote sensing data. International Journal of Remote Sensing, v. 26(7), pp. 1477-1491.

Moung-Jin, L., Won-Kyong, S., Joong-Sun, W., Inhye, P. and Saro, L. (2014). Spatial and temporal change in landslide hazard by future climate change scenarios using probabilistic-based frequency ratio model. Geocarto International, v. 29(6), pp. 639-662.

Petley, D.N. (2008). The global occurrence of fatal landslides in 2007. Geophysical Research Abstracts, v. 10, pp. 3.

Pradhan, B. and Lee, S. (2009). Landslide risk analysis using artificial neural network model focusing on different training sites. International Journal of Physical Sciences, v. 3(11), pp. 1-15.

Pradhan, B., Chaudhari, A., Adinarayana, J. and Buchroithner, M.F. (2012). Soil erosion assessment and its correlation with landslide events using remote sensing data and GIS: a case study at Penang Island, Malaysia. Environmental Monitoring and Assessment, v. 184, pp. 715-727.

Reichenbach, P., Rossi, M., Malamud, B.D., Mihir, M., and Guzzetti, F. (2018). A review of statistically-based landslide susceptibility models. Earth Science Reviews, v. 180, pp. 60-91.

Sangra, R., Singh, Y., Bhat, G.M., Pandita, S.K. and Hussain, G. (2017). Geotechnical investigation on slopes failures along the Mughal Road from Bafliaz to Shopian, Jammu and Kashmir, India. Journal of the Geological Society of India, v. 90, pp. 616-622.

Shahabi, H., Khezri, S., Ahmad, B.B., and Hashim, M. (2014). RETRACTION: Landslide susceptibility mapping at central Zab basin, Iran: A comparison between analytical hierarchy process, frequency ratio and logistic regression models, v. 2, pp. 4-8.

Singh, Y., and Bhat, G.M. (2010). Role of basin morphometric parameters in landslides along the national highway-1A between Udhampur and Batote, Jammu and Kashmir, India: a case Study. Himalayan Geology, v. 31(1), pp. 43-50.

Singh, Y. and Bhat, G.M. (2011). Landslide investigations: morphometric and geotechnical approach-a case study from Northwest Himalaya, India. Lambert Academic Publications, v. 5, p. 113.

Singh, Y., Ul Haq, A., Bhat, G.M., Pandita, S.K., Singh, A., Sangra, R. and Kotwal, S.S. (2018). Rainfall-induced landslide in the active frontal fold–thrust belt of Northwestern Himalaya, Jammu: dynamics inferred by geological evidences and Ground Penetrating Radar. Environmental Earth Sciences, v. 77, pp. 1-17.

Tien Bui, D., Pradhan, B., Lofman, O. and Revhaug, I. (2012). Landslide susceptibility assessment in Vietnam using support vector machines, decision tree, and Naive Bayes Models. Mathematical Problems in Engineering, v. 7, pp. 12-19.

Van Westen, C.J., Castellanos, E. and Kuriakose, S.L. (2008). Spatial data for landslide susceptibility, hazard, and vulnerability assessment: An overview. Engineering Geology, v. 102(3-4), pp. 112-131.

Yilmaz, I. (2009). Landslide susceptibility mapping using frequency ratio, logistic regression, artificial neural networks and their comparison: a case study from Kat landslides (Tokat-Turkey). Computers & Geosciences, v. 35(6), pp. 1125-1138.

JOURNAL INDIAN ASSOCIATION OF SEDIMENTOLOGISTS ISSN NO 2582 – 2020
Vol. 40, Issue II, 2023, pp. 49-56
DOI: https://doi.org/10.51710/jias.v40iII.328

Microtextures and trapped diatoms on quartz grain surfaces in the Acapulco Beach, Mexican Pacific: An insight into palaeoenvironment

John S. Armstrong-Altrin[1, 2], V. Balaram[3], Mayla A. Ramos-Vázquez[4, *], Jayagopal Madhavaraju[5], Sanjeet K. Verma[4], and Rathinam Arthur James[2]

[1] Universidad Nacional Autónoma de México, Instituto de Ciencias del Mar y Limnología, Unidad de Procesos Oceánicos y Costeros, Ciudad Universitaria, Ciudad de México 04510, México

[2] Department of Marine Sciences, Bharathidasan University, Tiruchirappalli, 620024, Tamil Nadu, India

[3] CSIR-National Geophysical Research Institute (NGRI), Hyderabad -500 007, India

[4] División de Geociencias Aplicadas, Instituto Potosino de Investigación Científica y Tecnológica (IPICYT), Camino a la Presa San José 2055, San Luis Potosí 78216, México

[5] Estación Regional del Noroeste, Instituto de Geología, Universidad Nacional Autónoma de México, Hermosillo, Sonora, México

[*] E-mail Address: mayla.ramos@ipicyt.edu.mx

ABSTRACT

In this study, we report Scanning Electron Microscopy (SEM) images of quartz grains in the Acapulco beach, Mexican Pacific. The morphology of quartz grains is angular, sub-angular, sub-rounded, rounded, and well-rounded. The variations in the morphology of quartz grains are indicating both nearby and distance sources. The rounded and well-rounded grains support for a long transport distance and a distal source. Microtextures of mechanical and chemical origins are identified in quartz grains. The mechanical features include, bulbous edges (ble), elongated depression (ed), parallel striations, crater, meandering ridges (mr), arcuate steps, conchoidal fractures (cf), v-shaped marks (v-s), and broken grain. These mechanical features indicate the combination of fluvial, aeolian, and subaqueous environments. The conchoidal fractures are characteristic of crystalline rocks. Arcuate steps and meandering ridges are indicating a high wave energy. The striations on grain surfaces are due to collision between two grains, probably during an aeolian transport.

The chemical features include adhered particles (ap), solution pit (sp), silica globule, crystal overgrowth (crg), precipitation, and trapped diatoms. The solution pits and precipitation are indicating the diagenetic processes in a silica saturated coastal environment. A few grains are associated with both mechanical and chemical features, suggesting a dual environment, probably littoral and marine. Trapped diatoms identified in quartz grains are *Cocconeis guttata* and *coccolith*.

Keywords: SEM, sand grains, microtextures, beach sediments, active margin. Pacific Ocean

INTRODUCTION

Microtextures of quartz grains are one of the widely applied techniques to infer the palaeoenvironment of a particular region (Machado et al. 2016; Ramos-Vázquez et al., 2023; Saha and Sinha, 2023). Although microtextures on quartz grains are influenced by the medium of transport, their types are distinct for the fluvial, littoral, and aeolian environments. Hence, the combination of different features in a single quartz grain is reliable to predict the paleoenvironment (Costa et al., 2019; Darshan et al., 2022). In general, the microtextures in quartz grains are due to grain-to-grain collision during transport, either by wind or water, and their types are varying, depends on the energy in the depositional environment or medium of transport. In fact, rounded and angular quartz grains indicate long and short transport distance, respectively (Mathur et al. 2009; Armstrong-Altrin, 2020). Several authors documented that conchoidal fractures, arcuate steps, striations, and linear fractures are typical of mechanical origin. Similarly, other studies grouped solution pits, adhered particles, and trapped diatoms on quartz grain surfaces into chemical origin. On the other hand, a quartz grain dominated by both chemical and mechanical origin are subjected to a heterogenous provenance. Hence, differentiating the microtexture types on quartz grain surface by SEM is a powerful tool to predict the palaeoenvironment (Madhavaraju et al. 2021; Passchier et al., 2021).

In Mexico, a very few authors studied the microtextures of quartz grains recovered from the coastal sediments. Some of them are briefly discussed below: Madhavaraju et al. (2021)

analyzed the sand grains in the Gulf of California beach and Ramos-Vázquez (2023) described various types of microtextures of quartz grains in the Puerto Chiapas beach, Mexican Pacific. Others discussed the morphology of sands grains recovered from dunes, along the Mexican Pacific coast (Kasper-Zubillaga 2009; Mejía-Ledezma et al., 2020). Recently, Ramos-Vázquez and Armstrong-Altrin (2021a, b) and Armstrong-Altrin et al. (2021, 2022), studied the palaeoenvironment of the Gulf of Mexico coastal region, based on the surface features of quartz grains obtained by SEM images. However, studies on quartz grain surface features from the Mexican Pacific coast is very little. In this study, we report the microtextures of quartz grains recovered in the Acapulco beach sediments in the Mexican Pacific coast, Mexico. The objective of this study to identify the microtextures and to infer the palaeoenvironment.

STUDY AREA

The Acapulco beach (16°50´22.52" N and 99°51´03.12" W) is in the Guerrero State, Mexican Pacific coast, southern part of Mexico (Fig. 1). About 10 sediment samples were collected in the Acapulco beach and ~ 20-30 quartz grains were selected for SEM study. In the Guerrero Stata rocks are dominated by: (1) granites and granitoids of Early Paleocene; (2) volcanic rocks of intermediate to acid composition, mostly of Early Tertiary age; (3) sedimentary rocks of Mesozoic to Tertiary ages; and (4) Quaternary alluvium. Sediments in the Acapulo beach are supposed to derive from the Guerrero terrane (Verma et al., 2017, 2020). The Guerrero terrane is associated with Late Jurassic to Early Cretaceous igneous and sedimentary rocks considered to be developed in an intra-oceanic setting (Ortega-Gutiérrez, et al., 2004). The major rivers that discharge relatively near to Acapulco beach is Cihuatlán. A warm humid climate prevails with an average annual maximum temperature of 28°C and a minimum of 22°C, whereas during summer raining with a variation from 2 to 15mm (CONANP, 2003).

METHODOLOGY

SCANNING ELECTRON MICROSCOPY - SEM

Quartz grains were picked from 10 sediment samples (~ 2 kg each) under the binocular microscope. The quartz grains were treated with 5% diluted hydrochloric acid solution to remove soluble carbonates. The grains were dried at 50° C and were coated with thin gold film (Armstrong-Altrin and Natalhy-Pineda, 2014). The JEOL JSM6360LV - SEM equipped with secondary electron detector is used to infer microtextures, which is located at Instituto de Ciencias del Mar y Limnología (ICML), Universidad Nacional Autónoma de México (UNAM).

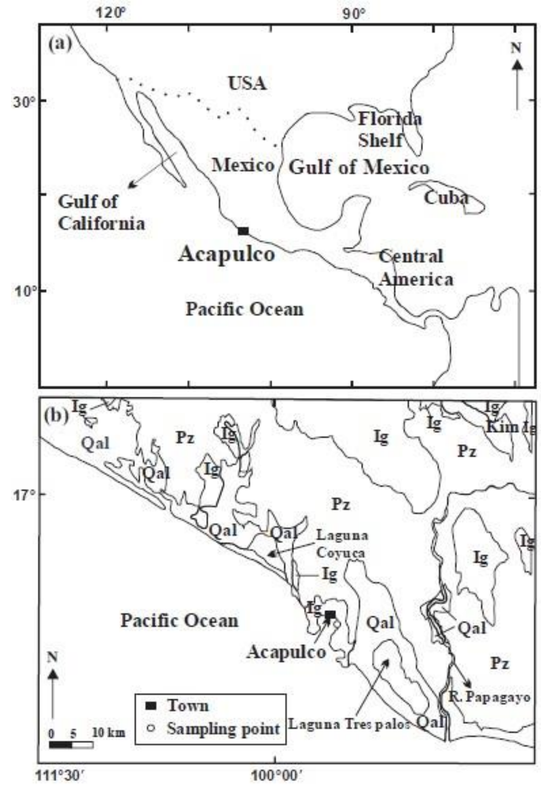

Fig. 1 Simplified geological map of the study area showing sample location (Modified after Armstrong-Altrin, 2009; CONANP, 2003). (a) Map showing location of the Acapulco beach, Mexico; (b) Volcanic and sedimentary units are: Ig = intrusive igneous rocks; Ige = extrusive igneous rocks (andesite); Jss = sedimentary rocks (lower Jurassic); Mi = intrusive rocks (Mesozoic); Pz = metamorphic rocks (Proterozoic); Qal = alluvium (Quaternary); Tiv = volcanic rocks (lower Tertiary); Tivc = volcanoclastic rocks (lower Tertiary); Tm = marine rocks (Tertiary; sandstone, mudstone); To = sandstone and limestone (Oligocene); Tsc = clastic rocks (upper Tertiary).

RESULTS

The different types of microtextures identified by SEM are shown in Figures 2 and 3. Based on their origin the microtextures are classified as Mechanical (Fig. 2) and Chemical types (Fig. 3). The morphology of quartz grains in the Acapulco beach are classified as angular (Fig. 2A), sub-angular (Fig. 2B), sub-rounded (Fig. 2C), rounded (Fig. 2D and E), and well-rounded (Fig. 2F and G).

MECHANICAL ORIGIN

The microtextures of mechanical origin identified in the quartz grains are listed below: well-rounded grains with bulbous edges (Fig. 2F and G) (ble), elongated depression (ed) (Fig. 2H), parallel striations (2I, J, K, and L), crater (2L), meandering ridges (mr) (Fig. 2M), arcuate steps (Fig. 2M), conchoidal fractures (cf) (Fig. 2N, O, and P), v-shaped marks (v-s) (Fig. 2P, Q, R, and S), and broken grain (Fig. 2T).

CHEMICAL ORIGIN

Microtextures of chemical origin includes, adhered particles (ap) (Fig. 3A, B, and C), solution pits (sp) (Fig. 3B, C, D, E, F, and G), silica globule (Fig. 3 H), crystal overgrowth (crg) (Fig. 3H, I, J, and L), precipitation (Fig. 3K and L), and trapped diatoms (Fig. 3 L, M, N, O, and P).

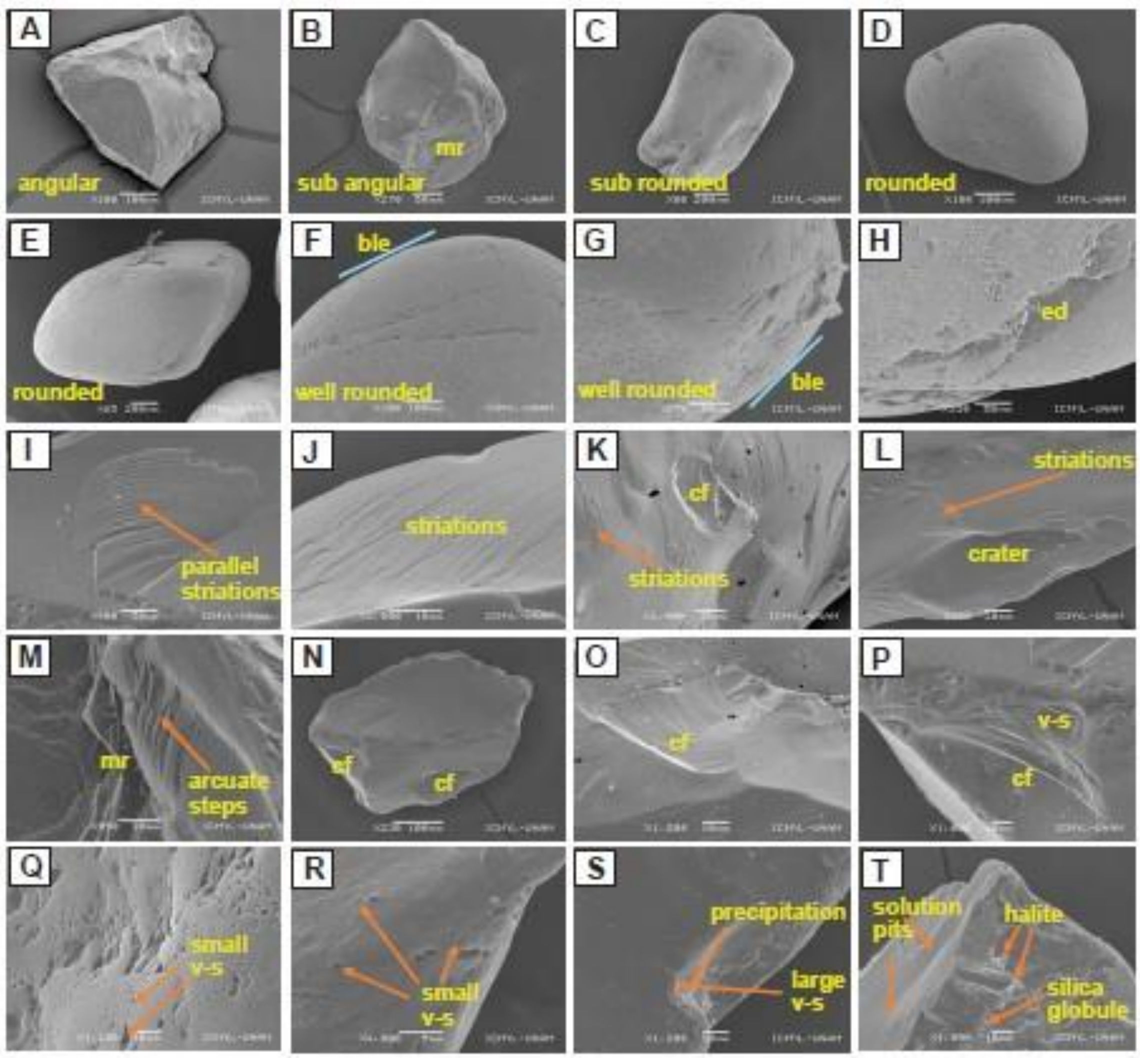

Fig. 2 Surface microtextures on quartz grains identified by SEM from the Acapulco beach, Mexican Pacific: (A) angular grain; (B) sub-angular grain; (C) sub-rounded grain; (D) rounded grain; (E) rounded; (F and G) well-rounded grains with bulbous edges (ble); (H) elongated depression (ed); (I, J, K, and L) parallel striations; (L) crater; (M) meandering ridges (mr); (M) arcuate steps; (N, O, and P) conchoidal fractures (cf); (P, Q, R, and S) v-shaped marks (v-s); (T) broken grain with chemical features

DISCUSSION

PALEOENVIRONMENTAL IMPLICATIONS

MECHANICAL FEATURES

The mechanical features identified in the Acapulco beach sands are indicating a high energy coastal environment. Rounded and sub-rounded grains are due to abrasion between two grains during transport, especially indicating a longer transport distance. The rounded grains with bulbous edges are indicating an aeolian transport and rolling of grains during saltation (Costa et al. 2013; Ramos-Vázquez and Armstrong-Altrin, 2019, 2020; Yhasnar et al., 2023). On the other hand, angular and broken quartz grains are indicating a short littoral transport. The combination of angular and well-rounded grains is revealing both proximal and distal sources. The parallel (Fig. 2I) and sub-parallel striations (Fig. 2J and L) on quartz grain surfaces are due to a collision between two grains during transport, either by wind or littoral transport. Meandering ridges and arcuate steps are indicating a grain to grain collision during saltation or suspension in a subaqueous coastal marine environment (Hossain et al., 2014; 2020). Similarly, meandering ridges are also indicating a long-distance transport of quartz grains in a fluvial environment (Madhavaraju et al., 2022). Meandering ridges may convert easily to elongated depressions due to large scale abrasion (Fig. 2H). A rare feature crater (Fig. 2L) identified in a quartz grain is indicating an impact between two grains with high energy, probably during wind transport. Later the impact point in a quartz grain is polished due to abrasion by wave action in a coastal environment. The conchoidal fractures are widely varying in size, i.e. small (Fig. 2K and N) and large (Fig. 2L and P). Few authors reported that large size conchoidal fractures with depressions of about 20-250 μm in size may indicate a glaciofluvial origin as well as a crystalline source (Mejía-Ledezma et al. 2020; Armstrong-Altrin et al., 2021). Similarly, v-s are triangular shaped pits, which are also common in the analyzed quartz grains and are varying widely in their size and frequency. Some of the v-s are large in size and are less in number (Fig. 2S). However, relative to large v-s, small size v-s are abundant and its distribution is high in a single grain (Fig. 2Q, and R; Fig. 3C). The origin of v-s is due to gouging and a mechanical collision between two grains. In general, v-s are suggesting a high energy subaqueous environment. However, other studies documented that v-s in quartz grains are suggesting both glaciofluvial and fluvial transport (Madhavaraju et al., 2009; Hossain et al., 2020). In summary, this study reveals the combination of microtextures derived by both wind and littoral transport.

CHEMICAL FEATURES

Chemical features are abundant in the quartz grains from the Acapulco beach. Adhering particles on grain surfaces are common, which are mostly fragmented rock pieces or other particles such as algae, microplastics, foraminifer, etc. (Fig. 3A and C). Adhering particles are highly reliable to infer the diagenetic characteristics of a particular depositional environment, i.e. shallow or deep water, marine or fresh water, and glacial or eolian (Bónová et al. 2020). Solution pits on quartz grains are varying widely in their size and shape, which are circular, sub-circular, and irregular in shapes (Fig. 3F), some of them are bigger in size, greater than 15 μm (Fig. 3G). In addition, few solution pits identified are smaller in size, similar to raindrop prints (Fig. 3C). Solution pits (Fig. 3B, C, D, E, F, and G) and precipitation (Fig. 3K and L) are indicating different stages of a diagenetic environment or chemical action in a marine environment, where water is saturated with silica. In fact, sea water acidification can also increase the intensity of solution activity in a marine environment. The frequency of solution pits is depending on the availability of silica solution and their time of stay in a particular marine environment. Similarly, the intensity of solution and precipitation in a marine environment is depending on the acidity of sea water, grain hardness and corrosion strength. The diagenetic features are relatively less in heavy minerals, such as magnetite, ilmenite, and zircon (Armstrong-Altrin, 2020). On the other hand, crystal overgrowth in quartz grains is frequently observed in many grains (Fig. 3H, I, J, and L), indicating an in-situ precipitation and an aquatic diagenetic environment. Crystal overgrowth in quartz grains are generally represented by halite crystals (Fig. I and J), but occasionally are associated with silica globules, due to silica precipitation (Fig. 3H).

In addition to chemical features, trapped diatoms are identified in many grains, which are well preserved and indicating a nutrient rich sea water (Fig. 3L, M, N, O, and P). An elliptically shaped diatom called *Cocconeis guttata* (Hustedt and Aleem 1951) is identified in a quartz grain surface, in a well-preserved form (Fig. 3O). It is interesting to note that the distribution of *Cocconeis guttata* was recorded from the coastal waters of England (Hustedt and Aleem 1951) and France (Riaux-Gobin, 1991). In 2003, it was recorded for the first time from the shallow coastal waters of the Gulf of Matías, southwestern Atlantic

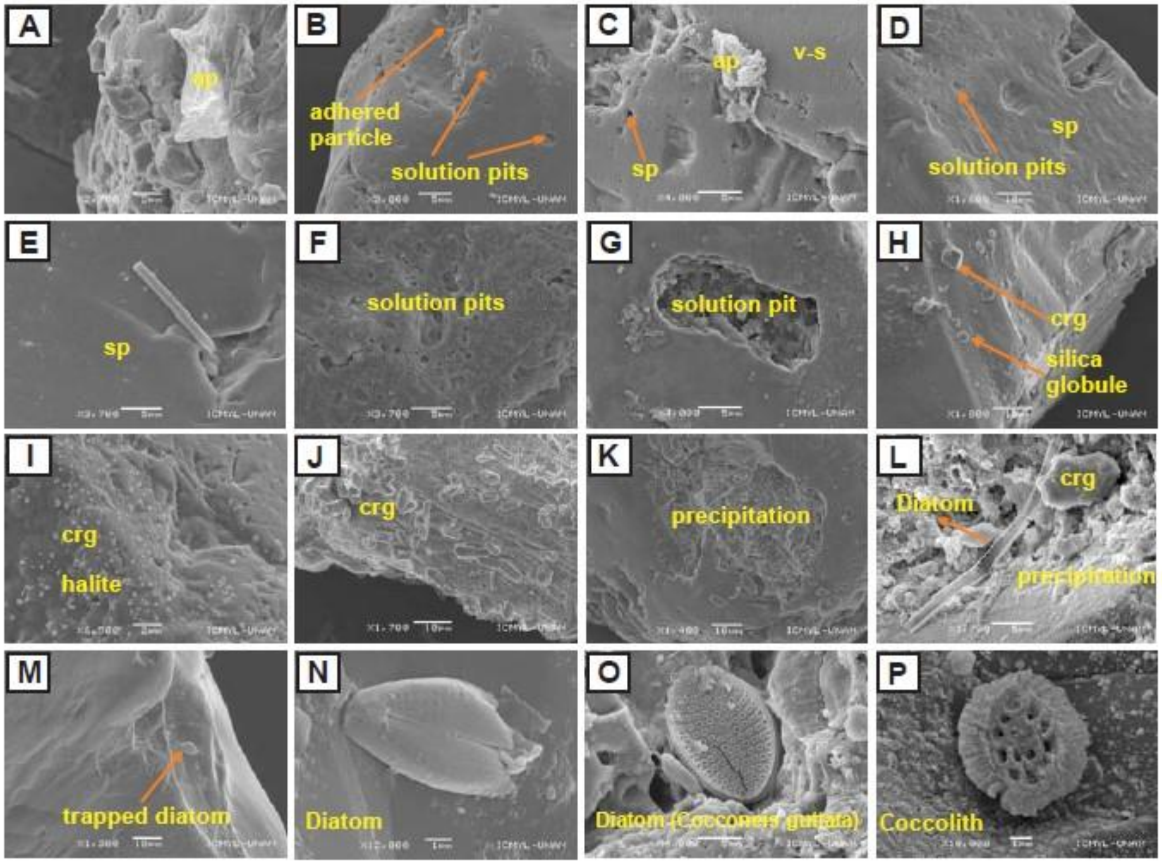

Fig. 3 Microtextures on quartz grain surfaces in the Acapulco beach, Mexican Pacific: **(A, B, and C)** adhered particles (ap); **(B, C, D, E, F, and G)** solution pits (sp); **(H)** silica globule (sg); **(H, I, J, and L)** crystal overgrowth (crg); **(3K and L)** precipitation; **(L)** diatom; **(M)** diatom; **(N)** enlarged view of previous image; **(O)** Diatom *Cocconeis guttata*; **(P)** Coccolith.

Ocean (Sar et al., 2003). Similarly, a fragmented disc shaped *coccolith* is identified (Fig. 3P), which is a single-celled organism, part of the phytoplankton, mostly 5-20 µm in diameter. *Coccoliths* form the part of calcite oozes, which are utilized in other studies to reconstruct the past climate (Arundhathy et al., 2021). Few quartz grains are with both mechanical and chemical features: 1) a broken grain with silica globule, halite, and solution pit (Fig. 2T) and 2) solution pits, adhering particles, and v-s (Fig. 3C), which are indicating a dual environment.

CONCLUSIONS

The morphology of quartz grains varies from angular to well-rounded, indicating the mixing of grains derived from the nearby and distal sources. The well-rounded grains in the Acapulco beach reveals that the sediments were partly supplied by the dunes and re-distributed along the coast by a littoral current. The microtextures on quartz grains in the Acapulco beach are classified as mechanical and chemical origin. The microtextures of mechanical origin includes well-rounded grains with bulbous edges, elongated depression, parallel striations, crater, meandering ridges, arcuate steps, conchoidal fractures, and v-shaped marks. Microtextures of chemical origin are represented by adhered particles, solution pits, silica globule, crystal overgrowth, precipitation, and trapped diatoms.

V-shaped marks, bulbous edges, and meandering ridges are indicating littoral and high-energy marine depositional environment. Parallel striations represent a high energy collision and abrasion during aeolian transport. The combination of v-s and solution pits in a single grain indicates that the grain was suffered by both littoral and a subaqueous marine environment (dual environment). The differences in surface features in quartz grains indicate that the sediments were transported to the Acapulco beach by aeolian and fluvial activities. Silica globules, solution and precipitation in quartz grains reveal a silica saturated marine environment. The diatoms like

Cocconeis guttata and *coccolith* are also identified on quartz grain surfaces.

ACKNOWLEDGEMENTS

This research work was financially supported by the PAPIIT (no: IN104824) and CONAHCyT (A1-S-21287) projects. We extend our sincere thanks to Laura E. Gómez Lizárraga for SEM study. We are grateful to Carlos Linares-López, Teodoro Hernández Treviño, Ricardo M. Domínguez, Eduardo Morales la Garza, Susana Santiago, and Arturo Ronquillo Arvizu for their assistance during the course of this study. Ramos-Vázquez is grateful to CONAHCyT for the postdoctoral scholarship (CVU: 595593). We acknowledge the ICML-Institutional project (no. 616) for providing transport facilities during sample collection.

AUTHOR CONTRIBUTION

John S. Armstrong-Altrin: Investigation, Writing - Review and Editing, Formal analysis, Resources, Funding acquisition. V. Balaram: Review and Editing. Mayla A. Ramos-Vázquez: Field work, SEM analysis. Jayagopal Madhavaraju: Methodology, Formal Analysis, Editing. Sanjeet K. Verma: Methodology, Formal Analysis, Review and Editing. Rathinam Arthur James: Data curation, Methodology, Formal analysis. All authors contributed equally in writing, reviewing, and editing the manuscript.

FUNDING

This work was supported financially by the Consejo Nacional de Ciencia y Tecnología (CONACyT; A1-S-21287) and Programa de Apoyo a Proyectos de Investigación e Innovación Tecnológica (PAPIIT; IN104824) projects.

CONFLICT OF INTEREST

The authors declare no conflict of interest

REFERENCES

Armstrong-Altrin, J.S. (2020). Detrital zircon U-Pb geochronology and geochemistry of the Riachuelos and Palma Sola beach sediments, Veracruz State, Gulf of Mexico: a new insight on palaeoenvironment. Journal of Palaeogeography, v. 9(4), no. 28.

Armstrong-Altrin, J.S. and Natalhy-Pineda, O. (2014). Microtextures of detrital sand grains from the Tecolutla, Nautla, and Veracruz beaches, western Gulf of Mexico, Mexico: implications for depositional environment and palaeoclimate. Arabian Journal of Geosciences, v. 7, pp. 4321-4333.

Armstrong-Altrin, J.S., Ramos-Vázquez, M.A., Hermenegildo-Ruiz, N.Y., Madhavaraju, J. (2021). Microtexture and U-Pb geochronology of detrital zircon grains in the Chachalacas beach, Veracruz State, Gulf of Mexico. Geological Journal, v. 56(5), pp. 2418-2438.

Armstrong-Altrin, J.S., Ramos-Vázquez, M.A., Madhavaraju, J., Marca-Castillo, M.E., Machain-Castillo, M.L. and Márquez-Garcia, A.Z. (2022). Geochemistry of marine sediments adjacent to the Los Tuxtlas Volcanic Complex, Gulf of Mexico: Constraints on weathering and provenance. Applied Geochemistry, v. 141, pp. 105321.

Arundhathy, M., Jyothibabu, R., Santhikrishnan, S., Albin, K.J., Parthasarathi, S. and Rashid, C.P. (2021). Coccolithophores: an environmentally significant and understudied phytoplankton group in the Indian Ocean. Environmental Monitoring and Assessment, v. 193, article number 144.

Bónová, K., Pánczyk, M., Bóna, J. (2020) Surface microtextures and new U-Pb dating of detrital zircons from the Eocene Strihovce sandstones in the Magura Nappe of the External Western Carpathians: Implications for their provenance. International Journal of Earth Sciences, v. 109, pp. 1565-1587.

CONANP (Comisión Nacional de Áreas Naturales Protegidas) (2003) Programa de Manejo de la Reserva de la Biosfera Barranca de Metztitlán. Comisión Nacional de Áreas Naturales Protegidas, SEMARNAT, México.

Costa, P.J.M., Andrade, C., Mahaney, W.C., Marques da Silva, F., Freire, P., Freitas, M.C., Janardo, C., Oliviera, M.A., Silva, T. and Lopes, V. (2013). Aeolian microtextures in silica spheres induced in a wind tunnel experiment: comparison with aeolian quartz. Geomorphology, v. 180-181, pp. 120-129.

Costa, P., Rasteiro, D., Figueirinhas, L. and Lario, J. (2019). The importance of coastal geomorphological setting as a controlling factor on microtextural signatures of the 2010 maule (Chile) tsunami deposit. Geologica Acta, v. 17(4), pp. 1-10.

Darshan, M. S, Shivanna, Ms., Rajuk, S. and Madesh, P. (2022). Microtextures on quartz grains in the Estuary sediments of Gurupura River, Dakshina Kannada district, Karnataka State, West coast, India. Journal Indian Association of Sedimentologists, v. 39(II), pp. 3-9.

Hossain, H.M.Z., Tarek, M., Armstrong-Altrin, J.S., Monir, M.U., Ahmed, M.T., Ahmed, S.I. and Hernandez-Coronado, C.J. (2014). Microtextures of detrital sand grains from the Cox's Bazar beach, Bangladesh: Implications for provenance and depositional environment. Carpathian

Journal of Earth and Environmental Sciences, v. 9(3), pp. 187-197.

Hossain, H.Z., Armstrong-Altrin, J.S., Jamil, A.H.M.N., Rahman, M.M., Hernandez-Coronado, C.J. and Ramos-Vazquez, M.A. (2020). Microtextures on quartz grains in the Kuakata Beach, Bangladesh: Implications for provenance and depositional environment. Arabian Journal of Geosciences, v. 13(7), no. 291.

Hustedt, F. and Aleem, A.A. (1951). Littoral diatoms from the Salstone, near Plymouth. Journal of the Marine Biological Association of the United Kingdom, v. 30, pp. 177-196.

Kasper-Zubillaga, J.J. (2009). Roundness in quartz grains from inland and coastal dune sands, Altaer Desert, Sonora, Mexico. Bulletin Sociedad Geologíca Mexicana, v. 61, pp. 1-12.

Madhavaraju, J., Lee, Y.I., Armstrong-Altrin, J.S. and Hussain, S.M. (2006). Microtextures on detrital quartz grains of upper Maastrichtian-Danian rocks of the Cauvery Basin, southeastern India: Implications for provenance and depositional environments. Geosciences Journal, v. 10, pp. 23-34.

Madhavaraju, J., García-Barragan, J.C., Hussain, S.M. and Mohan, S.P. (2009). Microtextures on quartz grains in the beach sediments of Puerto Peñasco and Bahia Kino, Gulf of California, Sonora, Mexico. Revista Mexicana de Ciencias Geologicas, v. 26, pp. 367-379.

Madhavaraju, J., Armstrong-Altrin, J.S., James, R.A. and Hussain, S.M. (2021). Palaeoenvironment and provenance signatures inferred from quartz grain Surface features: A case study from Huatabampu and Altata beaches, Gulf of California, Mexico. Journal of South American Earth Sciences, v. 111(1-11), No.103441.

Madhavaraju, J., Armstrong-Altrin, J.S., Selvaraj, K. and James, R.A. (2022). Microtextures on quartz grains from the Gulf of Mexico and the Mexican Pacific coastal sediments: Implications for sedimentary processes and depositional environment. Journal of Palaeogeography, v. 11(2), pp. 257-275.

Mathur, A.K., Mishra, V.P. and Singh, J. (2009). Study of quartz grain surface texture by electron microscopy-a tool in evaluating palaeoglacial sediments in Uttarakhand. Current Science, v. 96, pp. 1377-1382.

Mejía-Ledezma, R.O., Kasper-Zubillaga, J.J., Alvarez-Sánchez, L.F., Mendieta-Lora, M., Arellano-Torres, E., Tetlalmatzi-Martínez, J.L., Gonzalez Bermúdez, A., Patiño-Andrade, D. and Armstrong-Altrin. J.S. (2020). Surface textures of quartz and ilmenite grains from dune and beach sands of the Gulf of Mexico Coast, Mexico: implications for fluvial, aeolian and marine transport. Aeolian Research, v. 45, no. 100611.

Ortega-Gutiérrez, F., Solari, L., Solé, J., Martens, U., Gómez-Tuena, A., Morán-Icál, S., Reyes-Salas, M. and Ortega-Obregón, C. (2004). Polyphase, High-Temperature Eclogite-Facies Metamorphism in the Chuacús Complex, Central Guatemala: Petrology, Geochronology, and tectonic Implications. International Geology Review, v. 46, pp. 445-470.

Passchier, S., Hansen, M.A. and Rosenberg, J. (2021). Quartz grain microtextures illuminate Pliocene periglacial sand fluxes on the Antarctic continental margin. The Depositional Record, v,7:3, pp. 564-581.

Ramos-Vázquez, M.A. and Armstrong-Altrin, J.S. (2019). Sediment chemistry and detrital zircon record in the Bosque and Paseo del Mar coastal areas from the southwestern Gulf of Mexico. Marine and Petroleum Geology, v. 110, pp. 650-675.

Ramos-Vázquez, M.A. and Armstrong-Altrin, J.S. (2020). Provenance and palaeoenvironmental significance of microtextures in quartz and zircon grains from the Paseo del Mar and Bosque beaches, Gulf of Mexico. Journal of Earth System Science, v. 129, pp. 225.

Ramos-Vázquez, M.A. and Armstrong-Altrin, J.S. (2021a). Microtextures on quartz and zircon grain surfaces in the Barra del Tordo and Tesoro beaches, northwestern Gulf of Mexico. Arabian Journal of Geosciences, v. 14, pp. 949.

Ramos-Vázquez, M.A. and Armstrong-Altrin, J.S. (2021b). Provenance of sediments from Barra del Tordo and Tesoro beaches, Tamaulipas State, northwestern Gulf of Mexico. Journal of Palaeogeography, v. 10(20), pp. 1-17.

Ramos-Vázquez, M.A. (2023). Sediment provenance inferred by U-Pb ages of zircon grains in the Puerto Chiapas beach, Mexican pacific. Arabian Journal of Geosciences, v. 16, pp. 266.

Ramos-Vázquez, M.A., Verma, S.K., Armstrong-Altrin, J.S. and James, R.A. (2023). Provenance significance of quartz grain microtextures in the Salina Cruz and Puerto Angel Beaches, Oaxaca State, Mexican Pacific. Arabian Journal of Geosciences, v. 16, pp. 121.

Riaux-Gobin, C. (1991). Diatomees d une vasiere intertidale du Nord Finistere (Dourduff): genres Cocconeis, Campyloneis, Delphineis, Mastogloia et Raphoneis. Diatom Research, v. 6, pp. 125-135.

Saha, K. and Sinha, S. (2023). Distinguishing depositional environments in the beach–dune system of Chandipur, India, based on sediment texture and quartz grain surface features. Earth Surface Processes and Landforms, v. 48(6), pp. 1252-1266.

Sar, E.A., Romero, O. and Sunesen, I. (2003). Cocconeis Ehrenberg and Psammococconeis Garcia (Bacillariophyta) from the Gulf of San Matías, Patagonia, Argentina. Diatom Research, v. 18(1), pp. 79-106.

Verma, S.P., Rivera-Gómez, M.A., Díaz-González, L., Pandarinath, K., Amezcua-Valdez, A., Rosales-Rivera, M., Verma, S.K., Quiroz-Ruiz, A. and Armstrong-Altrin, J.S. (2017). Multidimensional classification of magma types for altered igneous rocks and application to their tectonomagmatic discrimination and igneous provenance of siliciclastic sediments. Lithos, v. 278-281, pp. 321-330.

Verma, S.P., López-Loera, H., Subramanyam, K.S. and Manikyamba, C. (2020). Geochemistry, petrogenesis, and tectonic setting of the Los Tuxtlas Volcanic Field, Mexico. Geological Journal, v. 55(12), pp. 8169-8185.

Yhasnar, M., Costa, P.J.M., Dourado, F., Martins, M.V.A., Feist, L., Bellanova, P. and Reicherter, K. (2023). Microtextural signatures in quartz grains and foraminifera from tsunami deposits of the Portuguese shelf. Geo-Marine Letters, v. 43(5).

ORCID ID

John S. Armstrong-Altrin: http://orchid.org/0000-0003-3910-5195
V. Balaram: https://orcid.org/0000-0002-8621-192X
Mayla A. Ramos-Vázquez: https://orcid.org/0000-0001-9155-4313
Sanjeet K. Verma: https://orcid.org/0000-0002-4390-5147
Rathinam Arthur_James: https://orcid.org/0000-0003-4536-4863

JOURNAL INDIAN ASSOCIATION OF SEDIMENTOLOGISTS ISSN NO 2582 – 2020
Vol. 40, Issue II, 2023, pp. 57-67
DOI: https://doi.org/10.51710/jias.v40iII.310

Texture and major element geochemistry of channel sediments in the Orsang and Hiren River Basins, Gujarat, India: Implications for provenance and weathering

Keshwala Nikunj[1], Maurya Shivam[1], Gurav Chandrakant[2] A. and More Laxman[1,3,*]
[1]Parul Institute of Applied Sciences, Parul University, Vadodara - 391760, Gujrat, India
[2]School of Earth Sciences, Punyashlok Ahilyadevi Holkar Solapur University, Solapur - 413255, Maharashtra, India
[3]Yashwantrao Chavan College of Science, Karad - 415124, Maharashtra, India
[*]Email Address: morelaxman70@gmail.com

ABSTRACT

Size, shape, degree of sorting, and composition of sediments in the river channels are controlled by climate, lithology, weathering, sorting, and medium of transportation. The present investigation is focused on the grain-size and geochemical analysis of the channel sediments of the Orsang and Hiren river basins. Major outcrops in the study area are Archaean granites, granitic gneisses, Upper Cretaceous to lower Eocene Deccan Volcanic Basalts (DVB), Quaternary sediments and minor proportion of Proterozoic low grade metamorphic rocks. The sediments are poorly to moderately sorted, very finely skewed, suggesting its derivation from heterogenous sources, while the kurtosis value indicates a high-energy depositional environment. The sediments are with gravelly sand texture and the mean grain size is varying from 581.9µm to 1284.2µm. The DVB provenance of the Hiren river basin and granitic provenance of the Orsang river basin is clearly reflected in the texture and geochemical composition of sediments. The TiO_2 and Fe_2O_3 contents of sediments from the Hiren river basin are distinctly higher and are comparable to the basalts of the Saurashtra region of the Deccan Province. Sediments collected after Orsang and Hiren rivers confluence and from Narmada river show higher concentration of felsic sources, indicating that Orsang river's sediment supply significantly outweighs Hiren rivers. The arkosic-litharenite nature points towards less transportation and moderate chemical weathering for the Orsang river sediments. The low Chemical Index of Alteration (CIA) values (Avg. 48.45 and 56.99 for Orsang and Hiren rivers, respectively) and A-CN-K plot also suggest the supply of sediments from minimally weathered detritus under a semi-arid condition.

Keywords: Sediments, Grain Size, Orsang River, Provenance, Transportation, Weathering

INTRODUCTION

River sediments are unconsolidated fragments of pre-existing rocks that have undergone both mechanical and chemical weathering. Both weathering and erosion contribute to the degradation of the rocks, but this degradation has different impact on different types of rocks (Joshua and Oyebanjo, 2010). The size and shape of sand grains in the river provide ideal information about transportation media (Bui et al., 1989); they also provide clues on sediment discharge rates and the environment during deposition of sediments (Gray and Simões, 2008; Williams, 2012). The distribution of sand grains is largely influenced by three key processes: sediment movement, sediment aggregation, and depositional mechanism (Wai et al., 2004). Sediment textures and geochemistry have been extensively used to extract information on provenance, weathering conditions, tectonics, fluvial processes, and paleoclimate conditions (Nesbitt and Young, 1982; Bhatia, 1983; McLennan et al., 1983; Taylor and McLennan, 1985; Wronkiewicz and Condie, 1987; Cullers et al., 1988; Fedo et al., 1995; Sharma et al., 2013). In this context, grain-size data provide clues to sediment provenance, transport history, depositional conditions, and classifying sedimentary facies and environments, which are largely controlled by the nature of the source rock and the transport agent (e.g., Folk and Ward, 1957; Friedman, 1979; Singh and Rajamani, 2001; Bernabeu et al., 2002; Guti errez-Mas et al., 2003; Benavente et al., 2005; Garzanti et al., 2011) while geochemical characteristics reveal the provenance, nature and degree of weathering at the source region of sediments, which is controlled by lithology, climate, and tectonics (Taylor and McLennan, 1985; Singh, 2009; Mondal et al., 2012; Hernández-Hinojosa et al., 2018). In addition, reworking also affects the chemical composition of sediments (McLennan, 1982; Cox and Lowe, 1995). Several authors have investigated the fluvial sediments of Indian rivers to understand the source and process controls on the geochemistry of sediments (Jain and Tandon, 2003; Juyal et al., 2006; Sanyal and Sinha, 2010; Garçon and Chauvel, 2014; Maharana et al., 2018). However, textural and geochemical studies on the fluvial sediments from Orsang and Hiren river basins, which are part of west-flowing river system, are yet to be studied. Additionally, distinctly different spatio-temporal geologic domains are traversed by Orsang and Hiren rivers, making them strongly suitable for understanding provenance control. The data generated in the present study will help to unravel the effect of weathering, provenance and variations in the textural and geochemical characteristics of sediments.

STUDY AREA

The Orsang river is one of the major tributaries of the Narmada river, which covers 4000 km^2 and has a total channel length of 135 km. It spreads over a geographical area extending from approximately 73°26'24" E to 74°20'24" E longitudes and 21°57'36" N to 22°35'24" N latitudes (Fig. 1). The Orsang river originates in the Aravalli Mountain ranges of Madhya Pradesh's Jhabua district and travels for about 20 kilometres in a south-westerly direction over the wide alluvial plain

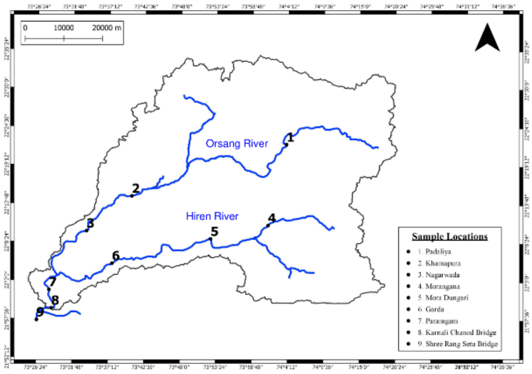

Figure 1. Basin Map of the Orsang and Hiren rivers.

before joining the Narmada river in Chandod, Gujarat. The south-flowing Bharaj river enters the Orsang river near Jetpur Pavi, and the southwest-flowing Hiren river joins further downstream at Chhota Udepur. The Kevdi-Kundal mountainous topography serves as the main water divide, separating the two distinct drainage zones. The general climatic condition of the study area is a moderate subtropical monsoonal climate very similar to other north-western peninsular river basins (Maharana et al. 2018). The Orsang river flows through deformed metamorphic and igneous rocks including granite, gneiss, quartzite, schist, limestone, phyllite, meta-subgreywacke and slate; while Hiren flows through predominantly basaltic terrain with few carbonatite patches (Merh, 1995; Chamyal et al., 2011; Shah et al., 2021). The stratigraphy of the study area ranges from the Archean to the Recent, with a gap of Palaeozoic rocks as in most of India. The northern and north-eastern regions of the basins expose the granitic and gneissic rocks of the Archean basement and the Proterozoic rocks (Champaner group). In the southeast region, the basement is covered by post-Cretaceous sediments and significant volcanic rocks (Fig. 2). The post-Cretaceous Intratrappean and Infratrappean sediments are exposed as scattered inliers, whereas younger volcanic rocks from the Deccan Traps and few Tertiary and Quaternary lithologies are well represented (Merh, 1995; Chamyal et al., 2011).

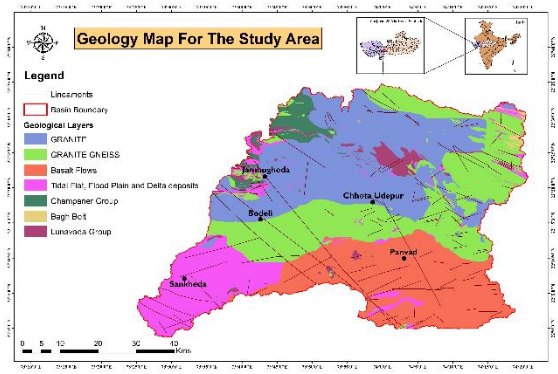

Figure 2. Geological map of the Orsang and Hiren river basins showing various lithological units. This map is extracted from Geological Society of India base map.

SAMPLING AND ANALYTICAL METHODS

For the study of the textural analysis and geochemistry, nine unconsolidated sediment samples were collected, i.e. three samples were collected from the Orsang and the Hiren river channels, two samples were collected after the confluence of the Orsang and Hiren rivers, and one sample was collected from the Narmada river. The sample locations were considered by i) the length of the river, ii) equal spacing of sampling site and iii) the geology of the basin. The location details are given in Table 1. One sample was taken from the Narmada river after the confluence of the Orsang river into the Narmada river. Such sites have been very important for the sample collection, especially for the geochemical study. The samples were collected after few inches of sediments in the surface layer was removed to prevent any contamination. Nearly 2 kg of sample was collected in a polythene bag and was dried under sunlight. After the removal of moisture from the samples, they were processed for sieve analysis and geochemistry. Before grain size analysis, the samples were treated with cold HCl and H_2O_2 to remove carbonates and organics, and then the grain size fractions were measured by dry sieving. The British Standard Sieve Analysis Method was adapted for the present work. For sieve analysis, a representative size of 300 gm from the collected samples was obtained by the coning and quartering method. Sieve analysis is carried out using the eight ASTM sieves, including 4750, 2000, 1000, 600, 300, 212, 150, 75 microns, and a pan. Sediments finer than 75 microns are collected into the pan, and 43 microns are assigned to them for processing the data through GRADISTAT program. The grain size data generated after sieving is listed in Table 2. The obtained data is processed in the GRADISTAT programme developed by Blott and Pye (2001). To measure the Mean, Sorting, Skewness and Kurtosis the Arithmetic method is

Table 1. Location details, sample type, textural group and sediment name for channel sediments from study area

Sample number	River name	Locations	Latitude (N)	Longitude (E)	Sample Type	Textural Group	Sediment Name
1	Orsang River	Padaliya	22°22'15"	74°3'56"	Unimodal, Poorly Sorted	Gravelly Sand	Very Fine Gravelly Coarse Sand
2		Khammapura	22°14'53.0"	73°40'38.0"	Bimodal, Poorly Sorted	Gravelly Sand	Very Fine Gravelly Coarse Sand
3		Nagarwada	22°09'57"	73°33'54"	Unimodal, Moderately Sorted	Slightly Gravelly Sand	Slightly Fine Gravelly Coarse Sand
4	Hiren River	Morangana	22°10'59"	74°1'18"	Bimodal, Poorly Sorted	Gravelly Sand	Fine Gravelly Coarse Sand
5		Moradungari	22°8'54"	73°52'30"	Unimodal, Moderately Sorted	Gravelly Sand	Very Fine Gravelly Coarse Sand
6		Garda	22°5'55"	73°37'41"	Unimodal, Poorly Sorted	Gravelly Sand	Fine Gravelly Coarse Sand
7	Orsang River (after confluence of above two basins)	Paramgam	22°01'42"	73°28'23"	Unimodal, Poorly Sorted	Gravelly Sand	Very Fine Gravelly Coarse Sand
8		Karnal Chanod Bridge	21°59'10"	73°28'40"	Unimodal, Moderately Sorted	Slightly Gravelly Sand	Slightly Very Fine Gravelly Coarse Sand
9	Narmada River	Seturam Bridge	21°57'27"	73°26'17"	Unimodal, Moderately Well Sorted	Gravelly Sand	Fine Gravelly Coarse Sand

Table 2: Basin wise grain size data generated after sieving of 300 gm sediment sample.

	Orsang River basin			Hiren River basin			Orsang River (After confluence)		Narmada River
Sample No.	1	2	3	4	5	6	7	8	9
Location	Padaliya	Khammapura	Nagarwada	Morangana	Moradungari	Garda	Paramgam	Karnali Chanod Bridge	Seturam Bridge
Aperture (microns)	Sediments Retained (g)	Sediments Retained (g)	Sediments Retained (g)	Sediments Retained (g)	Sediments Retained (g)	Sediments Retained (g)	Sediments Retained (g)	Sediments Retained (g)	Sediments Retained (g)
4750	7.9	14.1	4.35	35.0	14.6	13.8	28.2	-	8.38
2000	16.1	23.7	6.29	44.3	25.4	17.04	50.8	0.61	10.9
1000	72.9	75.3	27.03	55.5	83.5	38.5	86.2	8.31	32.3
600	131.6	112.2	125.8	63.6	141.5	114.2	84.1	116.9	215.3
300	42.6	37.18	102.5	44.3	21.3	79.8	22.9	118.7	28.8
212	18.8	20.51	26.2	37.5	6.16	26.6	10.2	42.4	1.17
150	4.11	7.7	1.8	8.6	1.47	4.72	4.61	5.87	0.1
75	4.11	5.34	3.03	7.16	3.36	3.16	8.15	4.5	0.84
43 (Pan)	0.71	3.14	2.13	3.11	2.35	1.65	3.02	1.63	0.63

adopted. Major elements were determined from bulk sediment samples by using an ElvaX Plus X-Ray Fluorescence (EDXRF) Spectrometer using pressed pellets. Pressed pellets were prepared by using collapsible aluminium cups. These cups were filled with boric acid and a few grams of the finely powdered sample and then pressed under a hydraulic press. For all elements, laboratory precision is better than 5%.

RESULTS

SEDIMENT TEXTURAL CHARACTERISTICS

In sedimentology, geomorphology, soil sciences, and sediment textural study involves estimation of the cumulative mass percentage of established size fractions of the total mass of sediment. There are different techniques that have been adopted to study the size distribution and textural characteristics of sediments, because of the shape and density variations of sediments, which include sieving, pipette hydrometers, X-ray attenuation, scanning electron microscopy, and laser diffraction. The mean value is the diameter, which represents the central gravity for the normal distribution of the frequency distribution (Inman, 1952). The second statistical property of grain size analysis is the sorting of grains. It has been studied using the dispersion of the sediment size. Skewness is the third statistical parameter, which measures the degree of asymmetry in the distribution. Kurtosis is a parameter that is used to measure the peakedness of the statistical distribution. Both skewness and kurtosis parameters are helpful for identifying the origin of sediments or sedimentary environments (Ruiz-Martínez et al., 2016). For the present study, the arithmetic method has been undertaken, and the obtained results are shown in Table 3.

The channel sediments of the Orsang river basin mainly consist of sand (72.5–99.3 %) and gravel (0.2–26.5 %), with a very low percentage of mud (0.2–1 %). The histograms for sediments peak around 600 microns in size. The Orsang river sediments are coarser than the sediments of the Himalayan rivers, corroborating the observations of Singh et al. (2007). In the Gravel-Sand-Mud diagram (Folk 1954), the sediments from the Orsang river basin mostly demonstrate gravelly sand texture (Fig. 3). Based on arithmetic method, average mean value of nine samples is 946.6 µm, sorting value is 734.5, Skewness measure is 1.98 and Kurtosis is 8.99. The lowest mean value is observed at Karnal Chanod site with 581.9 µm and highest is from Paramgam (1284 µm). The lowest sorting value is 296.6 obtained from the Karnal Chanod and highest is from Morangana (1079.6). The skewness lowest value is from Paramgam (0.953) and highest is from Seturam (3.002). The kurtosis lowest value is 2.84 from Paramgam and highest is from Karnal Chanod (19.15). The mean grain size values for all locations are listed in Table 3.

Table 3. Location wise textural parameters obtained by Arithmetic method

Sample number	River name	Locations	Arithmetic (Mm)			
			Mean (µm)	Sorting	Skewness	Kurtosis
1	Orsang River	Padaliya	984.7	713.9	1.9	7.1
2		Khammapura	1025.6	829.6	1.6	5.4
3		Nagarwada	722.1	515.0	3.0	15.4
4	Hiren River	Morangana	1055	1079.6	1.2	3.4
5		Moradungari	1121.8	808.4	1.6	5.5
6		Garda	836.9	735.9	2.3	8.3
7	Orsang River (after confluence of above two basins)	Paramgam	1284.2	1068.7	0.95	2.8
8		Karnal Chanod Bridge	581.9	296.6	2.32	19.2
9	Narmada River	Seturam Bridge	907.4	562.7	3.00	13.87

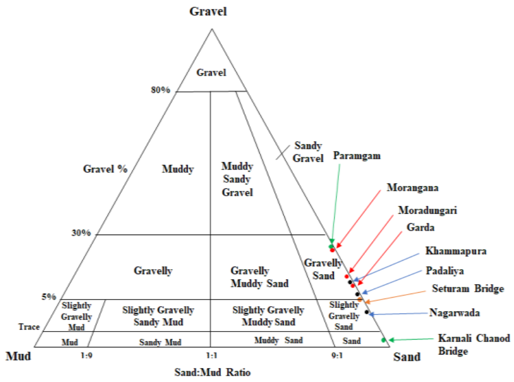

Figure 3. The Gravel-Sand-Mud ternary plot (after Folk, 1954) for Orsang and Hiren river basin sediments. Most of the channel sediments are plotted in the gravelly sand field.

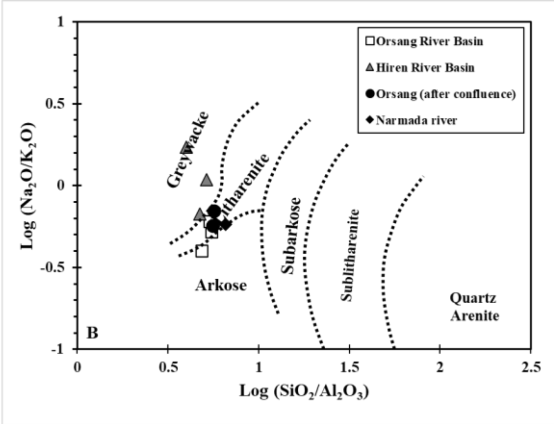

Figure 4. Log (Na_2O/K_2O) vs. log (SiO_2/Al_2O_3) classification plot (Pettijohn et al., 1972).

GEOCHEMISTRY

The geochemical characteristics of river sediments are an essential tool to understand diverse geological processes like the mobility of elements, paleoenvironmental conditions, degree of weathering, and diagenetic changes operating in any particular basin (Taylor and McLennan, 1985; Condie et al., 1992; Singh, 2009; Ramos-Vázquez and Armstrong-Altrin, 2021; Nayak and Singh, 2022). The major-element analyses of sandy channel sediments in the Orsang river basin are listed in Table 4. In the Log (Na_2O/K_2O) vs. Log (SiO_2/Al_2O_3) bivariate plot (Fig. 4; after Pettijohn et al., 1972), the sediments from the Orsang river basin are plotted in the arkose and litharenite fields, while Hiren river samples plotted in the greywacke field. The channel sediments show significant variations in their bulk chemistry, exhibiting the control of diverse sedimentological factors (Fig. 5). SiO_2 content of the samples ranges between 53.16 and 71.28 wt.%, and TiO_2 and Al_2O_3 concentrations vary between 0.2 and 2.2 wt.% and 9.41 and 14.23 wt.%, respectively. The CaO content varies from 3.43 to 18.4 wt.%, while the Fe_2O_3 content ranges from 1.07 to 10.44 wt.%. The TiO_2 and Fe_2O_3 values of sediments from the Hiren river basin are distinctly higher and are comparable to the basalts of the Saurashtra region of DVP (average: 2.23 wt.% and 11.53 wt.%; Laxman et al., 2022).

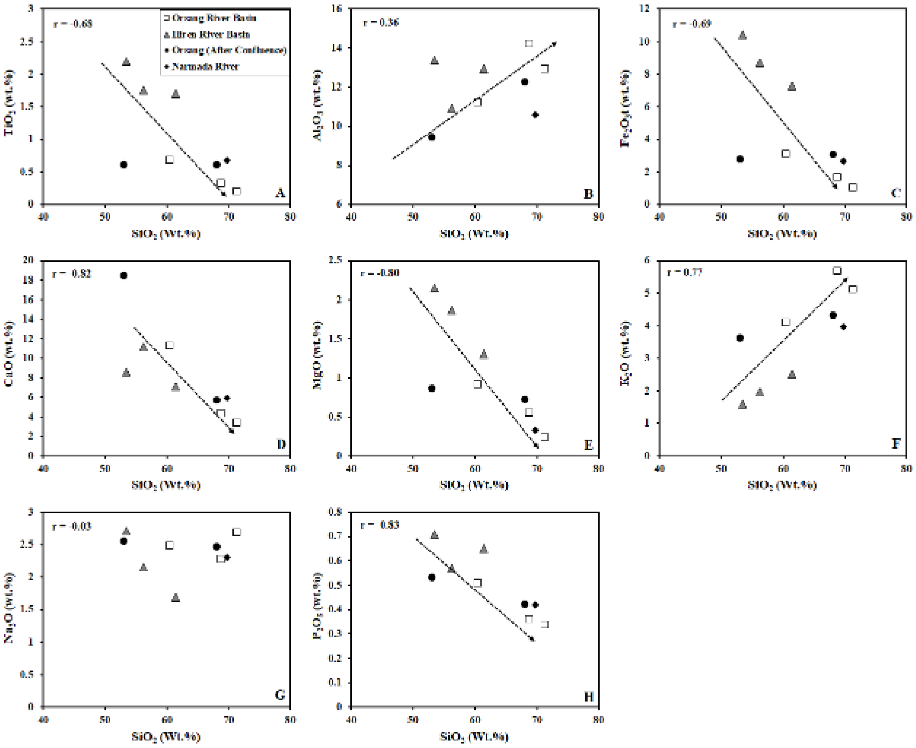

Figure 5. Harker variation plots of major oxides (wt. %) for channel sediments of the Orsang and Hiren river basins

The MgO values are also higher than the other parts of the Orsang river basin; the high TiO_2, Fe_2O_3, and MgO contents can be attributed to basaltic provenance. The Orsang river basin sediments have lower concentrations of MgO and P_2O_5, ranges from 1.2 to 7.4 wt. % and 0.24 to 0.15 wt. %, respectively. The low concentrations of MgO can be attributed to intermediate to felsic provenance. The K_2O (1.58–5.69 wt. %) of the study area is higher than the Na_2O

Table 4. Major element data (in wt.%) of the Hiren, Orsang and Narmada river channel sediments.

	Orsang River			Hiren River			Orsang River (after confluence)		Narmada River
	Location 1	Location 2	Location 3	Location 4	Location 5	Location 6	Location 7	Location 8	Location 9
Major Oxides	Padaliya	Khamapura	Nagarwada	Morangan	Moradungari	Garda	Paramgam	Karnali Chanod Bridge	Sree Rang Setu Ram Bridge
SiO_2	71.3	68.8	60.4	61.4	53.4	56.2	53.2	68.1	69.7
Al_2O_3	12.9	14.2	11.2	12.9	13.4	10.9	9.4	12.2	10.6
Fe_2O_3	1.1	1.7	3.1	7.3	10.4	8.7	2.7	3.0	2.7
TiO_2	0.2	0.3	0.7	1.7	2.2	1.8	0.6	0.6	0.7
CaO	3.4	4.4	11.3	7.1	8.6	11.2	18.4	5.6	5.9
Na_2O	2.7	2.3	2.5	1.7	2.7	2.2	2.5	2.5	2.3
K_2O	5.1	5.7	4.1	2.5	1.6	2.0	3.6	4.3	4.0
MgO	0.2	0.6	0.9	1.3	2.2	1.9	0.9	0.7	0.3
P_2O_5	0.3	0.4	0.5	0.7	0.7	0.6	0.5	0.4	0.4
LOI	2.1	1.2	4.9	2.8	4.3	4.1	7.4	1.5	2.9
Total	99.4	99.5	99.7	99.4	99.5	99.4	99.2	99.0	99.5

content (1.69–2.71 wt. %). The SiO_2 has a positive correlation with Al_2O_3 and K_2O (r = 0.36 and 0.77 respectively). However, the SiO_2 content of the Orsang river sediments shows negative correlations with TiO_2, Fe_2O_3, CaO, MgO, and P_2O_5 (Fig. 5). The strong negative correlation of SiO_2 with CaO (r = -0.83) suggests the mobility of CaO. The samples taken after the confluence of Orsang and Hiren rivers and sample from Narmada river plot in line with the Orsang river sediments suggesting the higher contribution of sediments from the Orsang river than the Hiren river (Fig. 5).

DISCUSSION

GRAIN SIZE ANALYSIS

The grain size analysis of sediments from the Orsang and Hiren River channels has been carried out by using the GRADISTAT program (Blott and Pye, 2001). The Arithmetic method has been utilized for present work, because it is a most reliable and suitable method for fluvial environment. The results are reported in Table 3. The sorting values show that sediments are poorly to moderately sorted and are very-fine skewed. The moderately well-sorted sediments suggest low and reasonably high energy current (Friedman, 1962; Blott and Pye, 2001). These values show that the sediments derived from the river channel are transported from various sources (Layade et al., 2019). The kurtosis lowest value shows very leptokurtic to extremely leptokurtic nature. These values suggest the high energy depositional environment (Friedman, 1962) and also implies that the central portions are better sorted at the tails and suggests that the samples are located at the water concentrated zone (Layade et al., 2019).

SOURCE ROCK CONTROL ON GRAIN SIZE

Source lithology, along with weathering and erosion processes, will have a significant impact on the sediment grain size produced in any particular region. For example, weathering of granite characteristically produces sand-sized quartz and feldspar grains, referring to the original mineral size of the source rock granite and clay minerals like kaolinite, smectite and illite (Banfield 1985; Pettijohn et al., 1987). The clays are generally formed due to the weathering of feldspars. In comparison, weathering of basalt produces much of the clay mineral varieties and lithic fragments, and very little sand-sized mineral grains (Pettijohn et al., 1987). To assess the provenance control on the grain size of river sediments, we selected samples that were contributed exclusively from granitic and basaltic sources. The Padaliya location sample from

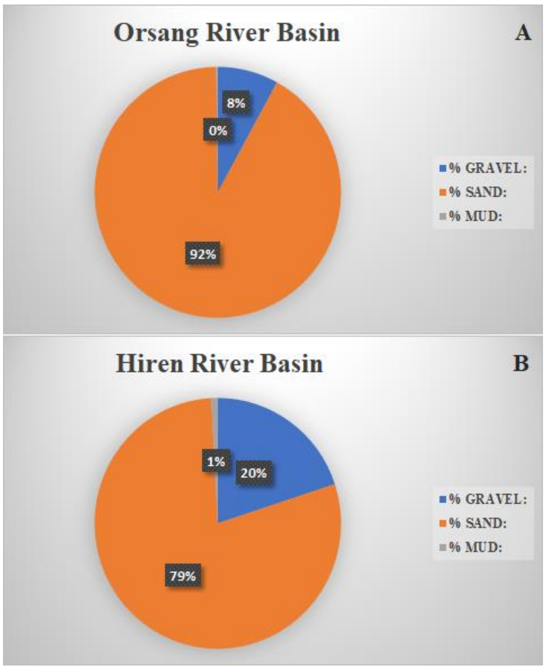

Figure 6. Distribution of Gravel, Sand, and Mud Percentages of Orsang (**A**) and Hiren (**B**) River Basins. The higher proportion of sand in the Orsang river sub-basin compared to the Hiren River sub-basin can be attributed to granitic and basaltic provenances, respectively

the Orsang river represents sediments derived from granitic rocks, while samples collected at Morangana and Moradungari locations from the Hiren river represent sediments derived from basaltic rocks. The granitic sample has 8% gravel and 92% sand while the sediment samples derived from basaltic rocks has 20% gravel, 79% sand, and 1% mud (Fig. 6). A higher proportion of sand in the Orsang river and a higher proportion of gravel and clay in the Hiren river samples can be attributed to granitic and basaltic provenances, respectively.

WEATHERING

The sorting of mineral grains and the degree of both chemical and physical weathering that sediments have undergone can be evaluated by the chemical composition of clastic sediments (McLennan, 1989; Cox and Lowe, 1996; Roddaz et al., 2006; Ramírez-Montoya et al., 2022; Ramos-Vázquez et al., 2022). To determine the impact of weathering and transport, the chemical index of alteration (CIA) values are calculated and are plotted in the Al_2O_3-(CaO+ Na_2O)-K_2O (A-CN-K; Fig. 7A) diagram (CIA: Nesbitt and Young, 1989). The CIA values indicate the intensity of chemical weathering and can be calculated by a formula [Al_2O_3/ (Al_2O_3 + CaO + Na_2O + K_2O)×100] in molecular proportions, where CaO is from the silicate fraction only. The CIA values of 50 to 60 suggest low weathering, 60 to 80 suggest moderate weathering, 80 to 100 suggest intense weathering, and un weathered rocks have CIA values of 50 or less than 50 (McLennan, 2001; Teng et al., 2004). The CIA values of Orsang river sediments range between 47.04 and 51.02, with an average of 48.45 suggesting incipient to moderate weathering in the semi-arid Orsang catchment, while Hiren river values are slightly higher than Orsang ranging from 54.23 to 60.97 with an average of 56.99, suggesting moderate weathering. The A-CN-K plot is extensively used to interpret CIA values, possible mineral phases, the weathering trend of the source rocks, and k-metasomatism (Nesbitt and Young, 1984). The un-weathered samples plot close to the Plagioclase-K feldspar join and the less weathered materials plot above the join line. In the A-CN-K plot (Fig. 7a), all the samples from the Orsang river basin plot close to the Plagioclase-k feldspar join, suggesting incipient to moderate chemical weathering under the semi-arid sub-tropical climatic conditions during deposition. The A-CN-K plot alone cannot adequately explain the impact of mafic minerals (olivine, pyroxene, biotite, and hornblende) on sediment chemistry. In order to comprehend how mafic components, impact sediment geochemistry, we also plotted the A-CNK-FM plot, which includes the molar fraction of Al_2O_3, CaO^* + Na_2O + K_2O and FeO + MgO (Nesbitt and Young, 1984). In the A-CNK-FM plot (Fig. 7B), the channel sediments of the Orsang river are plotted near the feldspar-FM join, whereas the Hiren river sub-basin is plotted around the smectite field more towards the FM apex. This implies that the channel sediments of the Hiren river sediments comprise a considerable number of mafic components supplied from Deccan basalts. The samples taken from after the confluence of Orsang and Hiren rivers and from Narmada river are suggesting felsic provenance, which points towards the higher contribution of sediments from Orsang river than the Hiren river (Fig. 7A and 7B).

Since the Deccan mafic rocks (tholeiite basalt) have contributed significantly to the Hiren sub-basin, another chemical index termed the Mafic Index of Alteration (MIA) has been used (Babechuk et al., 2014). The MIA is comparable to the A-CNK-FM plot (Nesbitt and Young, 1982, 1989), but the MIA has two forms that apply in oxidizing MIA (O) and reducing MIA (R) environments. Under oxidizing conditions, Fe (particularly Fe^{3+}) remains immobile and acts like Al, while in a reducing environment, Fe becomes mobile as Fe^{2+} moves out of the system. When applying the MIA to the Orsang and Hiren river samples, we inferred that in the A-CNKM-F diagram (Fig. 8A), the samples plot close and parallel to the A-CNKM line. The samples plot

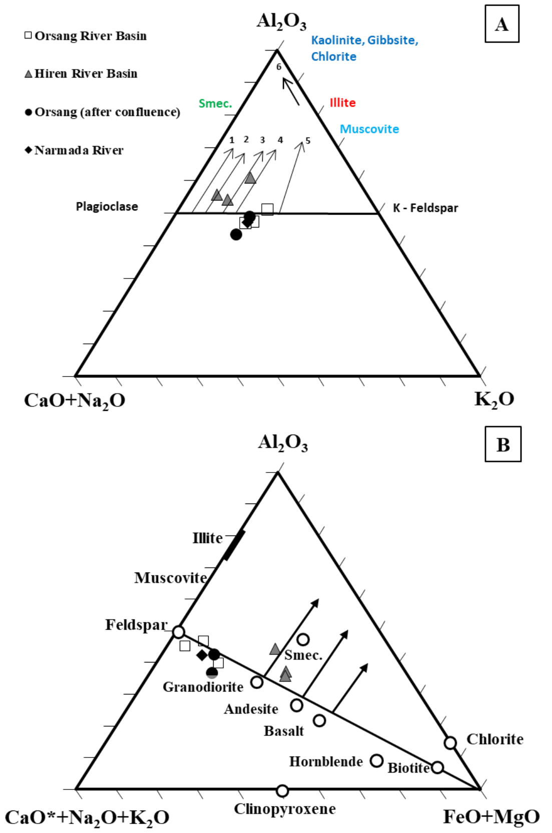

Figure 7. A) A-CN-K plot (Nesbitt and Young, 1984) and **B)** A-FM-CNK plot (Nesbitt and Young, 1989), showing the weathering trend of the Orsang river sediments. In the A-CN-K plot, the trend lines 1 = gabbro, 2 = tonalite, 3 = diorite, 4 = granodiorite, 5 = granite, and 6 = the weathering trend.

close to the CNKM corner, because of the addition of KM components with the CN component, whose concentration is retained during the incipient to moderate degree of weathering. In the Al_2O_3+Fe_2O_3 - MgO - CaO+Na_2O+K_2O diagram (Fig. 8B), where Fe retains with Al due to the immobile nature of Fe^{3+} under an oxidizing environment, the samples plot close to the AF-CNK join and away from the M (MgO) and CNK corners, indicating that Orsang and Hiren river samples have weathered in an oxidizing environment. The arkose-litharenite affinity of Orsang river sediments as depicted by the log Na_2O/K_2O vs. SiO_2/Al_2O_3 plot (Fig. 4), which supports our observation that the sediments have undergone minimal transportation and incipient to moderate chemical weathering. In summary, the low CIA values in our samples can be attributed to the supply of incipient to moderately weathered detritus from semi-arid oxidizing conditions.

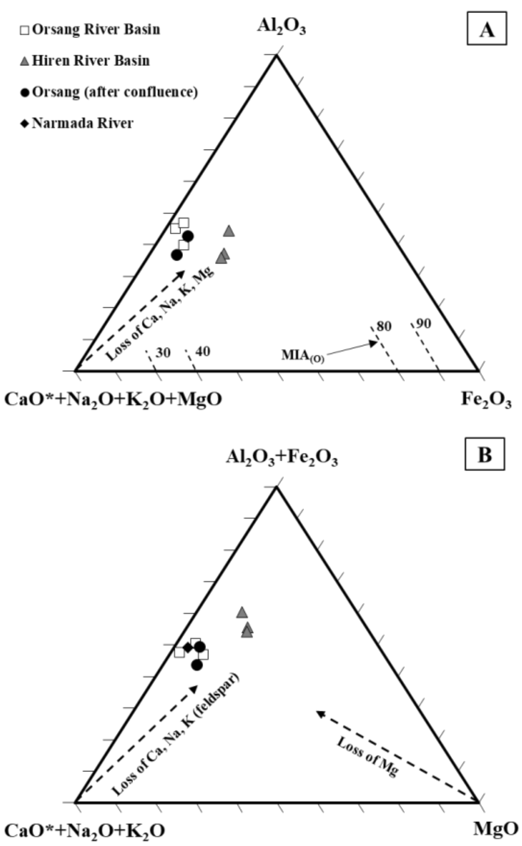

Figure 8. A) A-F-CNKM and **B)** AF-M-CNK plots (Nesbitt and Young, 1989 and Babechuk et al., 2017, respectively) showing Ca + Na + K + Mg loss from sediments. The basaltic provenance and oxidative weathering are reflected in the Fe_2O_3 concentration of the Hiren river sediments.

CONCLUSIONS

In this study, the grain size variations and geochemical characteristics of channel sediments in the Orsang and Hiren rivers are explored. The sediments from both rivers are poorly to moderately sorted, very finely skewed, indicating that the sediments derived from the river channel are transported from various sources. However, the kurtosis value indicates a very leptokurtic to extremely leptokurtic nature, indicating high energy depositional environment and sorting of the central portions. The observed variations in the grain sizes of Orsang and Hiren river basin sediments can be attributed to the provenance, degree of weathering and transportation. We inferred a higher proportion of sand and a lower proportion of gravel in the Orsang sediments due to their granitic source, but the Hiren river sediments composed of more gravel than the Orsang river, which might be due to their basaltic provenance. Sediments collected after the confluence of Orsang and Hiren rivers and from Narmada river points towards felsic provenance, which suggest that the proportion of sediment supply from Orsang river far outweighs that from Hiren River. The low CIA values and arkosic-litharenite nature of Orsang river sediments points towards less transportation and moderate chemical weathering, while Hiren river sediments CIA values point towards slightly higher degree of weathering. The sediments of Orsang and Hiren rivers are sourced from minimally weathered detritus from granitic and basaltic provenances, respectively and deposited in a semi-arid condition.

ACKNOWLEDGEMENTS

This manuscript is the outcome of Post Graduate dissertation project of Shivam Maurya and Nikunj Keshwala. We appreciate Dr. Trilok Akhani, Dean of Parul Institute of Applied Sciences, Vadodara for providing the all-essential facilities required for the research work. We also appreciate Dr. Vishal Ukey and other staffs of Department of Geology, Parul Institute of Applied Sciences, Vadodara for their help with laboratory procedures. We thank Om Minerals Lab & Trading, Gandhinagar, for their help in obtaining the geochemical data. We are grateful to the two reviewers, who reviewed our manuscript.

DECLARATION OF CONFLICTING INTEREST

The Authors hereby declare that they have no conflicting interests related to the research conducted and data reported in this paper.

REFERENCES

Babechuk, M.G., Widdowson, M. and Kamber, B.S. (2014). Quantifying chemical weathering intensity and trace element release from two contrasting basalt profiles, Deccan Traps, India. Chemical Geology, v. 363, pp. 56-75.

Banfield, J. F. (1985). The mineralogy and chemistry of granite weathering. The Australian National University (Australia).

Benavente, J., Gracia, F. J., Anfuso, G. and Lopez-Aguayo, F. (2005). Temporal assessment of sediment transport from beach nourishments by using foraminifera as natural tracers. Coastal Engineering, v. 52(3), pp. 205-219.

Bernabéu Tello, A. M., Medina Santamaría, R. and Vidal Pascual, C. (2002). An equilibrium profile model for tidal environments. Scientia Marina, v. 66(4), pp. 325-335.

Bhatia, M. R. (1983). Plate tectonics and geochemical composition of sandstones. The Journal of geology, v. 91(6), pp. 611-627.

Blott, S.J. and Pye, K. (2001). GRADISTAT: a grain size distribution and statistics package for the analysis of unconsolidated sediments. Earth Surf. Process. Landforms, v. 26, pp. 1237–1248.

Bui, E.N., Mazzullo, J.M. and Wilding, L.P. (1989). Using quartz grain size and shape analysis to distinguish between aeolian and fluvial deposits in the Dallol Bosso of Niger (West Africa). Earth Surf. Process. Landforms, v. 14, pp. 157-166.

Chamyal, L. S., Malassé, A. D., Maurya, D. M., Raj, R., Juyal, N., Bhandari, S., Pant, R. K. and Gaillard, C. (2011). Discovery of a robust fossil Homo sapiens in India (Orsang River Valley, Lower Narmada Basin, Gujarat): possible continuity with Asian Homo erectus. Acta Anthropologica Sinica, v. 30(02), pp. 158.

Condie, K. C., Noll Jr, P. D. and Conway, C. M. (1992). Geochemical and detrital mode evidence for two sources of Early Proterozoic sedimentary rocks from the Tonto Basin Supergroup, central Arizona. Sedimentary Geology, v. 77(1-2), pp. 51-76.

Cox, R. and Lowe, D. R. (1996). Quantification of the effects of secondary matrix on the analysis of sandstone composition, and a petrographic-chemical technique for retrieving original framework grain modes of altered sandstones. Journal of Sedimentary Research, v. 66(3), pp. 548-558.

Cox, R., Lowe, D. R. and Cullers, R. L. (1995). The influence of sediment recycling and basement composition on evolution of mudrock chemistry in the southwestern United States. Geochimica et Cosmochimica Acta, v. 59(14), pp. 2919-2940.

Cullers, R. (1988). Mineralogical and chemical changes of soil and stream sediment formed by intense weathering of the Danburg granite, Georgia, USA. Lithos, v. 21(4), pp. 301-314.

Fedo, C. M., Wayne Nesbitt, H. and Young, G. M. (1995). Unraveling the effects of potassium metasomatism in sedimentary rocks and paleosols, with implications for paleoweathering conditions and provenance. Geology, v. 23(10), pp. 921-924.

Folk, R. L. (1954). The distinction between grain size and mineral composition in sedimentary-rock nomenclature. The Journal of Geology, v. 62(4), pp. 344-359.

Folk, R. L. and Ward, W. C. (1957). Brazos River bar [Texas]; a study in the significance of grain size parameters. Journal of sedimentary Research, v. 27(1), pp. 3-26.

Friedman, G.M., (1962). On Sorting, Sorting Coefficients, and the Lognormality of the Grain-Size Distribution of Sandstones. The Journal of Geology, v. 70, pp. 737-753.

Friedman, G. M. and Sanders, J. E. (1978). Principles of sedimentology. New York: John Wiley Sons.

Friedman, G.M. (1979). Differences in size distributions of populations of particles among sands of various origins: addendum to IAS Presidential Address. Sedimentology, v. 26, pp. 859–862.

Garçon, M. and Chauvel, C. (2014). Where is basalt in river sediments, and why does it matter? Earth and Planetary Science Letters, v. 407, pp. 61-69.

Garzanti, E., Andó, S., France-Lanord, C., Censi, P., Vignola, P., Galy, V. and Lupker, M. (2011). Mineralogical and chemical variability of fluvial sediments 2. Suspended-load silt (Ganga–Brahmaputra, Bangladesh). Earth and Planetary Science Letters, v. 302(1-2), pp. 107-120.

Gray, J. R. and Simões, F. J. (2008). Estimating sediment discharge. Sedimentation engineering–processes, measurements, modelling, and practice, manual, v. 110, pp. 1067-1088.

Gutiérrez-Mas, J. M., Moral, J. P., Sánchez, A., Domínguez, S. and Muñoz-Pérez, J. J. (2003). Multicycle sediments on the continental shelf of Cadiz (SW Spain). Estuarine, Coastal and Shelf Science, v. 57(4), pp. 667-677.

Inman, D.L. (1952). Measures for Describing the Size Distribution of Sediments. Journal of Sedimentary Research, v. 22, pp. 125-145.

Jain, M. and Tandon, S. K. (2003). Quaternary alluvial stratigraphy and palaeoclimatic reconstruction at the Thar margin. Current Science, pp. 1048-1055.

Joshua, E. O. and Oyebanjo, O. A. (2010). Grain-size and heavy mineral analysis of River Osun sediments. Australian Journal of Basic and Applied Sciences, v. 4(3), pp. 498-501.

Juyal, N., Chamyal, L. S., Bhandari, S., Bhushan, R. and Singhvi, A. K. (2006). Continental record of the southwest monsoon during the last 130áka: evidence from the southern margin of the Thar Desert, India. Quaternary Science Reviews, v. 25(19-20), pp. 2632-2650.

Laxman, M. B., Nagaraju, B., Nagaraju, K. and Kumar, K.V. (2022). Spatial variations in the geochemical characteristics of basalts from the Deccan Volcanic Province, India: Role of mixing and assimilation fractional crystallisation. Journal of Earth System Science, v. 131(3), pp. 186.

Layade, G., Ogunkoya, C., Makinde, V. and Ajayi, K. (2019). Assessment and Analysis of Precambrian Basement Soil Deposits Using Grain Size Distribution. Materials and Geoenvironment, v. 66, pp. 235-243.

Maharana, C., Srivastava, D. and Tripathi, J.K. (2018). Geochemistry of sediments of the Peninsular rivers of the Ganga basin and its implication to weathering, sedimentary processes and provenance. Chemical Geology, v. 483, pp. 1-20.

Martins, L.R. (1965). Significance of skewness and kurtosis in environmental interpretation. Journal of Sedimentary Research, v. 35, pp. 768–770.

McLennan, S.M. (1982). On the geochemical evolution of sedimentary rocks. Chemical Geology, v. 37(3-4), pp. 335-350.

McLennan, S.M. (1989). Rare earth elements in sedimentary rocks; influence of provenance and sedimentary processes. Reviews in Mineralogy and Geochemistry, v. 21(1), pp. 169-200.

McLennan, S.M. (2001). Relationships between the trace element composition of sedimentary rocks and upper continental crust. Geochemistry, Geophysics, Geosystems, v. 2(4).

McLennan, S. M., Taylor, S. R. and Eriksson, K. A. (1983). Geochemistry of Archean shales from the Pilbara Supergroup, western Australia. Geochimica et Cosmochimica Acta, v. 47(7), pp. 1211-1222.

Merh, S. S. (1995). Geology of Gujarat. GSI Publications, v. 2(1).

Mondal, M.E.A., Wani, H. and Mondal, B. (2012). Geochemical signature of provenance, tectonics and chemical weathering in the Quaternary flood plain sediments of the Hindon River, Gangetic plain, India. Tectonophysics, v. 566, pp. 87-94.

Nayak, G.N. and Singh, K.T. (2022). Source, processes, and depositional environments of estuarine mudflat core sediments, central western coast of India. In: Armstrong-Altrin JA, Pandarinath K, Verma S. (Eds.), Geochemical Treasures and Petrogenetic Processes. pp. 123-152.

Nesbitt, H. W. and Young, G.M. (1984). Prediction of some weathering trends of plutonic and volcanic rocks based on thermodynamic and kinetic considerations. Geochimica et Cosmochimica acta, v. 48(7), pp. 1523-1534.

Nesbitt, H. W. and Young, G.M. (1989). Formation and diagenesis of weathering profiles. The Journal of Geology, v. 97(2), pp. 129-147.

Nesbitt, H. and Young, G.M. (1982). Early Proterozoic climates and plate motions inferred from major element chemistry of lutites. Nature, v. 299(5885), pp. 715-717.

Nesbitt, H., and Young, G M. (1982). Early Proterozoic climates and plate motions inferred from major element chemistry of lutites. nature, v. 299(5885), pp. 715-717.

Pettijohn, F.J., Potter, P.E., Siever, R., Pettijohn, F.J., Potter, P.E. and Siever, R. (1972). Petrographic classification and glossary. Sand and Sandstone, pp. 149-174.

Pettijohn, F. J., Potter, P.E. and Siever, R. (1987). Sand and sandstone. Springer Science & Business Media.

Ramírez-Montoya, E., Madhavaraju, J., González-León, C.M., Armstrong-Altrin, J.S. and Monreal, R. (2022). Detrital Zircon Geochemistry in the Morita Formation, Northern Sonora, Mexico: Implications for Origin and Source Rock Type. In:

Armstrong-Altrin, J.A., Pandarinath, K., Verma, S. (Eds.), Geochemical Treasures and Petrogenetic Processes. pp. 315-350.

Ramos-Vázquez, M.A. and Armstrong-Altrin, J.S. (2021). Provenance of sediments from Barra del Tordo and Tesoro beaches, Tamaulipas State, northwestern Gulf of Mexico. Journal of Palaeogeography, v. 10 (20), pp. 1-17.

Ramos-Vázquez, M.A., Armstrong-Altrin, J.S., Madhavaraju, J., Gracia, A. and Salas-de-León, D.A. (2022). Mineralogy and geochemistry of marine sediments in the Northeastern Gulf of Mexico. In: Armstrong-Altrin, J.A., Pandarinath, K., Verma, S. (Eds.), Geochemical Treasures and Petrogenetic Processes. pp. 153-183.

Roddaz, M., Viers, J., Brusset, S., Baby, P., Boucayrand, C. and Hérail, G. (2006). Controls on weathering and provenance in the Amazonian foreland basin: Insights from major and trace element geochemistry of Neogene Amazonian sediments. Chemical Geology, v. 226(1-2), pp. 31-65.

Ruiz-Martínez, G., Rivillas-Ospina, G.D., Mariño-Tapia, I. and Posada-Vanegas, G. (2016). SANDY: A Matlab tool to estimate the sediment size distribution from a sieve analysis. Computers & Geosciences, v. 92, pp. 104-116.

Sanyal, P. and Sinha, R. (2010). Evolution of the Indian summer monsoon: synthesis of continental records. Geological Society, London, Special Publications, v. 342(1), pp. 153-183.

Sharma, A., Sensarma, S., Kumar, K., Khanna, P.P. and Saini, N.K. (2013). Mineralogy and geochemistry of the Mahi River sediments in tectonically active western India: Implications for Deccan large igneous province source, weathering and mobility of elements in a semi-arid climate. Geochimica et Cosmochimica Acta, v. 104, pp. 63-83.

Singh, M., Singh, I. B. and Müller, G. (2007). Sediment characteristics and transportation dynamics of the Ganga River. Geomorphology, v. 86(1-2), pp. 144-175.

Singh, P. (2009). Major, trace and REE geochemistry of the Ganga River sediments: influence of provenance and sedimentary processes. Chemical Geology, v. 266(3-4), pp. 242-255.

Singh, P. and Rajamani, V. (2001). Geochemistry of the floodplain sediments of the Kaveri River, southern India. Journal of sedimentary Research, v. 71(1), pp. 50-60.

Taylor, S. R. and McLennan, S.M. (1985). The continental crust: its composition and evolution.

Teng, F. Z., McDonough, W. F., Rudnick, R. L., Dalpé, C., Tomascak, P. B., Chappell, B. W. and Gao, S. (2004). Lithium isotopic composition and concentration of the upper continental crust. Geochimica et Cosmochimica Acta, v. 68(20), pp. 4167-4178.

Wai, O.W.H., Wang, C.H., Li, Y.S. and Li, X.D. (2004). The formation mechanisms of turbidity maximum in the Pearl River estuary, China. Marine Pollution Bulletin, v. 48, pp. 441–448.

Williams, M. (2012). River sediments. Philosophical Transactions of the Royal Society A: Mathematical, Physical and Engineering Sciences, v. 370(1966), pp. 2093-2122.

Wronkiewicz, D. J. and Condie, K.C. (1987). Geochemistry of Archean shales from the Witwatersrand Supergroup, South Africa: source-area weathering and provenance. Geochimica et Cosmochimica Acta, v. 51(9), pp. 2401-2416.